Structural/functional analysis of complement proteins and inhibitions

by

Xin Xu

B.S., Hebei Medical University, 2012
M.S., Kunming Medical University, 2016

AN ABSTRACT OF A DISSERTATION

submitted in partial fulfillment of the requirements for the degree

DOCTOR OF PHILOSOPHY

Department of Biochemistry and Molecular Biophysics
College of Arts and Sciences

KANSAS STATE UNIVERSITY
Manhattan, Kansas

2022

Abstract

The complement system is an important component of innate immunity that fulfills diverse roles in defense and homeostasis, typically conferring protection against accumulating debris and eliminating pathogens. Overactivation or inappropriate activation of the complement system contributes to many inflammatory diseases. Tight regulation and inhibition of complement activators are paramount to prevent inappropriate activation, which has led to an emphasis on the development of therapeutic complement inhibitors. Activation of the central complement component, C3, is required for amplification of complement and is achieved through two different multi-subunit proteases called C3 convertases. Of these, the so-called Alternative Pathway (AP) C3 Convertase is responsible for a majority of the C3 activation products *in vivo*, which renders it an attractive target for inhibitor discovery. Moreover, among many components in the complement system, another molecule, factor H (FH), whose principal function is to inhibit the activity of the complement system, is a complement control protein. FH associates with the surface of human cells, thereby it ensures the complement system is directed towards pathogen rather than host cells.

An opportunistic pathogen, Group B *Streptococcus* (GBS), colonizes the gastrointestinal and vaginal epithelium of a large population of healthy women. Therefore, sometimes it causes ascending intrauterine infection during parturition and creates a risk of serious disease in newborn infants. The β protein is a large, multifunctional surface protein of GBS being investigated as a potential vaccine candidate. As a component of innate immunity, the complement system plays a role in defense against GBS. It has been previously reported that the GBS β protein binds to FH, yet how this occurs at the molecular level remains unclear.

In this study, we defined the FH binding site on β protein using a combination of structural and functional analysis. We also identified and characterized two Slow Off-rate Modified DNA

Aptamers (SOMAmers) that inhibit the AP by binding to factor B (FB), the essential pro-protease of the AP. Together, our studies have defined the FH binding site within the GBS β protein and suggested that molecules that target this site may interfere with FH binding at the GBS cell surface. Ultimately, this work could inform vaccine development and promote our understanding of the β protein in the pathogenesis of *Streptococcal* diseases. The results also demonstrated potent inhibition of the AP by SOMAmers and expanded the pipeline of FB-binding molecules with favorable pharmacologic properties.

Structural/functional analysis of complement proteins and inhibitions

by

Xin Xu

B.S., Hebei Medical University, 2012
M.S., Kunming Medical University, 2016

A DISSERTATION

submitted in partial fulfillment of the requirements for the degree

DOCTOR OF PHILOSOPHY

Department of Biochemistry and Molecular Biophysics
College of Arts and Sciences

KANSAS STATE UNIVERSITY
Manhattan, Kansas

2022

Approved by:

Major Professor
Dr. Brian V. Geisbrecht

Copyright

Abstract

The complement system is an important component of innate immunity that fulfills diverse roles in defense and homeostasis, typically conferring protection against accumulating debris and eliminating pathogens. Overactivation or inappropriate activation of the complement system contributes to many inflammatory diseases. Tight regulation and inhibition of complement activators are paramount to prevent inappropriate activation, which has led to an emphasis on the development of therapeutic complement inhibitors. Activation of the central complement component, C3, is required for amplification of complement and is achieved through two different multi-subunit proteases called C3 convertases. Of these, the so-called Alternative Pathway (AP) C3 Convertase is responsible for a majority of the C3 activation products *in vivo*, which renders it an attractive target for inhibitor discovery. Moreover, among many components in the complement system, another molecule, factor H (FH), whose principal function is to inhibit the activity of the complement system, is a complement control protein. FH associates with the surface of human cells, thereby it ensures the complement system is directed towards pathogen rather than host cells.

An opportunistic pathogen, Group B *Streptococcus* (GBS), colonizes the gastrointestinal and vaginal epithelium of a large population of healthy women. Therefore, sometimes it causes ascending intrauterine infection during parturition and creates a risk of serious disease in newborn infants. The β protein is a large, multifunctional surface protein of GBS being investigated as a potential vaccine candidate. As a component of innate immunity, the complement system plays a role in defense against GBS. It has been previously reported that the GBS β protein binds to FH, yet how this occurs at the molecular level remains unclear.

In this study, we defined the FH binding site on β protein using a combination of structural and functional analysis. We also identified and characterized two Slow Off-rate Modified DNA

Aptamers (SOMAmers) that inhibit the AP by binding to factor B (FB), the essential pro-protease of the AP. Together, our studies have defined the FH binding site within the GBS β protein and suggested that molecules that target this site may interfere with FH binding at the GBS cell surface. Ultimately, this work could inform vaccine development and promote our understanding of the β protein in the pathogenesis of *Streptococcal* diseases. The results also demonstrated potent inhibition of the AP by SOMAmers and expanded the pipeline of FB-binding molecules with favorable pharmacologic properties.

Table of Contents

List of Figures x

List of Tables xii

Acknowledgements xiii

Dedication xiv

Chapter 1 - Introduction 1

Complement Pathways and its Activation 1

Complement Factor H and its relationship with Group B *Streptococcus* β Protein 3

Complement Factor B and its Binding to SOMAmers 6

References 7

Chapter 2 - Expression, purification, and characterization of a human complement component C3 analog that lacks the C-terminal C345c domain 12

Abstract 13

Introduction 14

Methods 17

Results 23

Discussion 37

Acknowledgments 41

References 41

Chapter 3 - Inhibition of the Complement Alternative Pathway by Slow Off-Rate Modified DNA Aptamers that Bind with Picomolar Affinity to Factor B 44

Abstract 45

Introduction 46

Materials and methods 50
Results 58
Discussion 79
Acknowledgments 82
References 83
Chapter 4 - Group B *Streptococcus* Surface Protein β: Structural Characterization of a Novel Complement Factor H-binding Motif and its Contribution to Immune Evasion 87
Abstract 88
Introduction 89
Materials and Methods 91
Results 104
Discussion 130
Acknowledgements 135
References 135
Chapter 5 - Conclusion 142
References 144
Appendix A - Copyright Permissions 146

List of Figures

Figure 1.1. Complement Cascade. 2

Figure 1.2. Complement activation regulation by factor H. 4

Figure 2.1. Structural Representation of the Activation and Degradation of Human Complement Component C3 and Two Recombinant Analogs. 16

Figure 2.2. Annotated Pre-Pro-Protein Sequences of Both C3 Analogs. 18

Figure 2.3. Primary and Tertiary Structures of Human C3 and Two Engineered C3 Analogs. ... 25

Figure 2.4. Characterization of Stable CHO Cell Lines Expressing Two Different Human C3 Analogs. 27

Figure 2.5. Initial Purification of a Human C3 Analog by Immobilized Metal-ion Affinity Chromatography. 28

Figure 2.6. Final Purification of a Human C3 Analog by Size Exclusion Chromatography. 29

Figure 2.7. Activation of a Human C3 Analog by TEV Protease Digestion. 31

Figure 2.8. Peptide Coverage Map of the Truncated C3 Analog Before and Following Activation by TEV Protease. 33

Figure 2.9. Evaluation of the conformational state of human C3 and C3c analogs by their ligand binding profiles. 35

Figure 2.10. Both the human C3 analog and its C3c-like activation product bind to the C3/b/c ligand TRX-4W9A. 37

Figure 3.1. Sequence-Function Relationships of FB-Binding SOMAmers. 60

Figure 3.2. Nuclease and Serum Stability of FB-Binding SOMAmers. 63

Figure 3.3. FB-Binding SOMAmers Inhibit the AP, but not the CP of Complement. 64

Figure 3.4. Structural Analysis of SL1103 Bound to FB. 66

Figure 3.5. Supporting Data Pertaining to the SL1103/FB and SL1102/FB Crystal Structures. . 68

Figure 3.6. Supporting Data Pertaining to the SL1103 SOMAmer Structure. 73

Figure 3.7. Proposed Mechanism for AP Inhibition by FB-Binding SOMAmers..... 74

Figure 3.8. FB-Binding SOMAmers Reagents Inhibit Formation of the AP Pro-C3 Convertase.76

Figure 3.9. FB-Binding SOMAmers Reagents Inhibit Formation of the AP C3 Convertase..... 77

Figure 3.10. Cross Species Reactivity of FB-Binding SOMAmers Reagents. 78

Figure 4.1. A Protease-Stable Domain within the B75KN Region of GBS β Harbors a Binding Site for Factor H. 107

Figure 4.2. Structural Analysis of B75KN-CTD and Identification of its FH-binding Site. 111

Figure 4.3. The B75KN Region of β protein Binds FH in the CCP3 and CCP4 Modules. 115

Figure 4.4. Supporting Information for the B75KN/FH Crosslinking Study. 116

Figure 4.5. β Protein Expression Suppresses C3b Deposition onto the Bacterial Surface. 120

Figure 4.6. FH Bound by β Protein Retains its Complement Regulatory Activities. 125

Figure 4.7 Supporting Information for the Convertase Decay Study. 127

Figure 4.8. The B75KN Domain of β protein Suppresses Bacterial Phagocytic Killing Through a FH-Independent Mechanism. 130

List of Tables

Table 2.1. Rate and dissociation constants for TRX-4W9A binding obtained by surface plasmon resonance[a]. 37

Table 3.1. Distribution of Factor B-binding SOMAmers. 61

Table 3.2. X-ray Diffraction Data Collection and Refinement Statistics. 69

Table 4.1. Interaction Parameters for Various β Fragments with Immobilized Human FH[a] 108

Table 4.2. X-ray Diffraction Data Collection and Refinement Statistics 112

Table 4.3. Identities of Peptide Crosslinks Between the B75KN Region of β and Human FH . 117

Acknowledgements

First and foremost, I would like to express my overwhelming and sincerest appreciation to my advisor Dr. Brian Geisbrecht for their incredible and constant support throughout my Ph.D. studies. His collective knowledge, insights, and unending patience have been a source of security that have aided my growth as a research scientist. It has been a privilege and my pleasure to have him as my advisor.

I want to extend my thanks to my doctoral committee members Dr. Ho Ng, Dr. Anna Zolkiewska, Dr. Philip Hardwidge, and Dr. Peter Sues, for taking the time to serve on my committee. I would also like to thank my previous committee member, Dr. Zhilong Yang, for the guidance in adapting here in the U.S.

Extra thanks to current and previous members of our lab and Dr. Erika Geisbrecht's lab. Without them, I could not have had a colorful life both in and out of the lab. A special thanks to Dr. Timothy Herdendorf for guiding me in enzyme experiments. In addition, I would like to thank Dr. Simranjot Bawa and Dr. Ashish Kumar, who provided me with lots of precious advice in preliminary examination and job interviews.

I also want to express my sincerest gratitude to the staff and faculty of the entire Biochemistry and Molecular Biophysics Department for providing the facilities, education, and support during the 4.5 years. I felt lucky that I chose here in the K-state to pursue my Ph.D. degree.

Finally, I would like to thank my family and friends for being supportive, persistent, and patient all these years. Thank you for being my constant cheerleaders.

Dedication

To my mother, Yingxia Chang, for always nurturing my passions and pursuits wherever they led.

To my father, Xiaodong Xu, for unending patience, moral support, constant encouragement and understanding.

To my husband, Da Zhang, for always kindling my ambitions by pushing me to strive to be the best version of myself.

Thank you all for your unconditional love.

This work would not have been possible without your faith in my abilities.

Chapter 1 - Introduction

Complement is an evolutionarily conserved branch of the innate immune system that makes numerous contributions to human health and disease. Although complement is best known for its ability to recognize and eliminate of invading microorganisms, roles for complement in coordinating the overall immune response and in promoting developmental processes are now widely understood (1). Complement also contributes to inflammation-driven tissue injury, which occurs during ischemia and reperfusion processes, vasculitis, arthritis, and many other diseases (2). In recent years, complement has received considerable attention owing to a growing appreciation of its links to several prominent diseases, including systemic vasculitis (2) and Alzheimer's Disease (3-5). There are no broadly applicable reagents for the therapeutic regulation of excessive complement activation, but some agents in development might provide useful anti-complement therapies in the near future (6).

Complement Pathways and Their Activation

Complement activity has traditionally been thought to arise from three different pathways. However, contemporary evidence suggests that these are better viewed as two initiation routes, which are the classical (CP) and lectin pathways (LP), and an amplification route, the alternative pathway (AP) (1) (Figure 1.1). The CP and LP use distinct pattern recognition molecules to recognize surface-bound Ig molecules and carbohydrates, respectively. Activation of either pathway results in the splitting of C2 and C4 to form the CP or LP C3 convertase (7). At this point, the CP and LP are merged into a single pathway. The process of forming the C3 convertase, also called C4bC2a, requires activation of C4, which covalently deposits on nearby surfaces where it binds a pro-protease, called C2, in an Mg^{2+}-dependent manner. Then the C3 convertase cleaves

the next component, C3. The activated form C3 is known as C3b. It also deposits covalently on the surface and forms a Mg^{2+}-dependent complex with a separate pro-protease, Factor B (FB). The C3b-bound form of FB can be cleaved by another enzyme, Factor D (FD). This results in another metastable enzyme called the AP C3 convertase. Both forms of C3 convertase subsequently cleave C5 into C5a and C5b (an anaphylatoxin) (8,9). C5b binds to C6-C9 to form the membrane attack complex (MAC) that promotes lysis of microbes or cell injury in cases where complement regulatory proteins are deficient (7).

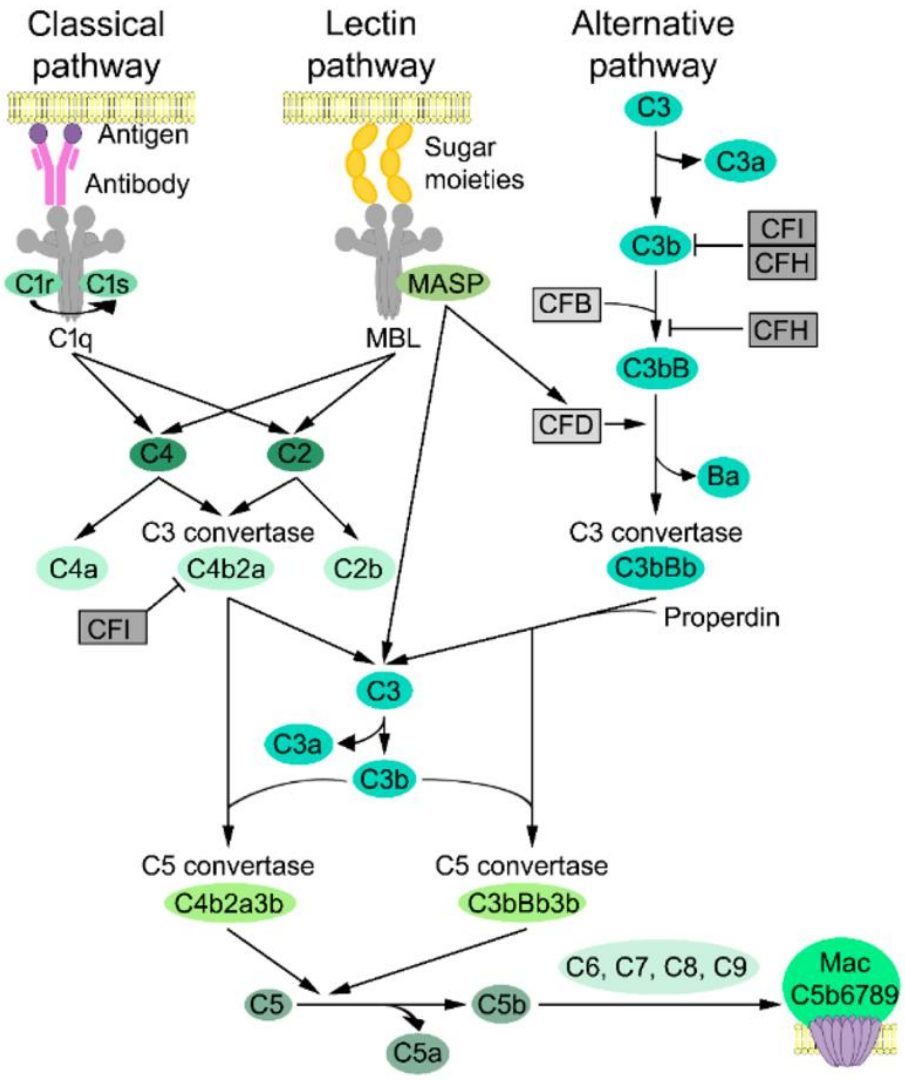

Figure 1.1. Complement Cascade.

The complement system can be activated via two initiation routes and an amplification route. (1) The classical pathway is typically activated by antigen-antibody complexes on the cell surface. The C1 complex consists of C1q, C1r, and C1s molecules, and cleaves serum proteins C4 and C2. C4b binds to the target cell surface and C2a binds C4b and forms the complex C4b2a, which is the classical pathway C3 convertase. (2) The lectin pathway is activated by mannose-binding lectins (MBLs) binding to carbohydrate ligands on the surface of pathogens. Activated MBL-associated serine proteinase (MASP)-2 in the MBL-MASP-2 complex cleaves C4 and C2. MASP-1/3 can activate complement factor D (FD). (3) The alternative pathway is the amplification route, which is activated by any permissive surface. Constant spontaneous breakdown of C3 takes place at a low level in plasma and by the surfaces of microbes and generates C3b. Complement factor B (FB) binds to C3b and forms the pro-convertase complex C3bB. Complement factor D (FD) cleaves C3b-bound FB to Ba and Bb. The fragment Bb stays associated with C3b and the fully active C3 convertase (C3bBb) is formed. Properdin stabilizes the AP C3 convertase. All three of these pathways lead to activation of the lytic/terminal pathway. C5b engages C6, C7, C8, and C9 to form the terminal membrane attack complex (MAC), which results in cell lysis. The activation of complement is strictly regulated to prevent damage to host cells. Complement factor I (FI) and complement factor H (FH) are the main inhibitors of complement pathways. FH competes with FB for binding to active C3b and inhibits the C3 convertase by displacing Bb from this complex. FI also cleaves FH-bound C3b to an inactive form and inhibits the classical pathway by cleaving C4b. Reused from Riihilä et al. 2019 (https://doi.org/10.3390/ijms20143550).

Complement Factor H and its relationship with Group B *Streptococcus* β Protein

Factor H (FH) is a fluid-phase regulator of the AP. It is a soluble, ~150 kDa protein composed of 20 short consensus repeat (SCR) domains or called complement control protein (CCP) modules (10) (Figure 1.2). FH is the main inhibitor of the AP whereby it acts through inhibition of the so-called self-amplification loop (11). The inhibition activities of FH are mediated by SCR domains 1-4 , which harbor a C3b-binding site (12). SCR7 contains binding sites for certain ligands, including glycosaminoglycans (GAGs) on host cellular surfaces, pentraxins, and malondialdehyde (MDA) epitopes generated by lipid peroxidation (13). The C-terminal SCR19-20 domains harbor binding sites for C3b/C3d, pentraxins, and sialic acid/GAGs, and thus anchor FH to host surfaces to attenuate complement attack (14,15). The different functions among these domains allow FH to restrict complement activation on host cells, thus allowing complement attack against non-self surfaces which lack membrane-bound complement regulators. Thus, FH has an important role in self-nonself discrimination by recognizing specific host surfaces (14-16).

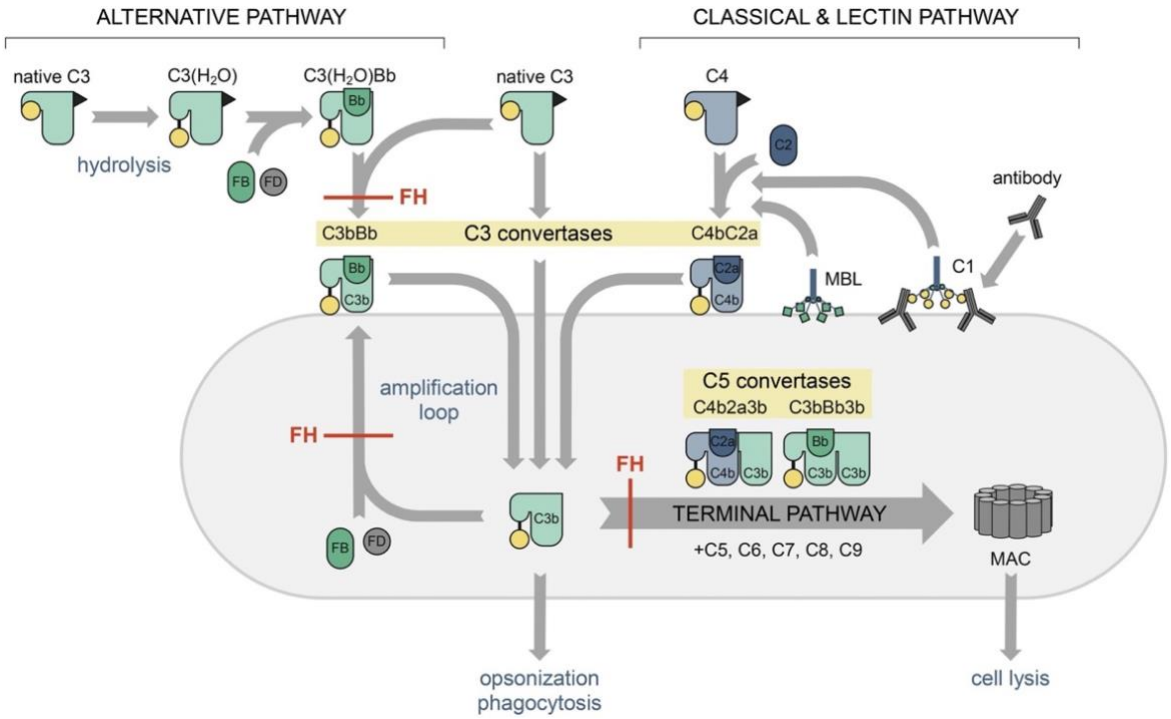

Figure 1.2. Complement activation regulation by factor H.

FH inhibits complement activation at the level of the central C3b molecule, whereby it blocks the amplification loop and terminal pathway. Reused from Cserhalmi et al. 2019. (https://doi.org/10.1016/j.smim.2019.101341).

Group B *Streptococcus* (GBS), alternatively known as *Streptococcus agalactiae*, is a beta-hemolytic Gram-positive bacterium, that has been shown to bind FH. GBS is a cause of morbidity or mortality in newborns and is increasingly associated with disease in pregnant women, diabetics, and elderly populations (17-20). In clinical cases, GBS is mostly recognized as an important pathogen of neonates (21). Neonatal GBS infections are classified as early onset disease (EOD), which occurs in the first seven days after birth, or late onset disease (LOD) that develops between seven days and ninety days postpartum (22,23). GBS can transmit vertically from mother to child before or during labor because of the aspiration of contaminated amniotic and bodily fluids, potentially resulting in invasive neonatal diseases, including pneumonia and meningitis (24-26). GBS has also been shown to be transmitted in breast milk, which may play a role in developing diseases such as sepsis and meningitis, especially in preterm infants (26,27). In the United States

and some other countries, colonization-positive maternal women are treated with intrapartum antibiotic prophylaxis (IAP) (28). Though IAP has aided in reducing EOD, it has little to no impact on LOD rates. Additionally, preliminary experimental evidence indicates IAP delays the development of healthy gut microbiota of the newborns, potentially increasing the risk for other types of infections, including *Escherichia coli* among others (29-31). Therefore, the administration of a suitable vaccine during pregnancy could provide better clinical outcomes, and may represent an alternative strategy to protecting newborns and young infants through transplacental antibody transfer and potentially reducing new vaginal colonization (32). Proteins such as alpha-C-protein (bca), beta-C-protein (bac), and epsilon/Alp1, Rib (rib) are embedded in the GBS bacterial surface and could be selected as candidate vaccine targets. Currently, glycan proteins (CPS) conjugate vaccines and protein based GBS vaccines are under development. The conjugate vaccines use GBS CPS as the primary target and enhance immunogenicity by forming a covalent conjugate to a protein carrier. However, the limitations of these vaccines are reflected in their pricing and the fact that they confer protection only against included serotypes (32). Protein vaccines use common GBS protein(s) as the vaccine target and have the potential to confer broad protection across serotypes. Moreover, they could be less complex and cheaper to manufacture. Nevertheless, the relationship between antibodies against surface proteins and the development of disease has not been established.

The beta-C-protein (bac), also called β protein, is expressed on the surface of several GBS serotypes. The expression of β protein elicits the production of antibodies that are protective against GBS infection (33). β protein is a 125 kDa surface protein, originally identified by its ability to bind immunoglobulin A (IgA) (34). Subsequently, it also has been found to bind with Siglec-7, an inhibitory molecule on natural killer (NK) cells (35). Moreover, CEACAM1 and

CEACAM5, which are cell surface proteins that regulate cell signaling and immunity, interact with an Ig superfamily (IgSF) fold domain within β protein (36). β protein has also been shown to bind FH, and the FH-binding region is tentatively located to the C-terminal half of the β protein (37,38). Most of its ligands have something to do with host immune response, suggesting that the β protein is an important immune evasion determinant of GBS. Understanding how these interactions occur, and how they influence the function of the host immune system, is critical for treating GBS diseases and the development of vaccines.

Complement Factor B and its Binding to SOMAmers

The discovery of FH variants and the alternative complement pathway in the pathophysiology of age related macular degeneration (AMD) subsequently led to the investigation of other complement factors for AMD associated complement activation or deregulation, including complement component 2 (C2) and FB (39,40). Indeed, in recent years, FB has been found in a relationship with a number of diseases including high glucose-induced podocyte injury, diabetic kidney disease, glomerular disease, paroxysmal nocturnal hemoglobinuria (PNH), etc. (41-43). As a key component of the alternative pathway, human complement factor B (FB) circulates in the blood and aids in amplification of complement activity (44). Thus, molecules that can inhibit the function of FB or even the AP of the complement have begun to attract research interest. Currently, a promising inhibitor, LNP023, has reached clinical trials. LNP023, or iptacopan as a trade name, is under phase 2 study in patients with PNH who have active hemolysis despite anti-C5 therapy (43). It is a highly selective, orally active, low molecular weight inhibitor that potently blocks AP activation *in vitro* and in mice (42). Other than this, no FB inhibitor is available for therapeutic applications. Nafamostat and peptide aldehydes are known as covalent inhibitors of FB, however both of these compounds lack specificity (45). The anti-FB Fab fragment TA106 is under

development at Alexion, but is still in pre-clinical research (46,47). Thus, the discovery of additional inhibitors is urgently needed.

Aptamers are oligonucleotides identified from large random sequence pools, where target-specific molecules are selected (48). Further evolution of aptamers exploits a systematic evolution of ligands by exponential enrichment (SELEX). During the last few years, scientists have used thousands of proteins, mostly human, as SELEX targets by applying a collection of modified pyrimidines with full substitution. Of these, SOMAmers (Slow Off-rate Modified Aptamers) are novel classes of aptamers with a more favorable pharmacokinetic/pharmacodynamic (PK/PD) profile. SOMAmers specific for different key components, including FB and C5, of the complement cascade, are currently under pre-clinical development and could be considered for further therapeutic applications (49). SOMAmers have proven as powerful substitutes for antibodies in diagnostic applications and the purpose of biomarker identification due to their exceptional recognition properties towards a variety of associated targets (50), such as the early diagnosis of Crohn's disease (51) and early detection of malignant pleural mesothelioma (52). The use of SOMAmers as inhibitory reagents carries advantages over traditional antibody-based immune therapies. The synthetic nature of SOMAmers also ensures availability and uniformity (50). With most investigations that target FB focusing on small molecules, Si-RNA (53), or monoclonal antibodies (47), whether SOMAmers might be the next promising inhibitor class to reach clinical studies remains to be determined through future investigation.

References

1. Hajishengallis, G., Reis, E. S., Mastellos, D. C., Ricklin, D., and Lambris, J. D. (2017) Novel mechanisms and functions of complement. *Nature immunology* **18**, 1288-1298

2. Chimenti, M. S., Ballanti, E., Triggianese, P., and Perricone, R. (2015) Vasculitides and the complement system: a comprehensive review. *Clinical reviews in allergy & immunology* **49**, 333-346
3. Ricklin, D., Reis, E. S., and Lambris, J. D. (2016) Complement in disease: a defence system turning offensive. *Nature Reviews Nephrology* **12**, 383-401
4. Ricklin, D., and Lambris, J. D. (2013) Complement in immune and inflammatory disorders: pathophysiological mechanisms. *The Journal of Immunology* **190**, 3831-3838
5. Ricklin, D., and Lambris, J. D. (2013) Complement in immune and inflammatory disorders: therapeutic interventions. *The Journal of Immunology* **190**, 3839-3847
6. Mizuno, M., and Morgan, B. (2004) The possibilities and pitfalls for anti-complement therapies in inflammatory diseases. *Current Drug Targets-Inflammation & Allergy* **3**, 87-96
7. Reddy, Y. N., Siedlecki, A. M., and Francis, J. M. (2017) Breaking down the complement system: a review and update on novel therapies. *Current Opinion in Nephrology and Hypertension* **26**, 123-128
8. Rawal, N., and Pangburn, M. K. (2003) Formation of high affinity C5 convertase of the classical pathway of complement. *Journal of Biological Chemistry* **278**, 38476-38483
9. Rawal, N., and Pangburn, M. K. (2001) Formation of high-affinity C5 convertases of the alternative pathway of complement. *The Journal of Immunology* **166**, 2635-2642
10. Zipfel, P. F., Jokiranta, T. S., Hellwage, J., Koistinen, V., and Meri, S. (1999) The factor H protein family. *Immunopharmacology* **42**, 53-60
11. Sánchez-Corral, P., Pouw, R. B., López-Trascasa, M., and Józsi, M. (2018) Self-damage caused by dysregulation of the complement alternative pathway: relevance of the factor H protein family. *Frontiers in immunology* **9**, 1607
12. Wu, J., Wu, Y.-Q., Ricklin, D., Janssen, B. J., Lambris, J. D., and Gros, P. (2009) Structure of complement fragment C3b–factor H and implications for host protection by complement regulators. *Nature immunology* **10**, 728-733
13. Józsi, M. (2017) Factor H family proteins in complement evasion of microorganisms. *Frontiers in immunology* **8**, 571
14. Morgan, H. P., Schmidt, C. Q., Guariento, M., Blaum, B. S., Gillespie, D., Herbert, A. P., Kavanagh, D., Mertens, H. D., Svergun, D. I., and Johansson, C. M. (2011) Structural basis for engagement by complement factor H of C3b on a self surface. *Nature structural & molecular biology* **18**, 463
15. Kajander, T., Lehtinen, M. J., Hyvärinen, S., Bhattacharjee, A., Leung, E., Isenman, D. E., Meri, S., Goldman, A., and Jokiranta, T. S. (2011) Dual interaction of factor H with C3d and glycosaminoglycans in host–nonhost discrimination by complement. *Proceedings of the National Academy of Sciences* **108**, 2897-2902
16. Meri, S. (2016) Self-nonself discrimination by the complement system. *FEBS letters* **590**, 2418-2434
17. Doran, K. S., and Nizet, V. (2004) Molecular pathogenesis of neonatal group B streptococcal infection: no longer in its infancy. *Molecular microbiology* **54**, 23-31
18. Saad, E. J., Baenas, D. F., Boisseau, C. S., García, M. J., Núñez, S. A., Sanchez, P. E., Balderramo, D. C., Hernández, D., and Caeiro, J. P. (2018) Streptococcus agalactiae bacteremia in non-pregnant adult patients at two teaching hospitals. *Revista Argentina de microbiologia* **50**, 280-284

19. Leclercq, S. Y., Sullivan, M. J., Ipe, D. S., Smith, J. P., Cripps, A. W., and Ulett, G. C. (2016) Pathogenesis of Streptococcus urinary tract infection depends on bacterial strain and β-hemolysin/cytolysin that mediates cytotoxicity, cytokine synthesis, inflammation and virulence. *Scientific reports* **6**, 1-14
20. Ruppen, C., Notter, J., Strahm, C., Sonderegger, B., and Sendi, P. (2018) Osteoarticular and skin and soft-tissue infections caused by Streptococcus agalactiae in elderly patients are frequently associated with bacteremia. *Diagnostic microbiology and infectious disease* **90**, 55-57
21. Thomas, L., and Cook, L. (2020) Two-component signal transduction systems in the human pathogen Streptococcus agalactiae. *Infection and immunity* **88**
22. Pediatrics, A. A. o. (2019) Prevention of Group B Streptococcal Early-Onset Disease in Newborns. *Pediatrics* **144**
23. Yadeta, T. A., Worku, A., Egata, G., Seyoum, B., Marami, D., and Berhane, Y. (2018) Vertical transmission of group B Streptococcus and associated factors among pregnant women: a cross-sectional study, Eastern Ethiopia. *Infection and drug resistance* **11**, 397
24. Li, S., Huang, J., Chen, Z., Guo, D., Yao, Z., and Ye, X. (2017) Antibiotic prevention for maternal group B streptococcal colonization on neonatal GBS-related adverse outcomes: a meta-analysis. *Frontiers in microbiology* **8**, 374
25. Shabayek, S., and Spellerberg, B. (2018) Group B streptococcal colonization, molecular characteristics, and epidemiology. *Frontiers in microbiology* **9**, 437
26. Zimmermann, P., Gwee, A., and Curtis, N. (2017) The controversial role of breast milk in GBS late-onset disease. *Journal of Infection* **74**, S34-S40
27. Trend, S., Strunk, T., Hibbert, J., Kok, C. H., Zhang, G., Doherty, D. A., Richmond, P., Burgner, D., Simmer, K., and Davidson, D. J. (2015) Antimicrobial protein and peptide concentrations and activity in human breast milk consumed by preterm infants at risk of late-onset neonatal sepsis. *PloS one* **10**, e0117038
28. Filkins, L., Hauser, J. R., Robinson-Dunn, B., Tibbetts, R., Boyanton, B. L., and Revell, P. (2020) American Society for Microbiology Provides 2020 Guidelines for Detection and Identification of Group B Streptococcus. *Journal of clinical microbiology*
29. Stearns, J. C., Simioni, J., Gunn, E., McDonald, H., Holloway, A. C., Thabane, L., Mousseau, A., Schertzer, J. D., Ratcliffe, E. M., and Rossi, L. (2017) Intrapartum antibiotics for GBS prophylaxis alter colonization patterns in the early infant gut microbiome of low risk infants. *Scientific reports* **7**, 1-9
30. Tapiainen, T., Koivusaari, P., Brinkac, L., Lorenzi, H. A., Salo, J., Renko, M., Pruikkonen, H., Pokka, T., Li, W., and Nelson, K. (2019) Impact of intrapartum and postnatal antibiotics on the gut microbiome and emergence of antimicrobial resistance in infants. *Scientific reports* **9**, 1-11
31. Toyofuku, M., Morozumi, M., Hida, M., Satoh, Y., Sakata, H., Shiro, H., Ubukata, K., Murata, M., and Iwata, S. (2017) Effects of intrapartum antibiotic prophylaxis on neonatal acquisition of group B streptococci. *The Journal of pediatrics* **190**, 169-173. e161
32. Kobayashi, M., Schrag, S. J., Alderson, M. R., Madhi, S. A., Baker, C. J., Sobanjo-ter Meulen, A., Kaslow, D. C., Smith, P. G., Moorthy, V. S., and Vekemans, J. (2019) WHO consultation on group B Streptococcus vaccine development: report from a meeting held on 27–28 April 2016. *Vaccine* **37**, 7307-7314
33. Bevanger, L. (1985) The Ibc proteins of group B streptococci: isolation of the α and β antigens by immunosorbent chromatography and test for human serum antibodies against

the two antigens. *Acta Pathologica Microbiologica Scandinavica Series B: Microbiology* **93**, 113-119
34. Russell-Jones, G., Gotschlich, E., and Blake, M. S. (1984) A surface receptor specific for human IgA on group B streptococci possessing the Ibc protein antigen. *The Journal of experimental medicine* **160**, 1467-1475
35. Fong, J. J., Tsai, C.-M., Saha, S., Nizet, V., Varki, A., and Bui, J. D. (2018) Siglec-7 engagement by GBS β-protein suppresses pyroptotic cell death of natural killer cells. *Proceedings of the National Academy of Sciences* **115**, 10410-10415
36. van Sorge, N. M., Bonsor, D. A., Deng, L., Lindahl, E., Schmitt, V., Lyndin, M., Schmidt, A., Nilsson, O. R., Brizuela, J., and Boero, E. (2020) Bacterial protein domains with a novel Ig-like fold bind human CEACAM receptors. *bioRxiv*
37. Jarva, H., Hellwage, J., Jokiranta, T. S., Lehtinen, M. J., Zipfel, P. F., and Meri, S. (2004) The group B streptococcal β and pneumococcal Hic proteins are structurally related immune evasion molecules that bind the complement inhibitor factor H in an analogous fashion. *The Journal of Immunology* **172**, 3111-3118
38. Areschoug, T., Stålhammar-Carlemalm, M., Karlsson, I., and Lindahl, G. (2002) Streptococcal β Protein Has Separate Binding Sites for Human Factor H and IgA-Fc∗. *Journal of Biological Chemistry* **277**, 12642-12648
39. Gold, B., Merriam, J. E., Zernant, J., Hancox, L. S., Taiber, A. J., Gehrs, K., Cramer, K., Neel, J., Bergeron, J., and Barile, G. R. (2006) Variation in factor B (BF) and complement component 2 (C2) genes is associated with age-related macular degeneration. *Nature genetics* **38**, 458-462
40. Jakobsdottir, J., Conley, Y. P., Weeks, D. E., Ferrell, R. E., and Gorin, M. B. (2008) C2 and CFB genes in age-related maculopathy and joint action with CFH and LOC387715 genes. *PloS one* **3**, e2199
41. Lu, Q., Hou, Q., Cao, K., Sun, X., Liang, Y., Gu, M., Xue, X., Zhao, A. Z., and Dai, C. (2021) Complement factor B in high glucose–induced podocyte injury and diabetic kidney disease. *JCI insight* **6**
42. Webb, N., Haraldsson, B., Schubart, A., Milojevic, J., End, P., Holbro, T., and Junge, G. (2020) MO042 LNP023: A NOVEL ORAL COMPLEMENT ALTERNATIVE PATHWAY FACTOR B INHIBITOR FOR THE TREATMENT OF GLOMERULAR DISEASE. *Nephrology Dialysis Transplantation* **35**, gfaa140. MO042
43. Risitano, A. M., Röth, A., Soret, J., Frieri, C., de Fontbrune, F. S., Marano, L., Alashkar, F., Benajiba, L., Marotta, S., and Rozenberg, I. (2021) Addition of iptacopan, an oral factor B inhibitor, to eculizumab in patients with paroxysmal nocturnal haemoglobinuria and active haemolysis: an open-label, single-arm, phase 2, proof-of-concept trial. *The Lancet Haematology* **8**, e344-e354
44. Lee, M. J., Na, K., Shin, H., Kim, C.-Y., Cho, J.-Y., Kang, C. M., Kim, S. H., Kim, H., Choi, H. J., and Lee, C.-k. (2021) Early Diagnostic Ability of Human Complement Factor B in Pancreatic Cancer Is Partly Linked to Its Potential Tumor-Promoting Role. *Journal of Proteome Research*
45. Schubart, A., Anderson, K., Mainolfi, N., Sellner, H., Ehara, T., Adams, C. M., Mac Sweeney, A., Liao, S.-M., Crowley, M., and Littlewood-Evans, A. (2019) Small-molecule factor B inhibitor for the treatment of complement-mediated diseases. *Proceedings of the National Academy of Sciences* **116**, 7926-7931

46. Noris, M., Mescia, F., and Remuzzi, G. (2012) STEC-HUS, atypical HUS and TTP are all diseases of complement activation. *Nature Reviews Nephrology* **8**, 622-633
47. Ricklin, D., and Lambris, J. D. (2013) Progress and trends in complement therapeutics. *Complement Therapeutics*, 1-22
48. Cox, J., Rajendran, M., Riedel, T., Davidson, E. A., Sooter, L. J., Bayer, T. S., Schmitz-Brown, M., and Ellington, A. D. (2002) Automated acquisition of aptamer sequences. *Combinatorial chemistry & high throughput screening* **5**, 289-299
49. Drolet, D., Zhang, C., O'Connell, D., Gupta, S., and Janjic, N. (2014) SOMAmer inhibitors of the complement system. in *7th international conference on complement therapeutics, Olympia*
50. Kraemer, S., Vaught, J. D., Bock, C., Gold, L., Katilius, E., Keeney, T. R., Kim, N., Saccomano, N. A., Wilcox, S. K., and Zichi, D. (2011) From SOMAmer-based biomarker discovery to diagnostic and clinical applications: a SOMAmer-based, streamlined multiplex proteomic assay. *PloS one* **6**, e26332
51. Torres, J., Petralia, F., Sato, T., Wang, P., Telesco, S. E., Strauss, R., Li, X.-j., Laird, R. M., Gutierrez, R. L., and Porter, C. K. (2020) Serum biomarkers identify patients who will develop inflammatory bowel diseases up to 5 years before diagnosis. *Gastroenterology* **159**, 96-104
52. Ostroff, R. M., Mehan, M. R., Stewart, A., Ayers, D., Brody, E. N., Williams, S. A., Levin, S., Black, B., Harbut, M., and Carbone, M. (2012) Early detection of malignant pleural mesothelioma in asbestos-exposed individuals with a noninvasive proteomics-based surveillance tool.
53. Borodovsky, A., Yucius, K., Sprague, A., Banda, N. K., Holers, V. M., Vaishnaw, A., Maier, M., Kallanthottathil, R., Charisse, K., and Kuchimanchi, S. (2014) Aln-CC5, an investigational RNAi therapeutic targeting C5 for complement inhibition. American Society of Hematology Washington, DC

Chapter 2 - Expression, purification, and characterization of a human complement component C3 analog that lacks the C-terminal C345c domain

This chapter has been published as a journal article in the Journal of Immunological Methods.

Kasra X. Ramyar[a,1], Xin Xu[a,1], Natalie M. White[a], Andrew Keightley[b], Brian V. Geisbrecht[a,*]

[a] Department of Biochemistry & Molecular Biophysics, Kansas State University, 141 Chalmers Hall, 1711 Claflin Road, Manhattan, KS 66506, United States of America

[b] School of Biological Sciences, University of Missouri-Kansas City, 5100 Rockhill Road, Kansas City, MO 64110, United States of America

[1] These two authors contributed equally to this work.

Abstract

The complement system consists of a series of soluble and cell-surface proteins that serve numerous roles in innate immunity, development, and homeostasis. Despite its many functions, the central event in the complement system is the proteolytic activation of the 185 kDa complement component 3 (C3) into its opsonin and anaphylatoxin fragments known as C3b (175 kDa) and C3a (10 kDa), respectively. The C3 protein is comprised of thirteen separate structural domains, several of which undergo extensive structural rearrangement upon activation to C3b. In addition to this, the C-terminal C345c domain found in C3, C3b, and the terminal degradation product, C3c (135 kDa), appears to adopt multiple conformations relative to the remainder of the molecule. To facilitate various structure/function studies, we designed two C3 analogs that could be activated to a C345c-less, C3c-like state following treatment with Tobacco Etch Virus (TEV) protease. We generated stably transfected Chinese Hamster Ovary (CHO) cell lines that secrete approximately 1.5 mg of the highest-expressing C3 analog per liter of conditioned culture medium. We purified this C3 analog by sequential immobilized metal ion affinity and size exclusion chromatographies, activated the protein by digestion with TEV protease, and purified the resulting C3c analog by a final size exclusion chromatography. The conformations and activities of our C3 and C3c analogs were assessed by measuring their binding profiles to known C3/b/c ligands by surface plasmon resonance. Together, this work demonstrates the feasibility of producing a C3 analog that can be site-specifically activated by an exogenous proteolytic enzyme.

Introduction

The complement system is an essential component of the human innate immune response, wherein it serves important roles in the detection and destruction of foreign organisms, recruitment of phagocytic cells, and clearance of immune complexes among others (1). Furthermore, recent work has expanded our understanding of the diverse contributions of complement to development, homeostasis, and inflammatory and degenerative diseases such as cancer and Alzheimer's Disease (2,3). Consisting of some 30 unique soluble and cell-surface retained proteins, the complement system can be triggered by three canonical routes known as the Classical, Lectin, and Alternative Pathways (1). Although the biochemical stimulus for initiating each of these pathways differs considerably, all three pathways converge at the level of activating the third component of complement, commonly known as C3 (185 kDa), into its C3b (175 kDa) and C3a (10 kDa) fragments (1,4,5). Whereas the C3a fragment exhibits physiological properties of an anaphylatoxin, the C3b fragment becomes covalently linked to nearby surfaces. C3b functions in this context as both an opsonin and hub for various protein-protein interactions that drive downstream processes within the complement system (1,4,5).

Under normal circumstances, C3 becomes activated through site specific proteolytic cleavage by transiently stable, multi-subunit serine proteases known as C3 convertases (1,4,5). C3 convertase assembly occurs in stepwise fashion and proceeds through the initial association of a pro-protease zymogen with a platform molecule, followed by cleavage into a fully active enzyme complex. The Classical and Lectin Pathways share a C3 convertase that forms when the zymogen C2 binds to the surface-linked platform molecule, C4b, and becomes activated by cleavage of C4b/C2 into C4b/C2a. Similarly, the Alternative Pathway C3 convertase forms when the zymogen factor B (B) binds to the surface-linked component, C3b, and becomes activated via cleavage of

C3b/B into C3b/Bb. It is the Alternative Pathway C3 convertase that is responsible for the remarkable self-amplifying nature of the complement system, as it contributes greater than 80% of the complement activation products generated under physiological conditions (6). Moreover, the convertase-mediated deposition of increasingly greater levels of C3b on surfaces causes a change in the substrate specificity of both convertases from C3 to C5 (7-9). Proteolytic activation of C5 into C5a and C5b represents the final enzymatic step in the complement system. It also sets the stage for key effector functions of complement, including the recruitment of phagocytic cells to the site of complement activation (via C5a) and formation of the terminal complement complex (via C5b) (1,4,5).

The structures of human C3 (10), as well as its activation products C3b (11) and C3c (10), have been extensively characterized by X-ray crystallography (12). This work has revealed that activation of C3 into C3b involves global conformational changes that serve to both create and destroy the various ligand binding sites responsible for the divergent functional properties of C3 and C3b (Figure 2.1). Most notably, while the eight macroglobulin-like domains that comprise the so-called "key ring" of C3 remain essentially static, both the CUB (for Complement C1r/C1s, Uegf, and Bmp1) and TED (for thioester-containing) domains undergo a large rotation and translation relative to the remainder of the molecule. One important consequence of this change is creation of a portion of the C3b binding site for the Alternative Pathway zymogen, fB (13). Subsequent degradation of C3b to C3c through the proteolytic activity of factor I in the presence of factor H removes the CUB-TED region, destroys this aspect of the fB binding site, and renders C3c incapable of interaction with fB. The remainder of the fB binding site is derived from the C345c domain (13). Although the C345c domain does not experience dramatic positional changes when compared to the CUB-TED region, the short linker which connects C345c to the key ring

appears partly capable of rotating around the axis defined by the longest dimension of the C3/b/c structure. Indeed, since the C345c domain appears to contribute the only binding site on C3b for Bb, such rotations have been proposed as critical for efficient proteolytic cleavage of substrate by the Alternative Pathway C3 convertase (14).

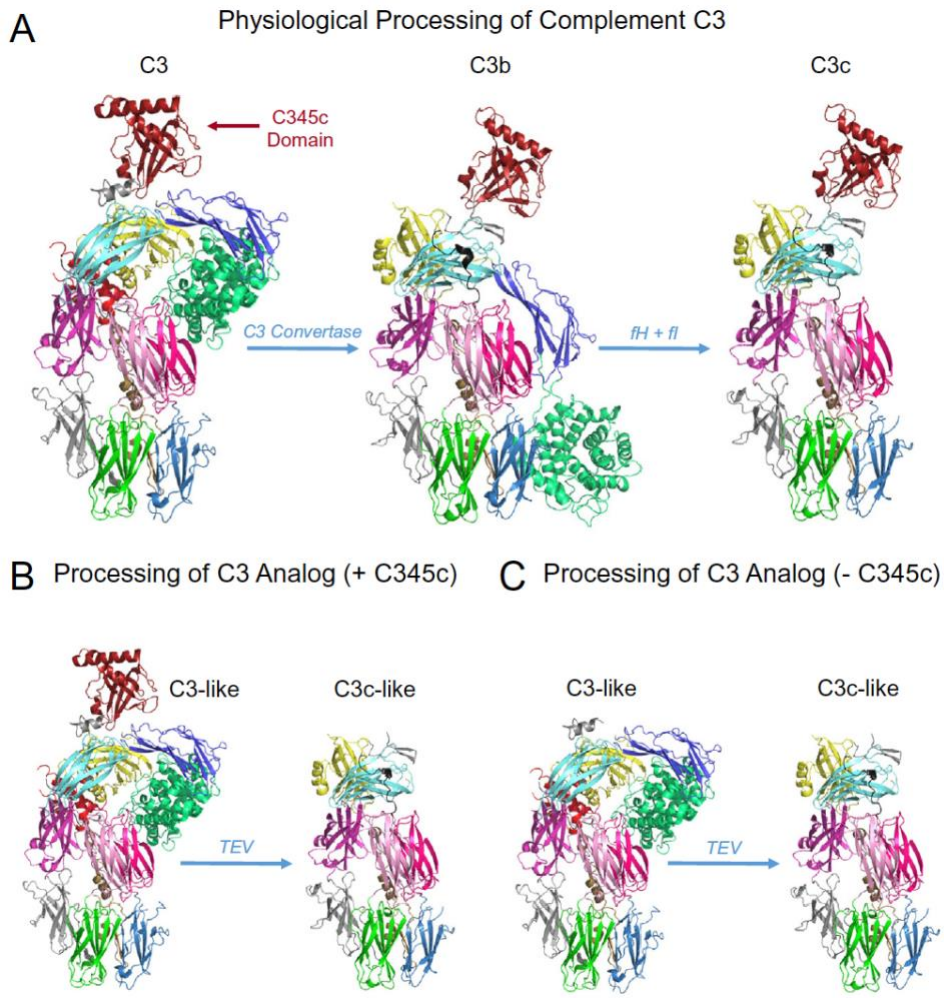

Figure 2.1. Structural Representation of the Activation and Degradation of Human Complement Component C3 and Two Recombinant Analogs.

(A) Structural representation of native C3, its activation into C3b via proteolysis by a C3 convertase, and the degradation of C3b into C3c via the activities of FH and fI. Images were drawn using PyMol from PDB entries 2A73 (10,11,15), and 2A74 (10), respectively. (B) Structural representation of a human C3 analog containing the C345c domain, followed by its activation by TEV protease to a C3c-like state that lacks the C345c domain. (C) Structural representation of a human C3 analog expressed without the C345c domain, followed by its activation by TEV protease to a C3clike state. The images in panels B and C were drawing using PyMol from the PDB entries 2A73 (10) and 2A74 (10), respectively.

Methods

Molecular Biology and Plasmid Construction

The coding sequence for each human C3 analog was assembled from a series of GeneBlock synthetic designer gene fragments (Integrated DNA Technologies, Coralville, IA) that had been individually subcloned into pBluescript II SK (+) and sequence confirmed. Following complete assembly of the human C3 analog sequences, the corresponding inserts were directionally subcloned into the mammalian cell expression vector pCI-neo with NheI and NotI sites at the 5′- and 3′-ends, respectively. The coding sequence and translation product for each human C3 analog is provided as supporting information (Figure 2.2). All plasmids were purified by isopyncic density gradient centrifugation over CsCl prior to use in cell culture applications.

Truncated C3 Analog Pre-Pro-Protein

MGPTSGPSLLLLLLTHLPLALGSPMYSIITPNILRLESEETMVLEAHDAQGDVPVTVTVHDFPGKKLVLSSEKTVLT
PATNHMGNVTFTIPANREFKSEKGRNKFVTVQATFGTQVVEKVVLVSLQSGYLFIQTDKTIYTPGSTVLYRIFTVNH
KLLPVGRTVMVNIENPEGIPVKQDSLSSQNQLGVLPLSWDIPELVNMGQWKIRAYYENSPQQVFSTEFEVKEYVLPS
FEVIVEPTEKFYYIYNEKGLEVTITARFLYGKKVEGTAFVIFGIQDGEQRISLPESLKRIPIEDGSGEVVLSRKVLL
DGVQNPRAEDLVGKSLYVSATVILHSGSDMVQAERSGIPIVTSPYQIHFTKTPKYFKPGMPFDLMVFVTNPDGSPAY
RVPVAVQGEDTVQSLTQGDGVAKLSINTHPSQKPLSITVRTKKQELSEAEQATRTMQALPYSTVGNSNNYLHLSVLR
TELRPGETLNVNFLLRMDRAHEAKIRYYTYLIMNKGRLLKAGRQVREPGQDLVVLPLSITTDFIPSFRLVAYYTLIG
ASGQREVVADSVWVDVKDSCVGSLVVKSGQSEDRQPVPGQQMTLKIEGDHGARVVLVAVDKGVFVLNKKNKLTQSKI
WDVVEKADIGCTPGSGKDYAGVFSDAGLTFTSSSGQQTAQRAELQCPQPAARRRRSVQLTEKRMDKVGKYPKELRKC
CEDGMRENPMRFSCQRRTRFISLGEACKKVFLDCCNYITELRRQHARASHLGLARENLYFQSIIAEENIVSRSEFPE
SWLWNVEDLKEPPKNGISTKLMNIFLKDSITTWEILAVSMSDKKGICVADPFEVTVMQDFFIDLRLPYSVVRNEQVE
IRAVLYNYRQNQELKVRVELLHNPAFCSLATTKRRHQQTVTIPPKSSLSVPYVIVPLKTGLQEVEVKAAVYHHFISD
GVRKSLKVVPENLYFQGIRMNKTVAVRTLDPERLGREGVQKEDIPPADLSDQVPDTESETRILLQGTPVAQMTEDAV
DAERLKHLIVTPSGSGEQNMIGMTPTVIAVHYLDETEQWEKFGLEKRQGALELIKKGYTQQLAFRQPSSAFAAFVKR
APSTWLTAYVVKVFSLAVNLIAIDSQVLCGAVKWLILEKQKPDGVFQEDAPVIHQEMIGGLRNNNEKDMALTAFVLI
SLQEAKDICEEQVNSLPGSITKAGDFLEANYMNLQRSYTVAIAGYALAQMGRLKGPLLNKFLTTAKDKNRWEDPGKQ
LYNVEATSYALLALLQLKDFDFVPPVVRWLNEQRYYGGGYGSTQATFMVFQALAQYQKDAPDHQELNLDVSLQLPSR
SSKITHRIHWESASLLRSEETKENEGFTVTAEGKGQGTLSVVTMYHAENLYFQSCNKFDLKVTIKPAPETEKRPQDA
KNTMILEICTRYRGDQDATMSILDISMMTGFAPDTDDLKQLANGVDRYISKYELDKAFSDRNTLIIYLDKVSHSEDD
CLAFKVHQYFNVELIQPGAVKVYAYYNLEESCTRFYHPEKEDGKLNKLCRDELCRCAEEHHHHHHHH

Full-length C3 Analog Pre-Pro-Protein

MGPTSGPSLLLLLLTHLPLALGSPMYSIITPNILRLESEETMVLEAHDAQGDVPVTVTVHDFPGKKLVLSSEKTVLT
PATNHMGNVTFTIPANREFKSEKGRNKFVTVQATFGTQVVEKVVLVSLQSGYLFIQTDKTIYTPGSTVLYRIFTVNH
KLLPVGRTVMVNIENPEGIPVKQDSLSSQNQLGVLPLSWDIPELVNMGQWKIRAYYENSPQQVFSTEFEVKEYVLPS
FEVIVEPTEKFYYIYNEKGLEVTITARFLYGKKVEGTAFVIFGIQDGEQRISLPESLKRIPIEDGSGEVVLSRKVLL
DGVQNPRAEDLVGKSLYVSATVILHSGSDMVQAERSGIPIVTSPYQIHFTKTPKYFKPGMPFDLMVFVTNPDGSPAY
RVPVAVQGEDTVQSLTQGDGVAKLSINTHPSQKPLSITVRTKKQELSEAEQATRTMQALPYSTVGNSNNYLHLSVLR
TELRPGETLNVNFLLRMDRAHEAKIRYYTYLIMNKGRLLKAGRQVREPGQDLVVLPLSITTDFIPSFRLVAYYTLIG
ASGQREVVADSVWVDVKDSCVGSLVVKSGQSEDRQPVPGQQMTLKIEGDHGARVVLVAVDKGVFVLNKKNKLTQSKI
WDVVEKADIGCTPGSGKDYAGVFSDAGLTFTSSSGQQTAQRAELQCPQPAARRRRSVQLTEKRMDKVGKYPKELRKC
CEDGMRENPMRFSCQRRTRFISLGEACKKVFLDCCNYITELRRQHARASHLGLARENLYFQSIIAEENIVSRSEFPE
SWLWNVEDLKEPPKNGISTKLMNIFLKDSITTWEILAVSMSDKKGICVADPFEVTVMQDFFIDLRLPYSVVRNEQVE
IRAVLYNYRQNQELKVRVELLHNPAFCSLATTKRRHQQTVTIPPKSSLSVPYVIVPLKTGLQEVEVKAAVYHHFISD
GVRKSLKVVPENLYFQGIRMNKTVAVRTLDPERLGREGVQKEDIPPADLSDQVPDTESETRILLQGTPVAQMTEDAV
DAERLKHLIVTPSGSGEQNMIGMTPTVIAVHYLDETEQWEKFGLEKRQGALELIKKGYTQQLAFRQPSSAFAAFVKR
APSTWLTAYVVKVFSLAVNLIAIDSQVLCGAVKWLILEKQKPDGVFQEDAPVIHQEMIGGLRNNNEKDMALTAFVLI
SLQEAKDICEEQVNSLPGSITKAGDFLEANYMNLQRSYTVAIAGYALAQMGRLKGPLLNKFLTTAKDKNRWEDPGKQ
LYNVEATSYALLALLQLKDFDFVPPVVRWLNEQRYYGGGYGSTQATFMVFQALAQYQKDAPDHQELNLDVSLQLPSR
SSKITHRIHWESASLLRSEETKENEGFTVTAEGKGQGTLSVVTMYHAENLYFQSCNKFDLKVTIKPAPETEKRPQDA
KNTMILEICTRYRGDQDATMSILDISMMTGFAPDTDDLKQLANGVDRYISKYELDKAFSDRNTLIIYLDKVSHSEDD
CLAFKVHQYFNVELIQPGAVKVYAYYNLEESCTRFYHPEKEDGKLNKLCRDELCRCENLYFQGEENCFIQKSDDKVT
LEERLDKACEPGVDYVYKTRLVKVQLSNDFDEYIMAIEQTIKSGSDEVQVGQQRTFISPIKCREALKLEEKKHYLMW
GLSSDFWGEKPNLSYIIGKDTWVEHWPEEDECQDEENQKQCQDLGAFTESMVVFGCPNHHHHHHHH

Figure 2.2. Annotated Pre-Pro-Protein Sequences of Both C3 Analogs.

Sequences of the pre-pro-protein for each human C3 analog are presented below. The secretion signal peptide is shown in dark yellow underlined letters, while the tetra-arginine motif cleaved by furin-class proteases during secretion is shown in blue underlined letters. The C-terminal octahistidine tag is also shown in blue underlined letters. TEV protease recognition sites are highlighted in yellow. The cysteine-to-serine mutation that removes the C3 thioester is shown in grey outline. Residues corresponding to the C3a (red), CUB (blue), TED (green), and C345c (rust) domains are colored identically to **Figure 2.1**and **Figure 2.3** to facilitate their identification.

Cell Lines, Transfection, Selection, and Amplification

A Chinese Hamster Ovary (CHO) cell line deleted for the gene encoding dihydrofolate reductase (dhfr -/-) was chosen for generating stably transfected mammalian cells expressing both human C3 analogs. All procedures involving routine culturing and maintenance of these cells, transfection by electroporation, and selection of stable transfectants were performed as described by Leahy and coworkers (16). Amplification of protein expression was carried out by culturing precursor cells in increasingly higher concentrations of methotrexate as previously described (16),

with the exception that clonal populations of cells were isolated using 3.2mm Bel-Art sterile paper cloning disks according to manufacturer's suggestions. Protein expression levels of individual clones were assessed by immunoblotting conditioned culture medium after 2-4 days of growth using either (i) an HRP-conjugated anti-human C3 goat IgG (MP Biomedicals) or (ii) a rabbit antibody recognizing human C3a (Calbiochem) followed by a goat anti-rabbit HRP conjugate (ThermoFisher).

Stably transfected CHO cell lines expressing the highest levels of human C3 analog were expanded into twenty 175-cm2 vented flasks and cultured at 37 °C in a humidified incubator containing 5% (v/v) CO2 in the atmosphere. Cells were maintained in a medium consisting of DMEM High Glucose (Corning cellgro number 10–013-CM) supplemented with 1% (v/v) Bovine Calf Serum, 1% (v/v) Non-Essential Amino Acids solution (HyClone number SH30238.01), and 1% (v/v) of a penicillin/streptomycin solution. The medium in all flasks was exchanged every 3–4 days. Conditioned culture medium was centrifuged following collection (20,000×g for 30 min) to remove cell debris and precipitated materials and stored at 4 °C until further use. Pilot experiments were also carried out using PowerCHO-3-CD serum free medium (Lonza Catalog Number 12-772Q) in place of DMEM High Glucose.

Protein Expression and Purification

Purification of the human C3 analog lacking the C345c domain was achieved through sequential immobilized metal ion affinity and size exclusion chromatographies carried out at room temperature on a GE Life Sciences AKTA pure FPLC system. Briefly, 2 L of clarified conditioned culture medium was concentrated ten-fold using a Millipore lab scale tangential flow filtration device equipped with 30 kDa nominal molecular weight cut-off filters. The buffer of the concentrated sample was exchanged to 20mM tris (pH 8.0), 500mM NaCl, 10mM imidazole (pH

8.0) according to the manufacturer's suggestions. Following clarification by 0.45 μm filtration, the exchanged sample was applied at a flow rate of 4 ml/min to a 5 ml HiTrap Chelating column (GE Life Sciences) that had been previously charged with 100mM NiSO4 and equilibrated in the sample buffer. The column was washed extensively with sample buffer, prior to eluting the bound proteins at a flow rate of 2 ml/min with a linear gradient over 7.5 column volumes to 20mM tris (pH 8.0), 500mM NaCl, 500mM imidazole (pH 8.0) while collecting 2 ml fractions. Fractions containing human C3 analog (as judged by SDS-PAGE performed under non-reducing conditions) were pooled and injected at a flow rate of 4 ml/min onto a Superdex S200 26/60 size exclusion chromatography column (GE Life Sciences) that had been previously equilibrated in phosphate-buffered saline (pH 7.4). Fractions of the column eluate (2 ml each) were collected and analyzed by SDSPAGE performed under non-reducing conditions. Fractions containing the human C3 analog were pooled, concentrated by ultrafiltration, and stored at 4 °C for further use.

Proteolytic Activation of the Human C3 Analog

The purified human C3 analog was activated by site-specific digestion with TEV protease fused to the C-terminus of *E. coli* maltose binding protein. MBP-TEV was added to the purified substrate at a 1: 50 mass ratios in PBS (pH 7.4). The reaction was allowed to proceed at 37 °C for approximately 48–72 h until it reached completion, as judged by SDS-PAGE performed under non-reducing conditions. Following activation, the human C3c analog was separated from the MBP-TEV fusion protease and other digestion products by size exclusion chromatography. The sample was injected at 0.5 ml/min onto a Superdex S200 10/300 GL column that had been previously equilibrated in PBS (pH 7.4) and fractions of the eluate (1 ml each) were collected. Fractions containing purified human C3c analog were pooled, concentrated by ultrafiltration, and stored at 4 °C until further use.

Protein Characterization by Mass Spectrometry

Samples of purified proteins were separated by SDS-PAGE performed under non-reducing conditions and stained with Coomassie blue. Excised gel bands corresponding to each sample were reduced, alkylated, and processed for in-gel trypsin digestion by standard methods (17). The extracted peptides were characterized by tandem mass spectrometry according to the methods described by Keightley and coworkers (17). Identification of the C3 and C3c analogs was performed using Mascot 2.4 (Matrix Science) with semi-trypsin specificity.

Surface Plasmon Resonance Studies of Ligand Binding Profiles

The ligand binding profiles of the human C3 and C3c analogs were compared qualitatively to those of purified human C3b and C3c (Complement Technologies, Tyler, TX) by Surface Plasmon Resonance (SPR) as a means of assessing the conformational state of both recombinant proteins. All experiments were performed at 25 °C on a Biacore T-200 instrument (GE Healthcare) at a flow rate of 30 μl/min and utilized a running buffer of HBS-T (20mM HEPES (pH 7.4), 140mM NaCl, and 0.005% (v/v) Tween-20). Experimental surfaces were prepared on a CMD200 sensor chip (Xantec Bioanalytics GmbH, Dusseldorf, Germany) by immobilizing the *S. aureus* complement inhibitor Efb-C (18), its inactive mutant Efb-C-RENE (18) (approximately 1200 RU each), and purified human complement factor H (Complement Technologies, Tyler, TX) (1384 RU) on separate flow cells using random amine chemistry. A reference surface was prepared by immediately injecting ethanolamine over a separate flow cell following activation. Five different samples of either native human C3b, the C3 analog, or its C3c counterpart representing a five-fold dilution series (625 nM maximum) were injected in ascending order of concentration over the surfaces for 2 min with a 1 min dissociation between injections, followed by a single 30 min dissociation phase following the final injection. Regeneration to baseline was obtained by three

consecutive 30 s injections of 0.1M glycine (pH 1.5). All reference-subtracted injection series were analyzed using a heterogenous ligand binding model (Biacore T-200 Evaluation Software v3.1).

A similar study was performed by injecting native human C3c, the C3 analog, and its C3c counterpart over a surface consisting of immobilized mouse monoclonal antibody, WM-1 (19). In this case, while a somewhat lower density of capture ligand was used (639 RU), both the analyte concentration series and regeneration to baseline parameters were identical to those described above. All reference- subtracted injection series were analyzed using a Langmuir kinetic binding model (Biacore T-200 Evaluation Software v3.1).

Surface Plasmon Resonance Experiments for Quantitative Comparison of Affinities

The functional properties of the human C3 and C3c analogs were also compared quantitatively to purified human C3c by measuring binding of the C3/b/c ligand, TRX-4W9A (20), to each protein by SPR. Experimental surfaces were prepared on a CMD200 sensor chip (Xantec Bioanalytics GmbH, Dusseldorf, Germany) by immobilizing C3 analog (2544 RU), C3c analog (1618 RU), and native human C3c (1402 RU) on separate flow cells using random amine chemistry. A reference surface was also prepared as described above. Nine different samples of TRX-4W9A representing a two-fold dilution series (5 μM maximum), as well as buffer alone, were injected in ascending order of concentration over the surfaces for 2 min and allowed to dissociate for 3 min. Regeneration to baseline was obtained by two consecutive 30 s injections of 2M NaCl. All reference-subtracted injection series were analyzed using both Langmuir kinetic and approach to equilibrium binding models (Biacore T-200 Evaluation Software v3.1). Values describing the various binding parameters from three replicate injection series were pooled to derive mean and standard deviations for each parameter.

Results

Practical Considerations for Expression Vector Design

Although it is translated from a single type of mRNA transcript, biogenesis of the matured C3 protein found in human serum is a relatively complex process (4). Following removal of a 22-residue signal peptide upon translocation into the endoplasmic reticulum, the human C3 pro-protein is modified by N-linked glycosylation. It also undergoes cleavage into α and β chains of 110 and 75 kDa, respectively, through the action of a furin family protease. Once separated, these chains are then covalently rebound to each other through formation of a single inter-chain disulfide bond. All told, these two chains give rise to thirteen discrete structural domains in the native C3 molecule (Figure 2.1and Figure 2.3) (10).

In addition to this, the native C3 protein contains an unusual isoglutamyl cysteine thioester that forms between the sidechains of Cys-1010 and Glutamine-1013 as part of its eponymous thioester-containing TED domain (numbering based on native C3 pre-pro-protein sequence). This thioester is highly reactive to nucleophilic attack but is largely protected from access to solvent in the structure of native C3 (10). Nucleophilic attack, be it through groups found on nearby cells, carbohydrates, or proteins, is enabled following activation of native C3 to C3b; this allows for covalent attachment of C3b and its well-known function as a both an opsonin and platform for Alternative Pathway C3 convertase assembly. At a structural level, the C3 to C3b conversion is characterized by a massive conformational change that creates what is essentially an entirely different protein in the process (Figure 2.1) (5,11).

Stepwise degradation of C3b is vital to the regulation of complement activity, as the products that result can no longer participate in formation of Alternative Pathway C3 convertases (1,4). Although several combinations of proteins may play a role in this process, the most common

scenario involves factor H-dependent proteolytic cleavage by factor I of the bonds between Arg-1303 and Ser-1304 and Arg-1320 and Ser-1321 producing iC3b, followed by cleavage of the bond between Arg-954 and Glu-955, yielding C3c (4,21). Whereas iC3b retains opsonin activity via its interaction with a number of cell-surface exposed complement receptors (1,5), C3c has been ascribed no known functions to date. Despite this fact, C3c has proven quite useful as a research tool because this fragment is comprised of the entire key ring region of the C3/b molecule, as well as the C345c domain (10). C3c has therefore found extensive use in structural studies for defining the binding sites of Compstatin (15), CRIg (22), and the SCIN family of *S. aureus*-derived complement inhibitors (23,24). Intriguingly, each of these co-crystal structures is characterized by relatively poor model-to-map correlation for the C345c domain. This suggests that the intrinsic dynamics of the C345c domain may negatively influence either the feasibility or quality of crystallographic studies involving C3c.

Our goal was to provide a facile route for mammalian cell expression and purification of a human C3 analog that lacked the flexible C345c domain, and which could be activated into a C3c-like state through digestion by an exogenous protease. We incorporated several features in our expression system in the light of the considerations outlined above (Figure 2.2and Figure 2.3). First, we maintained the signal peptide sequence found in the human C3 pre-pro-protein to direct efficient secretion of the recombinant protein into the culture medium. Second, we eliminated the potential for thioester formation by mutating the thioester cysteine to serine. Third, we incorporated TEV protease recognition sequences to allow for concurrent removal of the C3a domain as well as the entire CUB-TED region. This feature allows for conversion of the C3 analog to a C3c-like state, effectively bypassing the C3b and iC3b forms of the molecule. Fourth, we included a C-terminal octahistidine tag to permit straightforward first-step purification of the target

protein from the conditioned culture medium by Immobilized Metal-ion Affinity Chromatography. Finally, we prepared two different expression vectors to accomplish our goal of removing the C345c domain (Figure 2.2 and Figure 2.3). The first of these simply truncated the protein prior to the C345c domain by placement of a stop codon; the second vector included the C345c domain but replaced several residues N-terminal to this domain with a TEV protease recognition site so that this domain could be removed by site-specific proteolysis. We favored this combined approach in case that lack of the C345c domain might somehow unexpectedly influence expression levels, secretion, or stability of the recombinant C3 protein analogs.

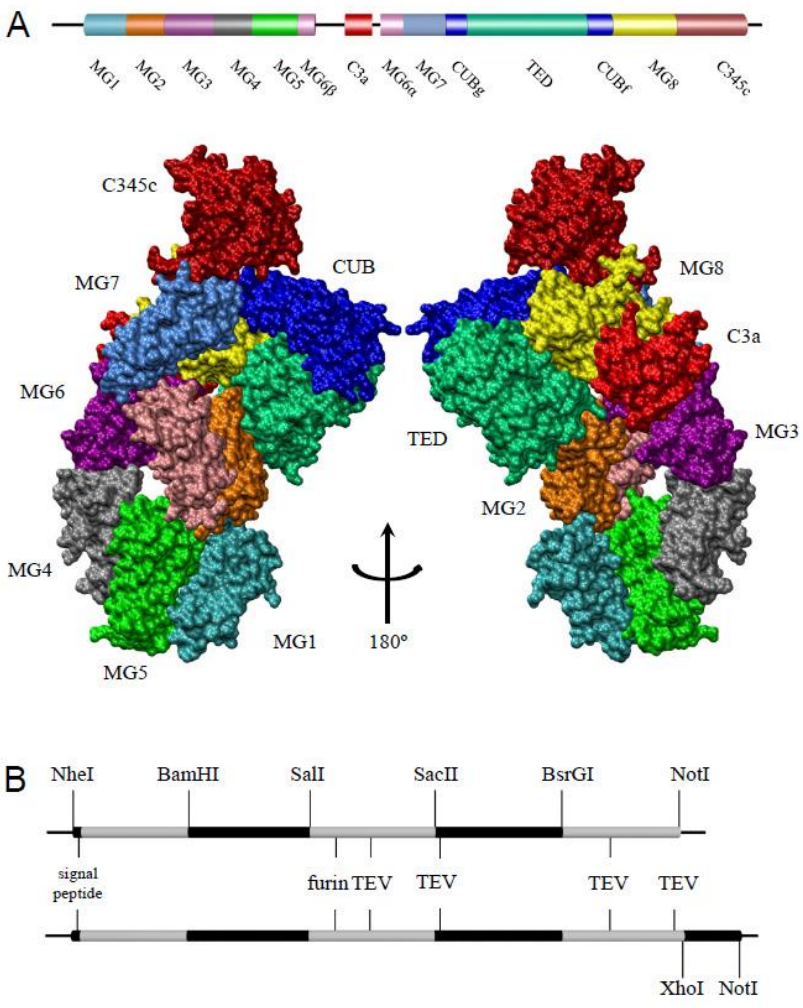

Figure 2.3. Primary and Tertiary Structures of Human C3 and Two Engineered C3 Analogs.

(A) Schematic representation of the domain boundaries in the human C3 pre-pro-protein and its comparison to the C3 crystal structure (PDB entry 2A73). The color scheme is derived from Janssen et al. (10). (B) A schematic representation of two analogs of human C3 assembled from synthetic GeneBlocks. Restriction enzyme sites used to complete the entire coding sequence are shown, as are various protease recognition sites in each construct. Note that the top diagram corresponds to the analog lacking the C345c domain, while the bottom diagram represents the analog with a TEV-cleavable C345c domain.

Generation of Stable Cell Lines Expressing Analogs of Human C3

We used electroporation to co-transfect dihydrofolate reductase deficient (dhfr-/-) CHO cells with a plasmid allowing for constitutive expression DHFR along with plasmids encoding either C3 analog (16). We then selected for stable transfectants by growing the recovering cells in nucleotide-free medium (16) and assayed individual clones for expression of human C3 epitopes by immunoblotting samples of conditioned culture medium. We subjected the highest-expressing cell line for each C3 analog to drug amplification by treatment with increasing concentrations of methotrexate (16). Following two rounds of amplification, we compared the three highest-expressing clones for each C3 analog to one another to determine which cell lines to carry forward for further investigation (Figure 2.4).

We found that the anti-C3a immunoreactive band produced by each clone was consistent with expression and secretion of the desired protein product. Moreover, we found that absence of serum did not adversely affect the stability of the either C3 analog, as judged by a lack of obvious change in the apparent molecular weight of the anti-C3a immunoreactive band when the cells were cultured in serum-free versus serum-containing medium. These results strongly suggested that the none of the modifications engineered into the C3 sequence had any globally deleterious consequences on protein stability. Nevertheless, we also observed that all three cell lines expressing the truncated C3 analog produced significantly higher levels of C3 protein than those expressing the full-length C3 analog. Of these, we found that cell lines 5UC3.12.2 and 5UC3.12.3

produced comparably high levels of the truncated C3 analog protein. Thus, we focused our subsequent efforts on large-scale purification and characterization of this molecule.

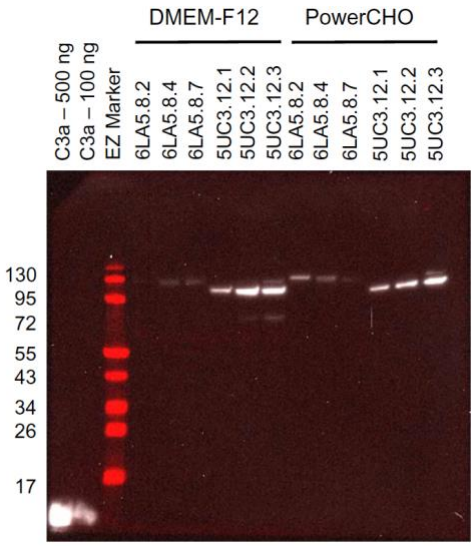

Figure 2.4. Characterization of Stable CHO Cell Lines Expressing Two Different Human C3 Analogs.

Stably transfected CHO cell lines expressing two different human C3 analogs were subjected to methotrexate amplification (16). Individual colonies resulting from amplification were isolated, cultured in either serum containing (DMEM) or serum-free (Power CHO) medium, and their supernatants were assayed for the presence of the human C3 analog by immunoblotting against C3a. Colonies expressing the C3 analog that lacked the C345c domain consistently produced higher levels of protein than those expressing the C3 analog with the C345c domain. Note that these samples were prepared under reducing conditions to emphasize the size difference in the α chains of these two different C3 analogs. Two different quantities of purified C3a were included as a control. Sample "EZ" corresponds to Pre-Stained Recombinant Protein Ladder (Fisher Bioreagents). Abbreviations that begin with "6LA5" and "5UC3" refer to individual colonies that were isolated for analysis.

Purification of a Human C3 Analog Lacking the C345c Domain

We expanded cell line 5UC3.12.3 to large scale culture in T-175 flasks and maintained the cells in DMEM medium supplemented with 1% (v/v) bovine serum and non-essential amino acids. We collected the conditioned culture medium every 3-4 days and began purification of the product once 2 L of medium were available. We used tangential flow filtration to concentrate the medium and exchange the buffer in preparation for immobilized metal-ion affinity chromatography by

FPLC. We applied the sample to a $Ni2^{+}$-charged chelating Sepharose column and washed extensively to remove unbound contaminants. We then eluted the bound proteins with a linear gradient of imidazole, which generated a large, asymmetric peak (2.5A, B). Analysis of the peak fractions by SDS-PAGE performed under non-reducing conditions revealed the presence of the polyhistidine-tagged human C3 analog in the later-eluting region of this peak (2.5).

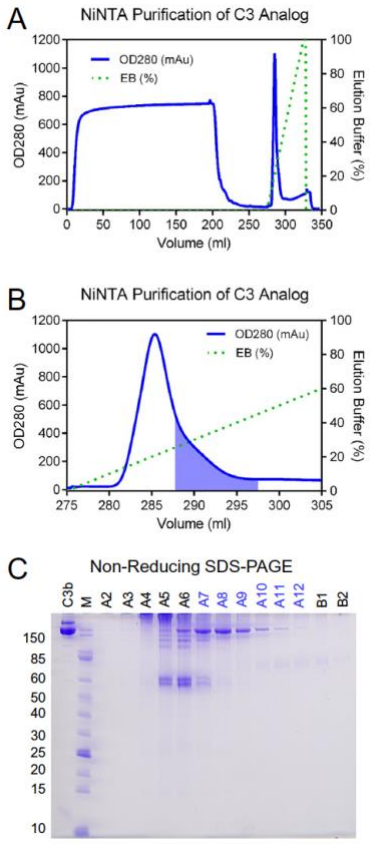

Figure 2.5. Initial Purification of a Human C3 Analog by Immobilized Metal-ion Affinity Chromatography.

A human C3 analog which lacked the C345c domain was purified by immobilized metal-ion affinity chromatography using 2 L of conditioned culture medium as the starting material. (A) Chromatogram showing elution of protein from the column (left y-axis) along with the relative concentration of elution buffer (right y-axis). (B) Magnified view of the chromatogram shown in panel A, with the fractions selected for pooling and further purification represented by the area shaded in purple. (C) Analysis of column fractions by SDS-PAGE performed under non-reducing conditions. Purified human C3b was included as a control. Lanes representing fractions that were collected for further purification are labeled with purple typeface. Sample "M" corresponds to a broad-range molecular weight standard (New England Biolabs). Names such as "A2", "A3", etc. refer to individual column fractions.

Since the main contaminants in the sample were a doublet of bands of approximately 60 kDa, we opted for further purification by Superdex S200 size-exclusion chromatography. The sample eluted from this column as two main peaks, the latter of which was characterized by shoulder that was not well-resolved by this column (Figure 2.6A, B). We analyzed the peak fractions by SDS-PAGE performed under non-reducing conditions and found that the later eluting peak contained highly purified human C3 analog (Figure 2.6C). Fractions corresponding to the center of this peak appeared to be devoid of obvious contaminants and were therefore pooled and concentrated by ultrafiltration to greater than 1 mg/ml protein. The final yield of purified human C3 analog was approximately 1.5 mg protein per liter of conditioned cultured medium.

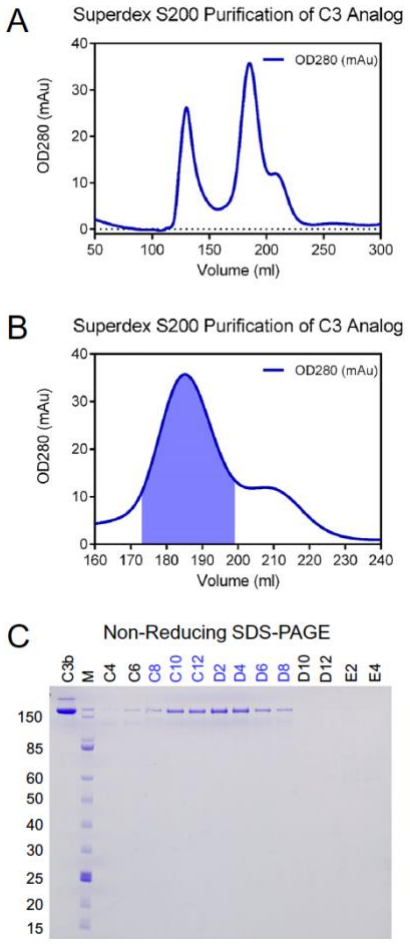

Figure 2.6. Final Purification of a Human C3 Analog by Size Exclusion Chromatography.

Fractions from the previous round of affinity chromatography were pooled and further purified by size exclusion chromatography on a Superdex S200 26/60 column. (A) Chromatogram showing elution of protein from the column. (B) Magnified view of the chromatogram shown in panel A, with the fractions selected for pooling represented by the area shaded in purple. (C) Analysis of column fractions by SDS-PAGE performed under non-reducing conditions. Purified human C3b was included as a control. Lanes representing fractions that were collected for further use are labeled with purple typeface. Sample "M" corresponds to a broad-range molecular weight standard (New England Biolabs). Names such as "C4", "C6", etc. refer to individual column fractions.

Activation the C3 Analog to its C3c-like State by TEV Protease Digestion

Whereas normal physiological activation of C3 to C3b requires the activity of a C3 convertase, the subsequent conversion of C3b to iC3b and then C3c requires separately the activity of factor I (Figure 2.1). By contrast, we designed the truncated human C3 analog to undergo activation to a C3c-like state by incorporating three separate TEV protease sites at positions corresponding to the domain boundaries which define C3a and the CUB-TED region (Figure 2.1, Figure 2.2 and Figure 2.3). We activated the purified human C3 analog by adding a recombinant TEV protease fusion protein (MBP-TEV) at a 1:50 mass ratio and incubating the reaction at 37 °C. Although many recombinant proteins can be cleaved to completion by MBP-TEV within 4-6 h (our unpublished observations), we found that the human C3 analog required digestion times of 48-72 h to approach completion. We purified the C3c analog from the remainder of the digestion reaction contents by size-exclusion chromatography and compared the starting material to the purified product (Figure 2.7). This revealed a large shift in electrophoretic mobility consistent with theoretical molecular weight of the human C3c analog (~115 kDa).

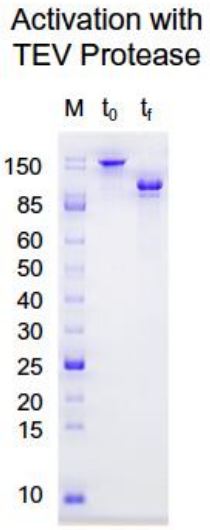

Figure 2.7. Activation of a Human C3 Analog by TEV Protease Digestion.

The purified human C3 analog was activated to its corresponding C3c-like state by digestion with a TEV protease fusion protein. Samples of both the starting material (to) and digestion product following purification by size-exclusion chromatography (tf) were analyzed by SDS-PAGE performed under non-reducing conditions. Sample "M" corresponds to a broad-range molecular weight standard (New England Biolabs).

We used proteomics methods as an independent means to establish the identities of the human C3 analog before and after activation by TEV protease. We prepared tryptic peptides of each sample following in gel digestion, separated the extracted peptides by reversed phase HPLC, and determined their sequences by tandem mass spectrometry. Peptide coverage for synthetic C3 was approximately 66%, based upon the open reading frame encoded by the truncated human C3 analog expression plasmid (Figure 2.8). We observed peptides corresponding to the predicted N-terminus of the protein (i.e. Ser-23) following removal of the signal sequence. We also detected peptides extending both N- and C-terminally from the tetra-arginine site (i.e. Arg-668 to Arg-671, numbering hereafter per the truncated C3 analog pre-pro-protein), but not contiguously through this region. This suggested that the C3 analog protein was correctly processed by a furin-class protease prior to secretion.

By contrast, peptide coverage for the putative human C3c analog decreased to 48% of the plasmid-encoded open reading frame (Figure 2.8). Closer inspection of the peptide coverage revealed loss of all peptides corresponding to the C3a region (i.e. Ser-671 to Arg-748), as well as those corresponding to all but the C-terminal extreme of the CUB-TED region (i.e. Gln-940 to Ala-1356). In this regard, we observed seven different peptides covering residues Met-1353 to Lys-1366, which included the TEV protease recognition site from Glu-1357 to Ser-1363. Together, these results suggested that cleavage in this region was not due to TEV protease activity, but rather a result of adventitious proteolysis by a contaminant present at trace levels in the activation reaction. However, we also found evidence for successful TEV protease digestion at the sites introduced to liberate C3a (i.e. Glu-749 to Ser-755) and at the N-terminal boundary of the CUB domain (i.e. Glu-935 to Gly-941), as judged by the presence of peptides derived from these TEV protease recognition sites in the C3c analog coverage map. When considered together, these proteomic data support our interpretation of the electrophoretic mobility change in the purified product following TEV digestion and confirmed the identify of this product as an analog of human C3c.

Figure 2.8. Peptide Coverage Map of the Truncated C3 Analog Before and Following Activation by TEV Protease.

The truncated C3 analog was activated by digestion with an MBP-TEV fusion protein, purified by size-exclusion chromatography and analyzed by SDS-PAGE. The protein bands were subjected to in-gel trypsinolysis and the extracted peptides were characterized by tandem mass spectrometry according to the methods described by Keightley et al. (17). Identification of the C3 and C3c analogs was performed using Mascot 2.4 (Matrix Science) with semi-trypsin specificity and is presented below. Matched peptides are shown in bold red for the truncated C3 analog (left panel) and its TEV-digestion product (right panel).

Functional Comparison of Human C3 and C3c Analogs with Purified Human C3b/c

Although our SDS-PAGE and proteomics data established the identity of the human C3 and C3c analogs at the chemical level, we sought further structural and functional validation of each protein. Since the large conformational changes that accompany C3 activation to C3b are known to create/expose numerous interaction sites that are otherwise unavailable in native C3 (5,11), the ligand binding profiles of activated forms of C3 vary considerably when compared to the native protein (4,5,25). In the past, we have extensively used SPR to characterize the

interactions of complement C3 and its proteolytic activation derivatives with various binding partners (18,20,26-28). Consistent with one such report (18), we confirmed here that native human C3b bound readily to a surface modified with a wild-type form of the staphylococcal innate immune evasion protein Efb-C, but not to a surface modified by a non-functional Efb-C double mutant (Figure 2.9A, B). We further determined that native human C3b bound well to a surface derivatized with the endogenous complement regulatory protein, factor H (Figure 2.9C). Significantly, we found that the human C3 analog bound only to the wild-type Efb-C surface (Figure 2.9D-F). This result strongly suggested that the human C3 analog has a solution conformation more similar to native C3 than to C3b, for while the Efb-C binding site within the TED domain is accessible in native C3 (18), the factor H binding site only becomes accessible upon activation to C3b (29).

Whereas most endogenous biological ligands exhibit selectivity for activated forms of C3 as described above, a number of exogenous interaction partners such as antibodies and peptides fail to display this type of binding preference. Along these lines, the mouse monoclonal antibody WM-1 has been reported to recognize the C3c fragment of the human C3 protein (19). Although no high-resolution structural information is available regarding the WM-1 binding site on human C3/c, the fact that WM-1 has been used in successful affinity purification of native C3 from serum samples (30) strongly suggests that the WM-1 epitope remains intact and exposed in C3/b/c. We therefore used a WM-1 derivatized SPR surface to further characterize the solution conformations of our recombinant human C3 and C3c analogs. We found that antibody WM-1 bound similarly to native human C3c (Figure 2.9G), as to the C3 (Figure 2.9H) and C3c (Figure 2.9I) analogs. This result provided further evidence regarding the structural integrity of the recombinant C3 and C3c analog proteins.

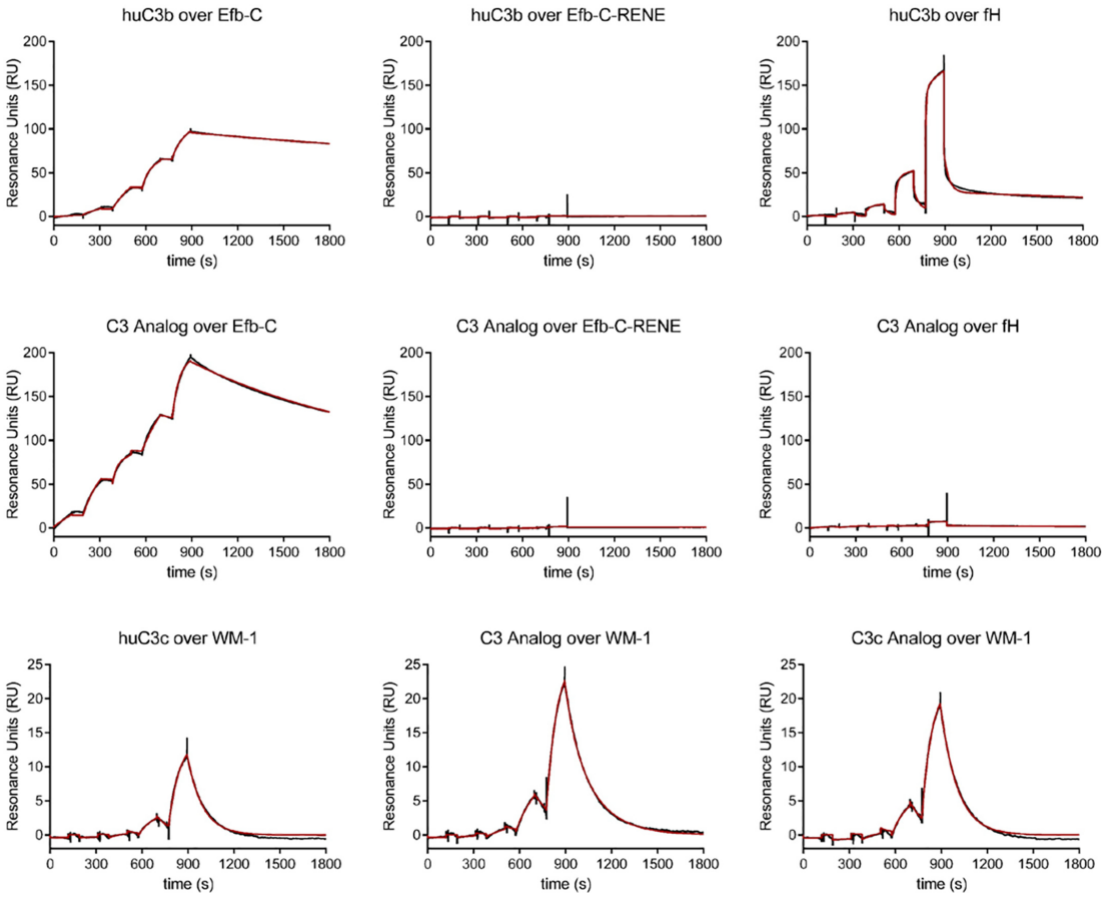

Figure 2.9. Evaluation of the conformational state of human C3 and C3c analogs by their ligand binding profiles.

Surface plasmon resonance was used to compare the ligand binding profiles of the human C3 analog and its C3c-like state with control proteins native human C3b (i.e. huC3b) and C3c (i.e. huC3c). (panels A-C) Single-cycle, reference corrected sensorgrams (black lines) and their corresponding fits (red lines) obtained following injection of a concentration series of human C3b over surfaces consisting of (A) *S. aureus* Efb-C, (B) its non-functional double mutant Efb-C-RENE, and (C) purified human complement factor H. (panels D-F) A similar set of experiments to those presented in panels A-C, except that a concentration series of the human C3 analog was injected over surfaces consisting of (D) Efb-C, (E) Efb-C-RENE, and (F) purified human complement factor H. (panels G-I) Single-cycle, reference corrected sensorgrams (black lines) and their corresponding fits (red lines) obtained following injection of a concentration series of (G) native human C3c, (H) the human C3 analog, and (I) the human C3c analog, over a surface consisting of immobilized monoclonal antibody WM-1.

Like monoclonal antibody WM-1, the peptidomimetic Compstatin (31) binds to a site within the "key ring" region that remains constant C3, C3b, and C3c (15). We previously described

a protein denoted TRX-4W9A, which consists of *E. coli* thioredoxin fused to a Compstatin variant comprised of entirely natural amino acids (20). TRX-4W9A was previously reported to bind site-specifically immobilized C3b with an equilibrium dissociation constant (K_D) of ~770 nM, as judged SPR (20). Consequently, we prepared biosensors of random amine immobilized human C3 analog, its C3c analog counterpart, and purified human C3c to characterize the interaction of these proteins with TRX-4W9A (Figure 2.10 and Table 2.1). We found that the C3 and C3c analogs bound TRX-4W9A with K_D values of 956 ± 26 and 1280 ± 96 nM, respectively. These values were in good agreement not only with one another, but with that we determined for purified human C3c as well (1350 ± 8 nM). When considered together, these data confirmed that our analogs of human C3 and C3c maintain proper solution conformations, as well as important functional properties associated with the C3/b/c protein.

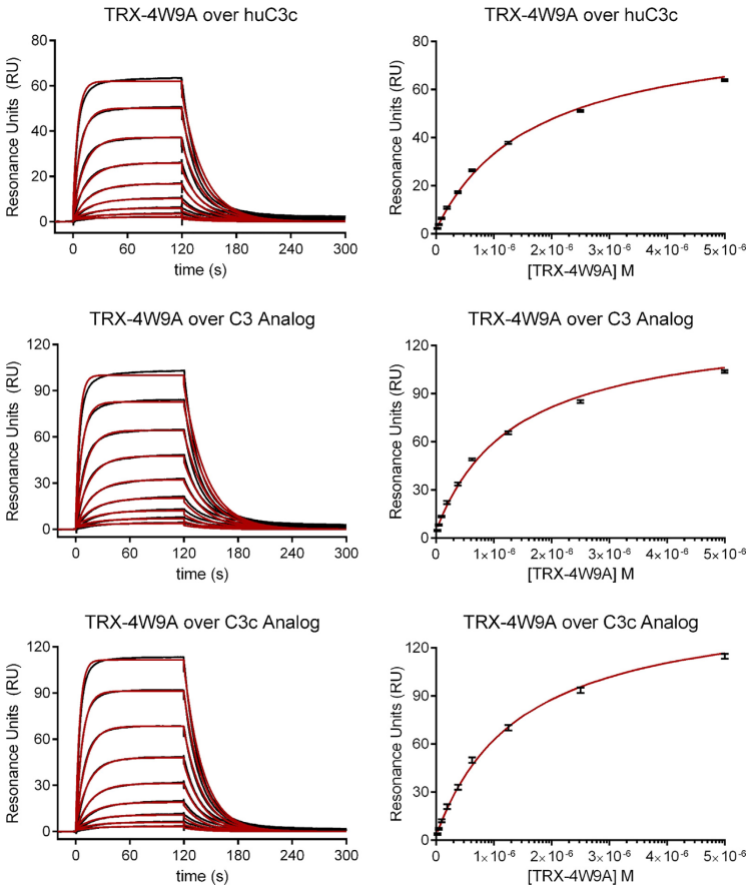

Figure 2.10. Both the human C3 analog and its C3c-like activation product bind to the C3/b/c ligand TRX-4W9A.

The interaction of soluble TRX-4W9A fusion protein to immobilized human C3 analog, its C3c-like counterpart, and purified human C3c (i.e. huC3c) was analyzed by Surface Plasmon Resonance. (A) Representative reference corrected sensorgrams obtained following injection of a dilution series of TRX-4W9A over the human C3 analog (black lines) and their corresponding fits to a 1:1 model (red lines). (B) Approach to equilibrium analysis for the experiment shown in panel A. The response level prior to injection stop for three replicate injections (black error bars) at each concentration was plotted and fit to a Langmuir binding isotherm (red lines). (C) Representative reference corrected sensorgrams obtained following injection of a dilution series of TRX-4W9A over the human C3c analog (black lines) and their corresponding fits to a 1:1 model (red lines). (D) Approach to equilibrium analysis for the experiment shown in panel C. The response level prior to injection stop for three replicate injections (black error bars) at each concentration was plotted and fit to a Langmuir binding isotherm (red lines). (E) Representative reference corrected sensorgrams obtained following injection of a dilution series of TRX-4W9A over purified human C3c (black lines) and their corresponding fits to a 1:1 model (red lines). (F) Approach to equilibrium analysis for the experiment shown in panel E. The response level prior to injection stop for three replicate injections (black error bars) at each concentration was plotted and fit to a Langmuir binding isotherm (red lines).

Table 2.1. Rate and dissociation constants for TRX-4W9A binding obtained by surface plasmon resonance[a].

Ligand	k_{on} ($M^{-1}s^{-1}$)	k_{off} (s^{-1})	K_D (nM)	Rmax (RU)
C3 analog	$4.17 \pm 0.14 \times 10^4$	$3.99 \pm 0.02 \times 10^{-2}$	956 ± 26	113 ± 10
C3c analog	$4.62 \pm 1.53 \times 10^4$	$5.98 \pm 2.33 \times 10^{-2}$	1280 ± 96	138 ± 5
Human C3c	$3.09 \pm 0.12 \times 10^4$	$4.18 \pm 0.14 \times 10^{-2}$	1350 ± 8	73.5 ± 14

[a] All values are reported as the mean ± standard deviation for three independent injection series over the same biosensor surface.

Discussion

A reliable source of recombinant protein permits a diverse array of structural and functional studies, including isotopic enrichment, incorporation of unnatural amino acids, and site-directed mutagenesis among others. Although prokaryotic expression systems are favored for most applications, many proteins that are normally secreted from human cells (e.g. complement components) require the use of eukaryotic expression hosts such as insect or mammalian cells. These systems allow for extensive post-translational modifications, secretion into the extracellular environment, and may provide a route to production of recombinant proteins that are otherwise

unapproachable. We chose CHO cells as our expression host in light of the complex biogenesis of C3 (Figure 2.1) and developed a stable cell line that allowed purification of approximately 1.5 mg of a human C3 analog lacking its C345c domain per liter of conditioned culture medium (Figure 2.4, Figure 2.5, and Figure 2.6). We showed that this recombinant product could be activated by TEV protease to a C3c-like state following release of both the C3a and CUB-TED regions (Figure 2.7). We then carried out a series of comparative SPR experiments to validate the conformational state of this recombinant protein before and after TEV activation. We found that the C3 analog selectively bound to *S. aureus* Efb-C but not complement factor H, consistent with the properties of native human C3 (Figure 2.9). We also determined that both the C3 and C3c-like states of the analog bound with high affinity to monoclonal antibody WM-1 (Figure 2.9) and the TRX- 4W9A fusion protein (Figure 2.10), which recognize distinct sites on the C3/b/c protein. Together, our work has demonstrated the feasibility of producing recombinant C3-like molecules that can be activated by an exogenous protease and retain biological function. In the future, we believe that similar approaches could be useful in answering structural and functional questions on central complement components and their interactions with one another.

Beginning with its initial synthesis as a pre-pro-protein to its terminal physiological degradation to C3c, an individual C3 molecule can undergo six or more different site-specific proteolytic reactions during its lifespan (4). This ordered series of biochemical transformations requires at least five different proteolytic enzymes, as well as their associated cofactors (4). To simplify this process in an *in vitro* setting, we introduced a series of TEV protease recognition sequences into the C3 pre-pro-protein under the premise that a highly specific exogenous protease might be able to mimic the reactions normally catalyzed by a C3 convertase and fI (4). Proteomic analysis of the purified C3 analog revealed that cleavage of the pre-pro-C3 signal peptide and

subsequent processing of the pro-protein into α and β chains occurred as expected (Figure 2.8). However, while we found that the purified C3 analog could be successfully activated into its corresponding C3c-like state following TEV digestion (Figure 2.2 and Figure 2.7), we also determined that bona fide TEV digestion occurred at only two of the three sites introduced into the C3 analog protein. This raised questions about the why two sites were cleaved efficiently during TEV digestion (i.e. Glu-749 to Ser-755 and Glu-935 to Gly-941), while the third appeared to be resistant (i.e. Glu-1357 to Ser-1363).

We examined the sequence and structures of C3/b/c to gain insight into why TEV cleavage failed at the C-terminal boundary of the CUB-TED region. Even though the sequence we introduced matched the most efficient TEV protease recognition site (32), the residue immediately following the substrate P1' site is Cys-1364. The sidechain of Cys-1364 forms a disulfide bond with the sidechain of Cys-1495, presumably stabilizing the eighth macroglobulin-like domain (MG8; Figure 2.2 and Figure 2.3). We suspect that this localized physical restriction interfered with substrate binding or efficient catalysis by the MBP-TEV fusion protein used in these studies. We favor this explanation over one based upon an argument of global steric hindrance, since the structure of C3b shows that the polypeptide chain both N- and C-terminally to the CUB-TED region lies in very close proximity to the "key ring", yet the TEV site introduced at positions Glu-935 to Gly-941 was efficiently processed by TEV (Figure 2.2 and Figure 2.7). It remains possible that TEV cleavage at this last position could still occur if more favorable reaction conditions were employed. In this regard, TEV protease is a thiol protease that requires the presence of reducing agent for maximal activity. Unfortunately, the presence of extensive intra- and inter-chain disulfide bonding in our C3 analog precluded inclusion of reagents like 2-mercaptoethanol or 1,4-dithiothreitol in our TEV activation reaction. The optimization of reaction conditions to include

milder reducing agents (e.g. varying ratios of reduced and oxidized glutathione) could be explored in future work, as could studies on similar C3 analogs designed to be cleaved by highly-specific, non-thiol proteases (e.g. Rhinovirus 3C-protease).

Despite the fact that TEV cleavage at the Glu-1357 to Ser-1363 site was unsuccessful, we determined that adventitious proteolysis in the area of Met-1353 to Tyr-1360 allowed for complete removal of the CUB-TED region from the truncated C3 analog. The resulting protein migrated as an ~115 kDa species in electrophoresis studies (Figure 2.7) and retained ligand-binding properties analogous to human C3c (Figure 2.9, Figure 2.10, and Table 2.1). Together, these data confirmed that the purified activation product had the structural and functional properties of C3c, but without the C-terminal C345c domain. This was the outcome that we intended. While there is room for improvement on what we have done thus far, we believe that our approach could be further refined and adapted for future work. For example, we chose to mutate Cys-1010 to eliminate the possibility for thioester formation in our C3 analogs. This mutation is beneficial in certain cases, as it eliminates the formation of disulfide-linked homodimers upon activation of C3. In other cases, the exposure of a unique cysteine sidechain can be used to modify the protein for downstream applications, in particular protein-protein interaction studies (20,24,26). Thus, we envision future functional studies involving a C3 analog which lacks the C345c domain but retains its thioester group. Separately, complement component C4 shares key structural with features C3, as well as several analogous functional properties relevant to the Classical and Lectin Pathways (1). We expect that C4 analogs could be designed, expressed, and purified so that site specific digestion by an exogenous enzyme like TEV protease would produce various C4 activation fragments and/or targeted deletion mutants thereof. Finally, C3b exists in an equilibrium distribution of open and closed conformers with apparently distinct functional profiles (33), and the same is likely true for

C4b as well (34). Thus, we believe it should be possible to use recombinant systems such as those described here to generate targeted mutations in C3 and/or C4 that selectively trap the activated form of these proteins in one conformational state or another. This should facilitate structure/function analyses of these conformers in isolation, and ultimately provide a more complete understanding of these central complement components.

Acknowledgments

The authors wish to acknowledge helpful discussions with Dr. Samuel Bouyain (School of Biological Sciences, University of Missouri-Kansas City) and Dr. Brandon L. Garcia (East Carolina University School of Medicine) during various stages of this project. This work was funded by grants AI113552, AI111203, and NS104767 from U.S. National Institutes of Health to B.V.G.

References

1. Ricklin, D., Hajishengallis, G., Yang, K., and Lambris, J. D. (2010) Complement: a key system for immune surveillance and homeostasis. *Nature immunology* **11**, 785-797
2. Ricklin, D., and Lambris, J. D. (2013) Complement in immune and inflammatory disorders: pathophysiological mechanisms. *The Journal of Immunology* **190**, 3831-3838
3. Hajishengallis, G., Reis, E. S., Mastellos, D. C., Ricklin, D., and Lambris, J. D. (2017) Novel mechanisms and functions of complement. *Nature immunology* **18**, 1288-1298
4. Sahu, A., and Lambris, J. D. (2001) Structure and biology of complement protein C3, a connecting link between innate and acquired immunity. *Immunological reviews* **180**, 35-48
5. Ricklin, D., Reis, E. S., Mastellos, D. C., Gros, P., and Lambris, J. D. (2016) Complement component C3–The "Swiss Army Knife" of innate immunity and host defense. *Immunological reviews* **274**, 33-58
6. Harboe, M., Ulvund, G., Vien, L., Fung, M., and Mollnes, T. (2004) The quantitative role of alternative pathway amplification in classical pathway induced terminal complement activation. *Clinical & Experimental Immunology* **138**, 439-446
7. Rawal, N., and Pangburn, M. K. (2000) Functional role of the noncatalytic subunit of complement C5 convertase. *The Journal of Immunology* **164**, 1379-1385

8. Rawal, N., and Pangburn, M. K. (2001) Formation of high-affinity C5 convertases of the alternative pathway of complement. *The Journal of Immunology* **166**, 2635-2642
9. Rawal, N., and Pangburn, M. K. (2003) Formation of high affinity C5 convertase of the classical pathway of complement. *Journal of Biological Chemistry* **278**, 38476-38483
10. Janssen, B. J., Huizinga, E. G., Raaijmakers, H. C., Roos, A., Daha, M. R., Nilsson-Ekdahl, K., Nilsson, B., and Gros, P. (2005) Structures of complement component C3 provide insights into the function and evolution of immunity. *Nature* **437**, 505-511
11. Janssen, B. J., Christodoulidou, A., McCarthy, A., Lambris, J. D., and Gros, P. (2006) Structure of C3b reveals conformational changes that underlie complement activity. *Nature* **444**, 213-216
12. Gros, P., Milder, F. J., and Janssen, B. J. (2008) Complement driven by conformational changes. *Nature Reviews Immunology* **8**, 48-58
13. Forneris, F., Ricklin, D., Wu, J., Tzekou, A., Wallace, R. S., Lambris, J. D., and Gros, P. (2010) Structures of C3b in complex with factors B and D give insight into complement convertase formation. *Science* **330**, 1816-1820
14. Rooijakkers, S. H., Wu, J., Ruyken, M., Van Domselaar, R., Planken, K. L., Tzekou, A., Ricklin, D., Lambris, J. D., Janssen, B. J., and Van Strijp, J. A. (2009) Structural and functional implications of the alternative complement pathway C3 convertase stabilized by a staphylococcal inhibitor. *Nature immunology* **10**, 721
15. Janssen, B. J., Halff, E. F., Lambris, J. D., and Gros, P. (2007) Structure of compstatin in complex with complement component C3c reveals a new mechanism of complement inhibition. *Journal of Biological Chemistry* **282**, 29241-29247
16. Leahy, D. J., Dann III, C. E., Longo, P., Perman, B., and Ramyar, K. X. (2000) A mammalian expression vector for expression and purification of secreted proteins for structural studies. *Protein expression and purification* **20**, 500-506
17. Keightley, J. A., Shang, L., and Kinter, M. (2004) Proteomic analysis of oxidative stress-resistant cells: a specific role for aldose reductase overexpression in cytoprotection. *Molecular & Cellular Proteomics* **3**, 167-175
18. Hammel, M., Sfyroera, G., Pyrpassopoulos, S., Ricklin, D., Ramyar, K. X., Pop, M., Jin, Z., Lambris, J. D., and Geisbrecht, B. V. (2007) Characterization of Ehp, a secreted complement inhibitory protein from Staphylococcus aureus. *Journal of Biological Chemistry* **282**, 30051-30061
19. Whitehead, A. S., Sim, R. B., and Bodmer, W. F. (1981) A monoclonal antibody against human complement component C3: the production of C3 by human cells in vitro. *European journal of immunology* **11**, 140-146
20. Garcia, B. L., Skaff, D. A., Chatterjee, A., Hanning, A., Walker, J. K., Wyckoff, G. J., and Geisbrecht, B. V. (2017) Identification of C3b-binding small-molecule complement inhibitors using cheminformatics. *The Journal of Immunology* **198**, 3705-3718
21. Xue, X., Wu, J., Ricklin, D., Forneris, F., Di Crescenzio, P., Schmidt, C. Q., Granneman, J., Sharp, T. H., Lambris, J. D., and Gros, P. (2017) Regulator-dependent mechanisms of C3b processing by factor I allow differentiation of immune responses. *Nature structural & molecular biology* **24**, 643-651
22. Wiesmann, C., Katschke, K. J., Yin, J., Helmy, K. Y., Steffek, M., Fairbrother, W. J., McCallum, S. A., Embuscado, L., DeForge, L., and Hass, P. E. (2006) Structure of C3b in complex with CRIg gives insights into regulation of complement activation. *Nature* **444**, 217-220

23. Garcia, B. L., Ramyar, K. X., Tzekou, A., Ricklin, D., McWhorter, W. J., Lambris, J. D., and Geisbrecht, B. V. (2010) Molecular basis for complement recognition and inhibition determined by crystallographic studies of the staphylococcal complement inhibitor (SCIN) bound to C3c and C3b. *Journal of molecular biology* **402**, 17-29
24. Garcia, B. L., Summers, B. J., Lin, Z., Ramyar, K. X., Ricklin, D., Kamath, D. V., Fu, Z.-Q., Lambris, J. D., and Geisbrecht, B. V. (2012) Diversity in the C3b convertase contact residues and tertiary structures of the staphylococcal complement inhibitor (SCIN) protein family. *Journal of Biological Chemistry* **287**, 628-640
25. Yang, K., Dinasarapu, A. R., Reis, E. S., DeAngelis, R. A., Ricklin, D., Subramaniam, S., and Lambris, J. D. (2013) CMAP: Complement map database. *Bioinformatics* **29**, 1832-1833
26. Ricklin, D., Tzekou, A., Garcia, B. L., Hammel, M., McWhorter, W. J., Sfyroera, G., Wu, Y.-Q., Holers, V. M., Herbert, A. P., and Barlow, P. N. (2009) A molecular insight into complement evasion by the staphylococcal complement inhibitor protein family. *The Journal of Immunology* **183**, 2565-2574
27. Garcia, B. L., Summers, B. J., Ramyar, K. X., Tzekou, A., Lin, Z., Ricklin, D., Lambris, J. D., Laity, J. H., and Geisbrecht, B. V. (2013) A structurally dynamic N-terminal helix is a key functional determinant in staphylococcal complement inhibitor (SCIN) proteins. *Journal of Biological Chemistry* **288**, 2870-2881
28. Summers, B. J., Garcia, B. L., Woehl, J. L., Ramyar, K. X., Yao, X., and Geisbrecht, B. V. (2015) Identification of peptidic inhibitors of the alternative complement pathway based on Staphylococcus aureus SCIN proteins. *Molecular immunology* **67**, 193-205
29. Wu, J., Wu, Y.-Q., Ricklin, D., Janssen, B. J., Lambris, J. D., and Gros, P. (2009) Structure of complement fragment C3b–factor H and implications for host protection by complement regulators. *Nature immunology* **10**, 728-733
30. Dodds, A. W. (1993) [3] Small-scale preparation of complement components C3 and C4. *Methods in enzymology* **223**, 46-61
31. Katragadda, M., Magotti, P., Sfyroera, G., and Lambris, J. D. (2006) Hydrophobic effect and hydrogen bonds account for the improved activity of a complement inhibitor, compstatin. *Journal of medicinal chemistry* **49**, 4616-4622
32. Kapust, R. B., Tözsér, J., Copeland, T. D., and Waugh, D. S. (2002) The P1′ specificity of tobacco etch virus protease. *Biochemical and biophysical research communications* **294**, 949-955
33. Chen, H., Ricklin, D., Hammel, M., Garcia, B. L., McWhorter, W. J., Sfyroera, G., Wu, Y.-Q., Tzekou, A., Li, S., and Geisbrecht, B. V. (2010) Allosteric inhibition of complement function by a staphylococcal immune evasion protein. *Proceedings of the National Academy of Sciences* **107**, 17621-17626
34. Woehl, J. L., Ramyar, K. X., Katz, B. B., Walker, J. K., and Geisbrecht, B. V. (2017) The structural basis for inhibition of the classical and lectin complement pathways by S. aureus extracellular adherence protein. *Protein Science* **26**, 1595-1608

Chapter 3 - Inhibition of the Complement Alternative Pathway by Slow Off-Rate Modified DNA Aptamers that Bind with Picomolar Affinity to Factor B

This chapter has been published as a journal article in the Journal of Immunology.

Xin Xu*, Chi Zhang†, Dalton T. Denton*, Daniel O'Connell‡, Daniel W. Drolet†, & Brian V. Geisbrecht*

*Department of Biochemistry & Molecular Biophysics, Kansas State University, Manhattan, KS 66506 U.S.A.

†SOMALogic, Inc., Boulder, CO 80301 U.S.A.

‡St. Andrew's School, Middletown, DE 19709 U.S.A.

Abstract

The complement system is an evolutionarily conserved component of innate immunity that fulfills diverse roles in defense and homeostasis. Inappropriate or overactivation of the complement system contributes to many inflammatory diseases, however, which has led to a renewed emphasis on development of therapeutic complement inhibitors. Activation of the central complement component, C3, is required for amplification of complement and is achieved through two different multi-subunit proteases called C3 convertases. Of these, the so-called Alternative Pathway (AP) C3 Convertase is responsible for a majority of the C3 activation products *in vivo*, which renders it an attractive target for inhibitor discovery. Here we report the identification and structural characterization of two Slow Off-rate Modified DNA Aptamers (SOMAmers) that inhibit the AP by binding to the pro-protease, factor B (FB). These SOMAmers, known as SL1102 (31 bases) and SL1103 (29 bases), contain uniform substitutions of 5-(N-2-naphthylethylcarboxyamide)-2'-deoxyuridine (2NEdU) for deoxythymidine. SL1102 and SL1103 bind to FB with Kd values of 49 and 88 pM, respectively, and inhibit activation of C3 and lysis of rabbit erythrocytes under conditions specific for the AP. Co-crystal structures of SL1102 (3.4 Å) and SL1103 (3.1 Å) bound to FB revealed that these SOMAmers recognize a site comprised primarily of domain CCP1 within FB. Consistent with these structures and previously published information, these SOMAmers inhibited FB binding to C3b and thereby blocked formation of the AP C3 convertase. Together, these results demonstrate potent inhibition of the AP by SOMAmers and expand the pipeline of FB-binding molecules with favorable pharmacologic properties.

Introduction

Complement is an ancient and evolutionarily conserved branch of the innate immune system that makes numerous contributions to human health and disease (1,2). Although complement is best known for its ability to recognize and facilitate elimination of invading microorganisms, roles for complement in coordinating the overall immune response, in repairing damaged tissue, and in promoting developmental processes are now widely understood (1,2). In recent years, complement has received considerable attention owing to a growing appreciation of its links to several prominent diseases such as cancer and Alzheimer's Disease (Reviewed in (3-7)). This has spurred a renewed interest in the discovery of complement-targeted therapeutics with many such candidates moving through various stages of pre-/clinical development (8).

Complement activity has traditionally been thought to arise from three different pathways (1,2). However, contemporary evidence suggests that these are better viewed as two initiation routes, (i.e. the classical (CP) and lectin pathways (LP)) and an amplification system (i.e. the alternative pathway (AP)) (1,2). The CP and LP use distinct pattern recognition molecules to recognize surface-bound Ig molecules and carbohydrates, respectively, and trigger the activation of pathway-specific proteases (i.e. C1s and MASP-1/2) that cleave complement C4. The activated form of C4, called C4b, is covalently deposited on nearby surfaces where it binds a pro-protease, called C2, in a Mg2+-dependent manner. Once C4b-bound C2 is cleaved by the pathway-specific proteases mentioned above, it forms a metastable enzyme known as the CP/LP C3 convertase (i.e. C4b2a) that cleaves the next component in the pathway, C3. The activated form C3, called C3b, is also deposited on the surface and forms a Mg2+-dependent complex with a separate pro-protease, Factor B (FB). Once C3b-bound FB is cleaved by Factor D (FD), it forms another metastable enzyme known as the AP C3 convertase (i.e. C3bBb). The AP C3 convertase provides

a powerful means for complement self-amplification as it generates additional C3b molecules from native C3. Indeed, while both forms of C3 convertase subsequently cleave C5 (9,10), studies have shown that the AP C3 convertase provides more than 80% of the downstream products that culminate in effector function (11,12). This strongly suggests that any molecules that perturb AP C3 convertase formation and/or function should likewise be powerful inhibitors of complement activity.

Extensive structural and biochemical analyses have provided a wealth of insight into the formation, function, and regulation of the AP C3 convertase (Reviewed in (13)). These have revealed numerous details on the protein-protein interactions, proteolytic reactions, and conformational transitions that are required to generate enzymatically active C3bBb from its molecular precursors. The existence of no fewer than 10 individual steps in this process underscores the size and complexity of the proteins involved, as well as the need to strictly control both the levels and activity of the AP C3 convertase *in vivo* (13). Although each of these steps theoretically provides a potential point for regulatory "fine-tuning" of the overall process, the most well-understood AP regulatory strategies manifest through C3b-binding molecules that influence two key events. In this regard, the primary endogenous inhibitor of the AP is the C3b-binding protein Factor H (FH) (13,14). FH not only dissociates the active convertase (i.e. "decay accelerating activity") but also prevents formation of new convertases by stimulating the proteolytic degradation of C3b to iC3b by Factor I (i.e. "cofactor activity"). Exogenous C3b-binding molecules that inhibit AP C3 convertase formation and function have also been identified and characterized. Among these are the monoclonal antibody, 3E7/H17 (15), and the innate immune evasion proteins Efb (16,17), Ehp (18), and SCINs (19-22) from the Gram-positive pathogen Staphylococcus aureus. Collectively, these molecules employ various ortho- and

allosteric mechanisms to impair convertase formation by blocking FB binding to C3b and/or prevent cleavage of the C3 substrate. These observations provide proof of concept that AP C3 convertase regulatory modes distinct from those typified by FH are achievable by macromolecules.

The structural and functional properties of FB itself also contribute to regulation by influencing the opposing processes of AP C3 convertase formation and decay. Human FB is an ~93 kDa protein. It is comprised of five independently folding domains that give rise to two functionally discrete regions denoted Ba and Bb (23). The Ba region (~30 kDa) accounts for roughly one-third of the molecule and is comprised of the first three domains, each of which adopts the canonical complement control protein fold (hereafter CCP1-CCP3). The Bb region (~60 kDa) accounts for roughly two-thirds of the molecule and is comprised of the latter two domains. The first of these is a von Willebrand Factor domain (vWF), which contributes the Metal Ion Dependent Adhesion Site (MIDAS) that coveys the Mg++-dependence of the AP. The second such domain is a serine protease (SP) motif that provides the catalytic machinery of the enzyme. Association of FB with C3b involves both Ba and Bb regions (24), although their contributions are mechanistically distinct (17,22,24,25). Whereas Ba contributes an initial fast association event that can be measured with Ba fragment alone or FB in the absence of divalent cations, Bb contributes the slower association event that is Mg++-dependent. Significantly, this latter reaction cannot occur on its own and must be coupled to the initial Ba-dependent event; this gives rise to an essential regulatory feature of the AP C3 convertase. Crystallographic studies of FB both free (23) and bound to C3b (25) have revealed the molecular details of the separate Ba and Bb contact sites with C3b. They have also highlighted key conformational transitions that FB undergoes which render it susceptible to cleavage and activation by FD only when in the C3b-bound state (23,25).

Thus, the surprisingly complex series of events that underlie FB binding to C3b and its subsequent activation by FD suggest that this process could be exploited for inhibitor development.

Aptamers are single-chain nucleic acid ligands directed against other biomolecules (26). They can be identified from combinatoric libraries of tremendous initial diversity through a process known as SELEX (Systematic Evolution of Ligands by EXponential enrichment) (27,28). While aptamers recognize their ligands with specificity, the paucity of hydrophobic groups present in conventional nucleotides has been an impediment to aptamers obtaining the high affinities characteristic of tightly binding protein-protein interactions (26). To circumvent this limitation, modified nucleotide bases with functional groups reminiscent of hydrophobic amino acid sidechains have been developed and employed in SELEX strategies (29,30). A large panel of aptamers with significantly improved affinities for their cognate ligands has since been identified using this approach (29). Owing to their unique physico/chemical properties, this new class of aptamers has been given the name SOMAmers, for Slow Off-rate Modified Aptamers. In addition to their improved affinities, SOMAmers can also be synthesized with 2'-O-methyl groups or 3'-3' inverted linkages; these modifications can increase the chemical stability of SOMAmers in complex mixtures like serum by impairing degradation by nucleases. As such, SOMAmers may represent a valuable tool for developing therapeutic inhibitors of complement proteins, many of which are serum-resident.

Here we identify and characterize structurally two sequences related SOMAmers that bind to human FB and potently inhibit functional assays specific for the AP. These SOMAmers, known as SL1102 and SL1103, contain 31 and 29 bases, respectively, and incorporate the unconventional nucleoside 5-(N-2-naphthylethylcarboxyamide)-2'-deoxyuridine (2NEdU) in lieu of deoxythymidine (31). Four of the seven 2NEdU found in these SOMAmers are especially

required for high-affinity binding to FB, as judged by analysis of synthetic analogs. Crystal structures of SL1102 and SL1103 bound to FB demonstrate that the SOMAmers recognize a motif lying at the juncture of the CCP1, CCP3, and vWF domains of the pro-protease. This prevents FB binding to C3b and formation of the AP C3 convertase. These results not only provide a unique description of complement inhibition by an aptamer-like molecule, but they also increase our understanding of the structure/function relationships of synthetic nucleic acid ligands.

Materials and methods

Materials

Unless otherwise stated, proteins, sera, zymosan-A and erythrocyte preparations were obtained from Complement Technologies (Tyler, TX). Human FB that had been purified from human serum was obtained from both Complement Technologies and Quidel.

Protein Labelling

Native human FB (Quidel) was labeled via primary amines with either Alexa Fluor® 488 (AF, Molecular Probes™) or biotin (Pierce, EZ-Link NHS-PEG4-biotin) according to manufacturer's directions. Briefly, FB (400 pM in 75 µL) was incubated for 16 hours at 4 °C with a 22-fold (AF) or 10-fold (NHS-PEG4-biotin) molar excess of reagent. Unreacted label was removed by ultrafiltration using Ultracel 3 kDa filters (Millipore) and buffer solution SB18T0.01 (40 mM HEPES (pH 7.5), 102 mM NaCl, 5 mM $MgCl_2$, 5 mM KCl, and 0.01% (v/v) TWEEN 20).

Modified Aptamer Discovery and Sequencing

Aptamer selection, with minor modifications, was performed using the SELEX-process as described elsewhere (29) using a DNA library 5'-B-B-

TTTTTTTTCCTTTCCTTGTTCTGTTGTTG-$(N)_{40}$-CAAGGTAGGTCGGCGTCACT that included 40 consecutive random nucleotide positions [$(N)_{40}$] and two 5'-biotins (B). The random region contained the modified nucleotide 5-(N-2-naphthylethylcarboxyamide)-2'-deoxyuridine (2NE) in place of dT. Flanking regions served as templates for amplification by polymerase chain reaction (PCR). Ten rounds of SELEX were performed using AF labeled-FB for rounds 1-4 and biotin labeled-FB for rounds 5-10. Binding steps were performed at 37 ^{o}C in buffer solution SB18T0.01, as described above. Incubation time was 60 minutes for round 1 and 15 minutes for all subsequent rounds. Approximate FB concentrations were 500 nM for round 1, 100 nM for rounds 2-5, and 33, 3.3, 1.0, 0.33 and 0.10 nM for rounds 6-10, respectively.

To separate protein-bound from unbound nucleic acids, AF-labeled protein was captured on protein G magnetic beads (Dynabeads®) via a rabbit IgG anti-AF antibody (Invitrogen, Molecular Probes) while biotinylated protein was captured on MYONE-SA paramagnetic beads (Invitrogen) SA. AF capture beads were prepared by incubating 70 µg of rabbit IgG anti-AF antibody with beads (10 mg) in 1 mL of SB18T0.05 buffer (as described for SB18T0.01 except with 0.05% [v/v] Tween 20). After a 30-minute incubation at 37 ^{o}C, beads were washed three times with 14 mL of SB18T0.05 and stored at 4 ^{o}C until use. Round 1 was performed using FB pre-immobilized on beads while all other rounds captured FB after a binding step in solution. A kinetic challenge consisting of 5 mM dextran sulfate and counter SELEX against capture beads and a protein competitor mixture (10 µM casein, 0.1% (w/v) HSA, and 10 µM prothrombin) was employed in rounds 2-10.

The round 10 enriched pool was amplified by PCR and the products purified by SDS-polyacrylamide gel electrophoresis (PAGE). Following buffer exchange, ion torrent sequencing was performed by SeqWright Genomic Services (GE Healthcare; Houston TX).

Aptamer Synthesis

Aptamers were synthesized by standard DNA phosphoramidite methods (32). The phosphoramidites for modified 2NEdU bases were synthesized as described elsewhere (30,33). For crystallography studies, aptamers were purified using ion-pairing reverse phase liquid chromatography, followed by desalting using Hi-Trap Sephadex G-25 columns (GE Life Sciences). Desalted aptamers were evaporated to dryness using a Genevac HT-12 system. The purified products were characterized by ultra-performance liquid chromatography (Waters ACQUITY System) and their identities confirmed by MALDI-TOF mass spectrometry.

Binding Affinity Determinations

Equilibrium binding constants (K_d) in solution were measured as described previously (29). Briefly, radiolabeled aptamer [^{32}P] was incubated at 37 ^{o}C with various FB concentrations and complexes were captured after 30 minutes using Zorbax PSM-300 resin (Agilent Technologies, Santa Clara, CA). Bound aptamer was quantified with a phosphorimager. The percent of maximum captured aptamer was plotted versus the logarithm of protein concentration and these data fitted to a four-parameter sigmoid dose-response model to determine the apparent K_d.

Nuclease Stability Assays

Aptamers (250 nM) were incubated with 0.2 units/mL of recombinant human DNase I (Cell Sciences) in a buffer consisting of 10 mM Tris HCl (pH 7.6), 2.5 mM $MgCl_2$, 0.5 mM $CaCl_2$ or with 140 units/mL of porcine DNase II (Worthington Biochemical) in a buffer consisting of 0.1 M sodium acetate (pH 4.6), 2.0 mM $MgCl_2$, 15 mM NaCl. Incubations were conducted at 37 °C in a total reaction volume of 100 µL. At the indicated times, a 15 µL aliquot was collected and the reaction stopped by adding an equal volume of 2x gel loading buffer [(93.85% (v/v) formamide, 0.2% (w/v) SDS, 20 mM Na_2EDTA, 0.05% (w/v) xylene cyanol and 0.1% (w/v) Orange G)] and

heating at 95 ºC for 2 minutes. Serum stability studies were performed in 90% (v/v) pooled human sera with 10% (v/v) phosphate buffered saline using a final aptamer concentration of 500 nM. Samples were processed as described by Gupta et al. (34). Briefly, aliquots were extracted with phenol-chloroform and concentrated using a YM-10 molecular weight cutoff filter (EMD Millipore). Digestion products for all studies were separated from full-length aptamer by PAGE (15% (w/v) polyacrylamide gel containing 8 M urea) using a Tris-borate buffer system. Electrophoresis was carried out for 20 minutes at 200 V. Aptamers were stained with 2 µM SYBR® Gold nucleic acid stain (Molecular Probes), imaged using a FlourChem®Q imager (Alpha Innotech) and quantified using AlphaView Q software with background subtraction. Data are presented as the percentage of full-length input aptamer. All aptamers used in these studies had a 5'-hydroxyl group and 3'-3'-linked dT cap.

Hemolysis Assays

AP hemolysis assays were conducted in a 100 µL reaction mixture consisting of 10 µL NHS, 55 µL of 0.1% (w/v) gelatin veronal buffer (GVB; Complement Technologies), 10 µL of 0.1M MgEGTA (Complement Technologies), 5 µL aptamer in ddH_2O to achieve the indicated final concentration, and 20 µL of rabbit erythrocytes ($5x10^8$/mL exchanged into GVB). After 30 minutes at 37 ºC, samples were centrifuged for 10 minutes at 200 x*g*, the supernatant diluted 4-fold, and absorbance determined at 412 nm. Percent lysis was determined by the equation: $100 - [100*(OD_{412,\ sample} - OD_{412,\ buffer} / (OD_{412,\ no\ inhibitor} - OD_{412,\ buffer})]$ and the IC_{50} was determined by a four-parameter fit. A similar procedure was employed when using 12% (v/v) FB-depleted serum, except that the erythrocytes were at $3.3x10^8$/mL and the GVB concentration was adjusted to allow for the additional serum and for a 5% (v/v) addition of 20 nM FB. Classical pathway assays were performed in a 75 µL reaction mixture by consisting of 1.5 µL of C5-depleted NHS, 46 µL of

GVB containing of 10 mM $MgCl_2$ and 10 mM $CaCl_2$ (GVB++). After addition of human FB (4 µL, 2 nM final concentration) and aptamer (7.5 µL) to achieve the desired concentration, 16 µL of antibody-sensitized sheep erythrocytes ($3.3x10^8$/mL exchanged into GVB++) was added. After 30 minutes at 37 °C, the samples were processed as described above. ANOVA with a Dunnett's post-test correction was performed by comparing all groups to the no inhibitor control.

C3a Detection Assay

C3a detection assays were performed in a 50 µL reaction mixture containing 5 µL NHS and 40 µL of GVB containing 10 mM MgEGTA. After addition of aptamer in water (2.5 µL) to achieve the desired concentration, reactions were initiated by adding 2.5 µL of preactivated zymosan-A (10 mg/mL). Following 30 minutes at 37 °C, zymosan was pelleted by centrifugation (10,000 x*g* for 4 minutes) and the desArg-C3a concentrations in the supernatant were determined by ELISA according to the manufacturer's directions (BD Biosciences, OptEIA™ human C3a).

Crystallization, X-Ray Diffraction Data Collection, and Structure Determination

Samples of SL1102 or SL1103 bound to FB were prepared by mixing a 1.05-fold molar excess of either aptamer with native FB that had been purified from human serum (Complement Technologies). Each sample was exchanged into 10 mM HEPES (pH 7.5), 50 mM NaCl using 3 kDa molecular weight cut-off ultrafiltration units (Merck Millipore) and concentrated to 5 mg/ml complex as judged by OD_{280} using the theoretical extinction coefficient for an equimolar complex. Plate-like crystals of the SL1102/FB complex were obtained within 3 to 7 days at 20 °C by vapor diffusion of hanging drops prepared by mixing 1 µL of complex with 1 µL of a precipitant solution consisting of 0.1 M HEPES (pH 7.5), 0.2 M ammonium acetate, 25% (w/v) polyethylene glycol 3,350 and equilibrating over 500 µL of precipitant solution. A similar procedure was used to obtain plate-like crystals of the SL1103/FB complex, with the exception that 0.1 M Bis-Tris (pH 6.5) was

used in the precipitant solution. Diffraction-quality samples were cryopreserved by quickly soaking crystals in their respective precipitant solutions supplemented with an additional 10% (w/v) polyethylene glycol 3,350 prior to flash-cooling in liquid N_2.

X-ray diffraction data were collected from radiation of 0.97243 Å wavelength using beamline 22-ID of the Advanced Photon Source at Argonne National Laboratory. Reflections were indexed in the space group $P2_1$, integrated, and scaled using the HKL-2000 package (35). Owing to the higher resolution of its diffraction data set, the structure of SL1103/FB was solved first. Briefly, PHASER (36) as implemented within the PHENIX software suite (37,38) was used to perform molecular replacement using the refined coordinates of human FB as a search model (PDB entry 2OK5 (23)). Upon placement of two copies of FB, initial electron density maps were calculated using bulk solvent scaling and B-factor refinement in PHENIX.REFINE (37,38). A preliminary model for SL1103 was constructed by initially identifying positions of aptamer-derived phosphate groups in the F_o-F_c map. The SL1103 model was completed by manual rebuilding following the identification of features in the $2F_o$-F_c and F_o-F_c maps consistent with the sequential 2NE bases at positions 26 and 27 of the aptamer. Positional and B-factor refinement in PHENIX.REFINE (37,38) were used to iteratively improve the model for both copies of the SL1103/FB complex by employing non-crystallographic symmetry restraints. The structure of SL1102/FB was solved by molecular replacement using the final model of SL1103 and FB (PDB entry 2OK5 (23)) as sequential search models in PHASER (36). Iterative model building and refinement was carried out using equivalent methods to those described for the SL1103/FB complex.

The final model for SL1103/FB consists of two complete copies of each aptamer including the 3’-inverse deoxythymidine cap (chains B and D), along with two copies of FB (chains A and

C). Residues XX, YY, and ZZ were not modeled in either copy of FB due to poor map quality. The final model for SL1102/FB differs in the presence of two additional bases found at the 5'- and 3'-ends, respectively, in each chain (chains B and D). However, neither of these chains includes a 3'-inverse deoxythymidine cap. The composition of the FB chains modeled in the SL1102/FB structure is identical to those in the SL1103/FB structure. A quantitative description of the cell constants, diffraction data quality, and properties of the final model for each complex can be found in Table 3.2.

Competition Binding Assays

Competition between SL1103 and FB (Complement Technologies) for binding to C3b was investigated using a surface-plasmon resonance (SPR) based approach on a BiaCore T-200 instrument. A NeutrAvidin (ThermoFisher Scientific)-derivatized CMD200M chip (Xantec Bioanalytics, GmbH; Dusseldorf, Germany) was prepared by standard amine coupling and used to capture human C3b that had been site-specifically biotinylated at Cys-1010 via EZ-link Maleimide-PEG_2-biotin (ThermoFisher Scientific) according to previously published protocols (19,20,39). A reference surface was prepared by injecting one flow cell with biotin alone (10 µM) to yield a final capture level of 87 RU (fc1). Replicate experimental surfaces containing 2583 (fc2), 2485 (fc3), and 2685 (fc4) RU of C3b-biotin were prepared thereafter by injecting dilute solutions of C3b-biotin (8 ng/µL) across the remaining flow cells.

All binding studies were carried out at 25 ˚C using a running buffer of HBST-Mg^{++} (20 mM HEPES (pH 7.4), 150 mM NaCl, 0.005% (v/v) Tween-20, and 10 mM $MgCl_2$) and a flow rate of 30 µL/min. Binding of FB to C3b was assessed by injecting a buffer blank followed by a two-fold dilution series of FB across eight different concentrations spanning 15.625 nM to 2 µM. Each injection cycle consisted of a 1-minute association phase, a 2 minute dissociation phase, and final

0.5 min phase where a solution of 2 M NaCl was used to regenerate the surface. Each reference-subtracted sensorgram series was analyzed using BiaCore T-200 Evaluation software and fit to a two-state reaction model that incorporates a single second-order association rate constant. Competition binding studies were conducted by including SL1103 at the desired concentration ratio relative to 2 µM FB and injecting the resulting analyte mixture as outlined above. Analysis of these sensorgram series was carried out as described above. Data were normalized by assigning a value of 100% to the signal resulting from injection of the competitor-free 2 µM FB sample immediately prior to the end of the association phase. Each experimental flow cell was normalized independently to account for the slight differences in C3b density. All plots were generated using GraphPad Prism v6.07.

Convertase Formation Assay

FB (Quidel) alone or with SL1102 was prepared at twice the indicated final concentrations in GVB containing 10 mM MgEGTA and the mixtures were incubated at room temperature for 15 minutes. An equal volume of the same buffer containing twice the indicated concentration of C3b, and FD (Quidel) was added and the mixture was incubated at 37 ^{o}C for 30 minutes. Proteins were then labeled with Alexa Fluor®647 according to the manufacturer's directions (Molecular Probes) and reactions stopped by the addition of 2x Tris-Glycine loading buffer. Reactions without SL1102, or without one or more of the protein components, were run in parallel. Proteins were resolved by SDS-PAGE (4-20% (w/v) Tris-Glycine, Novex) at 150 V for 1.5h. The gel was imaged at 632 nm using an AlphaImager®.

Miscellaneous

Calculation of buried surface areas and identification of potential polar interactions such as hydrogen bonds were performed using EBI-PISA (40). LigPlot was also used to illustrate

features of surface complementary and packing interactions (41). Structural superpositions and renderings of molecular structures and surfaces were generated by PyMol (http://www.pymol.org/).

Results

Identification and Characterization of Factor B Binding SOMAmers

We screened for chemically modified DNA aptamers that bind human factor B (FB) via 10 rounds of the SELEX-process using FB isolated from human serum and a DNA library containing a 40-nucleotide random region wherein 5-(N-2-naphthylethylcarboxyamide)-2'-deoxyuridine (2NEdU) was uniformly substituted for deoxythymidine (Figure 3.1A). Upon sequencing the enriched pool, we identified a family of sequence-related molecules that contained a 23-nucleotide consensus sequence that accounted for approximately 6% of the enriched library (Table 3.1). A single nucleotide insertion between positions 13 and 14 of the consensus was found in a minority of the sequences we obtained, including the most abundant sequence of the enriched SOMAmer pool. We truncated this most abundant sequence to a 31mer (SL1100) and to a 29mer (SL1101), both of which were synthesized with a 3'-3'-linked dT "cap" to enhance resistance to exonucleases (n.b. that SOMAmer lengths do not include this cap residue). We found that both truncated aptamers maintained incredibly high-affinity binding to FB in this configuration with a mean (95% confidence interval, CI) equilibrium dissociation constant (K_d) of 12 (6.2-17) pM for SL1100 and 12 (6.5-17) pM for SL1101 (Figure 3.1B).

We used single dT substitution scans in the context of SL1100 to determine which of the seven 2NEdU nucleotides were most critical to function of this SOMAmer family. Although FB-binding studies showed that all seven modified nucleotides are important to some degree, we

observed a clear distinction between substitutions for the three 2NEdU residues closest to the 5'-terminus when compared to the remaining four (Figure 3.1C). Whereas single dT substitutions within the first group reduced the affinities by approximately 12- to 14-fold, corresponding substitutions within the second group reduced the affinities from 770- to greater than 10,000-fold (Figure 3.1C). This strongly suggested that the bases near the 3'-region of the SOMAmers might contribute directly to the FB binding site.

We also carried out a separate substitution scan wherein a 3-carbon alkyl linker (C3-spacer) was incorporated for each base aside from those occupied by 2NEdU (Figure 3.1C). This substitution preserves the natural spacing of the aptamer chain, does not impact folding, and therefore allows the functional contributions for each nucleoside base to be determined (34). We found that all C3-spacer substitutions within the consensus sequence of the 29-mer, SL1101, reduced affinity for FB, although the magnitude of the loss was less than 10-fold for those bases at and proximal to the 5' and 3' termini. Interestingly, we also determined that the guanosine at position 18 could be replaced with a C3-spacer without loss of binding affinity, as was suggested by the family of sequences obtained from the initial enriched library (Table 3.1). In fact, deletion of this nucleoside entirely had no impact on FB-binding affinity of the SOMAmer (*Data Not Shown*).

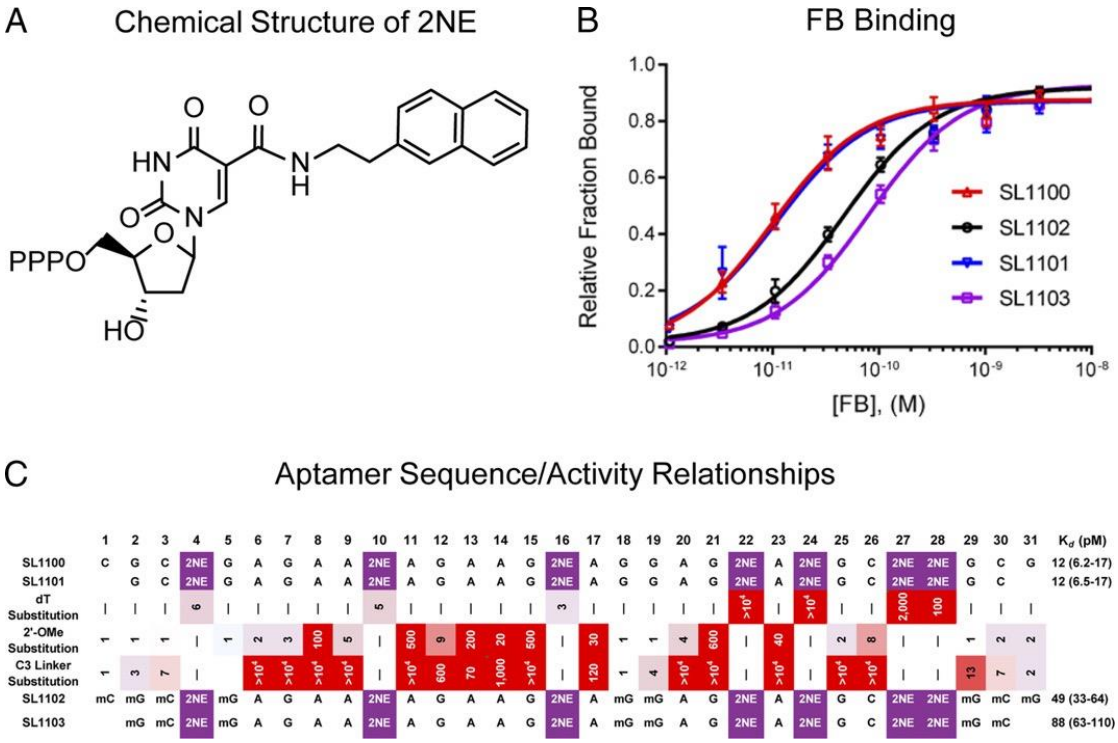

Figure 3.1. Sequence-Function Relationships of FB-Binding SOMAmers.

(A) Structure of 5-(N-2-naphthylethylcarboxyamide)-2'-deoxyuridine triphosphate (2NE) used to uniformly substitute for deoxythymidine in the SELEX library. The triphosphate is indicated as PPP. (B) Binding curves of aptamers as shown in panel C. Symbols represent mean (SEM) percent maximum binding for 7, 4, 11 and 8 independent determinations for SL1100, SL1101, SL1102 and SL1103, respectively. Data were fitted to a 4 four-parameter sigmoid dose-response model to determine the apparent equilibrium dissociation constants (K_d) for each interaction. (C) Sequence-function relationships and post-SELEX modification of the truncated aptamer, SL1100. Results of dT, C3 (3-carbon alkyl linker in place of the nucleoside), and 2'-OMe (2'-methoxy ribose) substitution scans are shown as the affinity ratio (K_d variant/K_d parent) for each single substitution. The effect on binding is also indicated by color, with affinity loss is red and affinity enhancement is blue, where color intensity is related to the magnitude of the change. A vertical dash (|) indicates that no affinity data were acquired. Sequences of SL1100, SL1101 and the 2'-OMe substituted aptamers SL1102 and SL1103 are shown where the position of a 2'-OMe ribose sugar is indicated with the letter "m" preceding the nucleobase designation. Equilibrium dissociation constants are given as the mean along with the confidence intervals (95% CI). (Experiments done by Somalogic, Inc.)

Table 3.1. Distribution of Factor B-binding SOMAmers.

Identical Copies	Equivalent Copies	Total	Sequence† 5'→3'
189	429	618	GACACGCtGAGAAtAGAAGtAGGAGtAtGCttGCGACCAC
113	71	184	tGAGAAtAGAAGtA-GAGtAtGCttAAGtAGGGCGtCAGtC
98	87	185	tCtGACCGAtGAGAAtAGAAGtA-GAGtAtGCttCGGtGGC
79	38	117	AAtCCCtGAGAAtAGAAGtAtGAGtAtGCttGGGtGGGA
25	104	129	AAGttGACACGGAGAAtAGAAGtA-GAGtAtGCttAGAtGt
17	23	40	AGAGAAtAGAAGtA-GAGtAtGCttGAGGttAtGGtCACGt
15	22	37	GCtGGCAtGAGAAtAGAAGtAGGAGtAtGCttGAACAGAC
10	27	37	tGCAGAGAAtAGAAGtA-GAGtAtGCttGCACCtAACAAGG
9	13	22	CGGAGAAtAGAAGtA-GAGtAtGCttAGCAGtGAAGGCtCCAGA
6	3	9	AACttAAGCAtGAGAAtAGAAGtA-GAGtAtGCttGCGtAC
5	6	11	GGtGCtGAAAAAtGCCAGAAtAGAAGtA-GAGtAtGCttGG
5	4	9	AGAGAAtAGAAGtA-GAGtAtGCttAAAGGAtGtAtCGGCt
3	3	6	CCACAAtAGCCGtGAGAAtAGAAGtACGAGtAtGCttGGCtCC
3	0	3	CtttGGCGCGGAGAAtAGAAGtA-GAGtAtGCttAGCtCCA
3	0	3	CtACtGtGCAGAGAAtAGAAGtA-GAGtAtGCttGCACCtAACAAGG
2	2	4	tGAGAAtAGAAGtA-GAGtAtGCttAAGAAAtGGGGAGAtG
2	1	3	ttGGCtGAGAAtAGAAGtAGGAGtAtGCttGCCtGGGCAC
2	1	3	*GAGAAtAGAAGtA-GAGtAtGCttAGGtAtGAAGGCtCCAGG
2	0	2	*GAGAAtAGAAGtA-GAGtAtGCttAGGttGGGGCtACCAtCA
2	0	2	AGAGAAtAGAAGtA-GAGtAtGCttCAAGGCAGAGCAGGGCA
2	0	2	GtGAAGCAGtGAGAAtAGAAGtA-GAGtAtGCttAAGCGGt

†The sequence in grey represents the consensus obtained following SELEX.
*This G occurred as part of the fixed region of the 5'-primer.
(Experiments done by Somalogic, Inc.)

DNA aptamers with modified nucleosides have been shown to possess increased resistance to nucleases in serum when compared to native DNA of the same sequence (34,42). Consistent with these observations, we found that *in vitro* stability of SL1100 against 90% normal human serum (NHS), 0.2 units/mL human recombinant DNase I, or 14 units/mL porcine DNase II was increased by 14-, 17- and 6-fold, respectively, when compared to a version of SL1100 in which all

seven 2NEdU residues were replaced with natural dT residues (SL1100dT; Figure 3.2). To further enhance nuclease resistance, we substituted 2'-*O*-methyl ribose (2'-OMe) for 2'-deoxyribose sugars where permitted. Positions that could tolerate a 2'-OMe group were determined by substitution scanning of SL1100 and resulted in the creation of aptamers containing nine and seven 2'-OMe residues for the 31-mer (SL1102) and 29-mer (SL1103), respectively (Figure 3.1C). This process increased the nuclease resistance of SL1102 by 3.4-fold against DNase I and 4-fold against DNase II. We also found that both SL1102 and SL1103 were completely stable for 96 hours at 37 ^{o}C in 90% (v/v) pooled NHS (Figure 3.2). However, we also noted that these 2'-OMe substitutions resulted in slight reductions in binding affinity (Figure 3.1B). The mean (95% CI) K_d for SL1102 was 49 (33-64) pM, which represented a 4-fold reduction from its parent molecule SL1100. Similarly, the mean (95% CI) K_d for SL1103 was 88 (63-110) pM, which equated to a 7.3-fold reduction from its parent molecule SL1101.

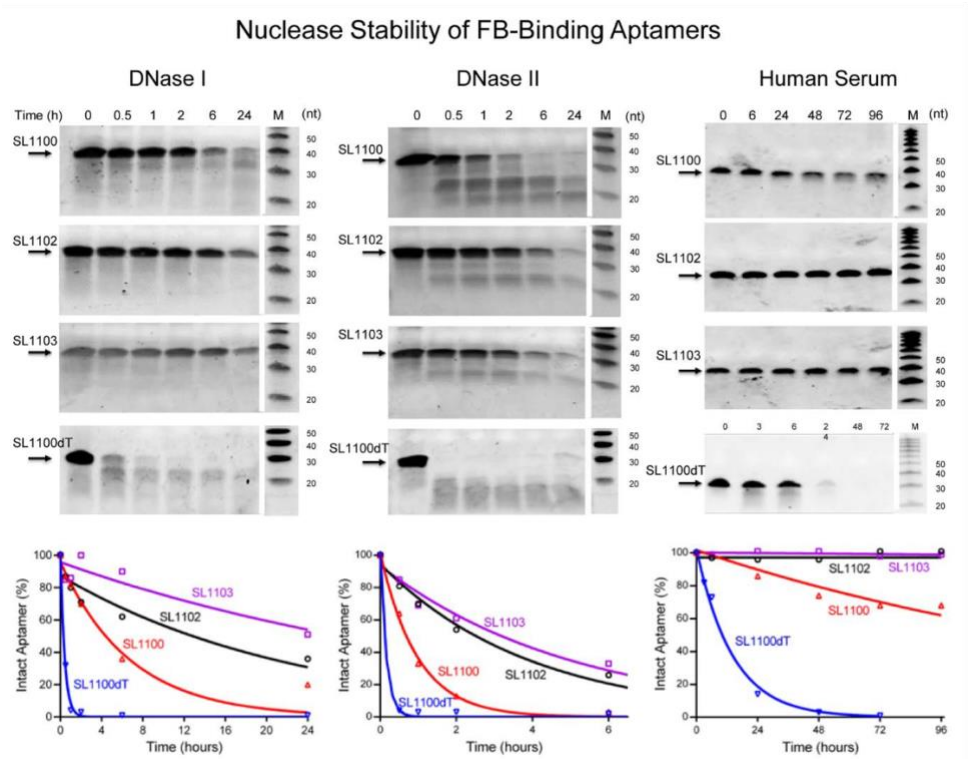

Figure 3.2. Nuclease and Serum Stability of FB-Binding SOMAmers.

(A) Digestion products resulting from treatment with either 0.2 U/mL human recombinant DNase I (left), 14 U/mL porcine DNase II (middle), or 90% (v/v) human serum (right) after the indicated number of hours (h) at 37 ^{o}C were separated from the full-length SOMAmer (indicated by arrows) by electrophoresis. Bands were visualized using SYBR Gold and the percentage of full-length aptamer that remained was determined by densitometry. DNA markers (M) were run on a different part of the gel; their size given as number of nucleotides (nt). (B) Plot of percent full-length SOMAmer remaining versus time corresponding to the data presented in panel A. Data were fit to a one-phase exponential decay model to estimate half-lives. Half-lives of SL1100dT, SL1100, SL1102 and SL1103 in DNase I are 0.28, 4.7, 16, and 29 h, respectively, while the corresponding estimates for DNase II are 0.11, 0.67, 2.7 and 3.5 h. The estimated half-life of SL100dT and SL1100 in human serum is 9.8 h and 135 h, respectively, while SL1102 and SL1103 were completely stable during the 96-h incubation period. (Experiments done by Somalogic, Inc.)

Factor B Binding SOMAmers Inhibit the Alternative Pathway of Complement

Although our initial studies demonstrated that this novel family of SOMAmers bound FB with high affinity, they did not determine whether these molecules had any effect on FB activity. We therefore examined the outcome of including these SOMAmers in various assays for complement function. We initially tested the ability of each SOMAmer to inhibit lysis of rabbit erythrocytes using 10% (v/v) NHS as a source of complement components and conditions specific for the AP (*please see Materials & Methods*). Significantly, we found that SL1100, SL1102, and SL1103 each inhibited lysis in a dose-dependent manner with IC_{50} values of 220, 200, and 280 nM, respectively (Figure 3.3A). FB is present at concentrations of ~200 µg/ml in human plasma, which corresponds to ~2 µM protein. As this value is greater than five orders of magnitude above the K_d of these SOMAmers for FB (Figure 3.1B), we repeated the rabbit erythrocyte lysis assay using 12% (v/v) FB-depleted NHS that had been fortified with 20 nM FB. Under these conditions, we found that SL1102 inhibited lysis with an IC50 value of 9.8 nM (Figure 3.3B). This suggested that the apparently weaker potency of the SOMAmers in our initial experiment was due to the

large quantities of FB present in NHS, rather than a change in their ability to bind to FB in complex mixtures.

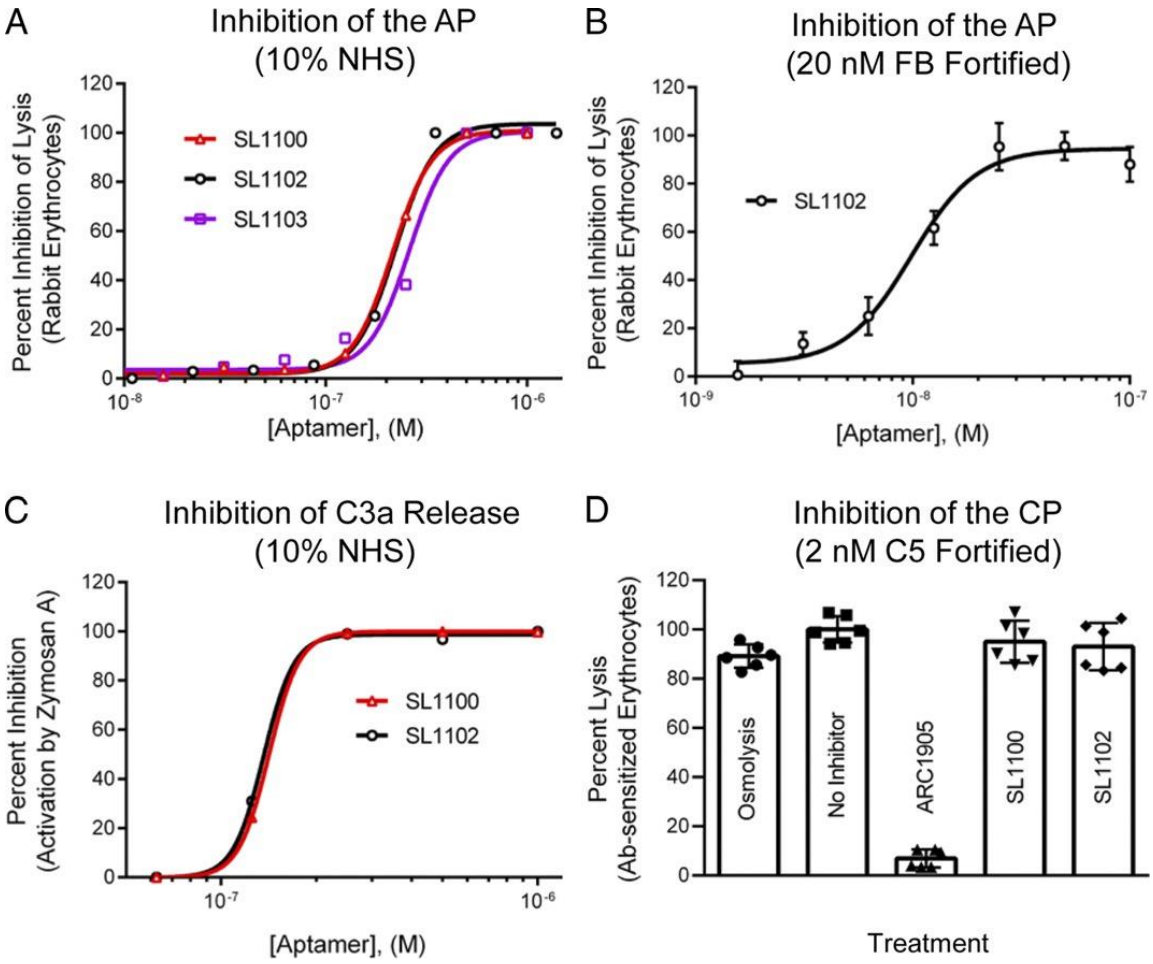

Figure 3.3. FB-Binding SOMAmers Inhibit the AP, but not the CP of Complement.

(A) FB-binding SOMAmers inhibit hemolysis of rabbit erythrocytes in the presence of 10% (v/v) NHS. The IC50 values for SL1100, SL1102 and SL1103 are 220, 200, and 280 nM, respectively. (B) SL1102 inhibits hemolysis of rabbit erythrocytes in the presence of 12% (v/v) FB-depleted NHS fortified with 20 nM of human FB. The mean ± SD of the percent lysis observed in three independent determinations is shown (IC50=9.8 nM). (C) FB-binding SOMAmers inhibit generation of C3a in 10% (v/v) NHS stimulated with zymosan-A. Both SL1100 and SL1102 blocked activation of C3 in a dose-dependent manner. (D) FB-binding SOMAmers do not inhibit the classical pathway of complement. The percent lysis of antibody-sensitized (Ab-sensitized) sheep erythrocytes in 2% (v/v) C5-depleted NHS fortified with 2 nM human C5 is shown as the mean ± SD (n=6). No significant difference in hemolysis was observed with the addition of either 2 μM SL1100 ($p=0.52$) or SL1102 ($p=0.25$) when compared to the no inhibitor control. The anti-C5 aptamer, ARC1905 (40 nM), served as a positive control and inhibited hemolysis ($p<0.001$). (Experiments done by Somalogic, Inc.)

Since FB is required for forming the AP C3 convertase, any inhibitors of FB activity should also disrupt C3 activation under conditions specific for the AP. To test this hypothesis for the FB-binding SOMAmers, we included various concentrations of SL1100 and SL1102 in an assay where zymosan-A was used to stimulate the complement activity of 10% (v/v) NHS in the presence of MgEGTA and then measured the levels of C3a that resulted. We observed dose-dependent inhibition of C3 activation by SL1100 and SL1102 with IC_{50} values well-matched to the concentration of FB, as judged by an ELISA specific for C3a (Figure 3.3C). As a control for specificity, we tested whether the same SOMAers could inhibit lysis of antibody-sensitized sheep erythrocytes in the presence of 2% (v/v) C5-depleted serum that had been fortified with 2 nM C5.

We found that including 2 μM of the C5-targeted aptamer ARC1905 (43) completely inhibited hemolysis, but neither SL1100 nor SL1102 had any impact on hemolysis when used at the same concentration (Figure 3.3D). Thus, this family of FB-binding SOMAmers act as specific inhibitors of the complement AP.

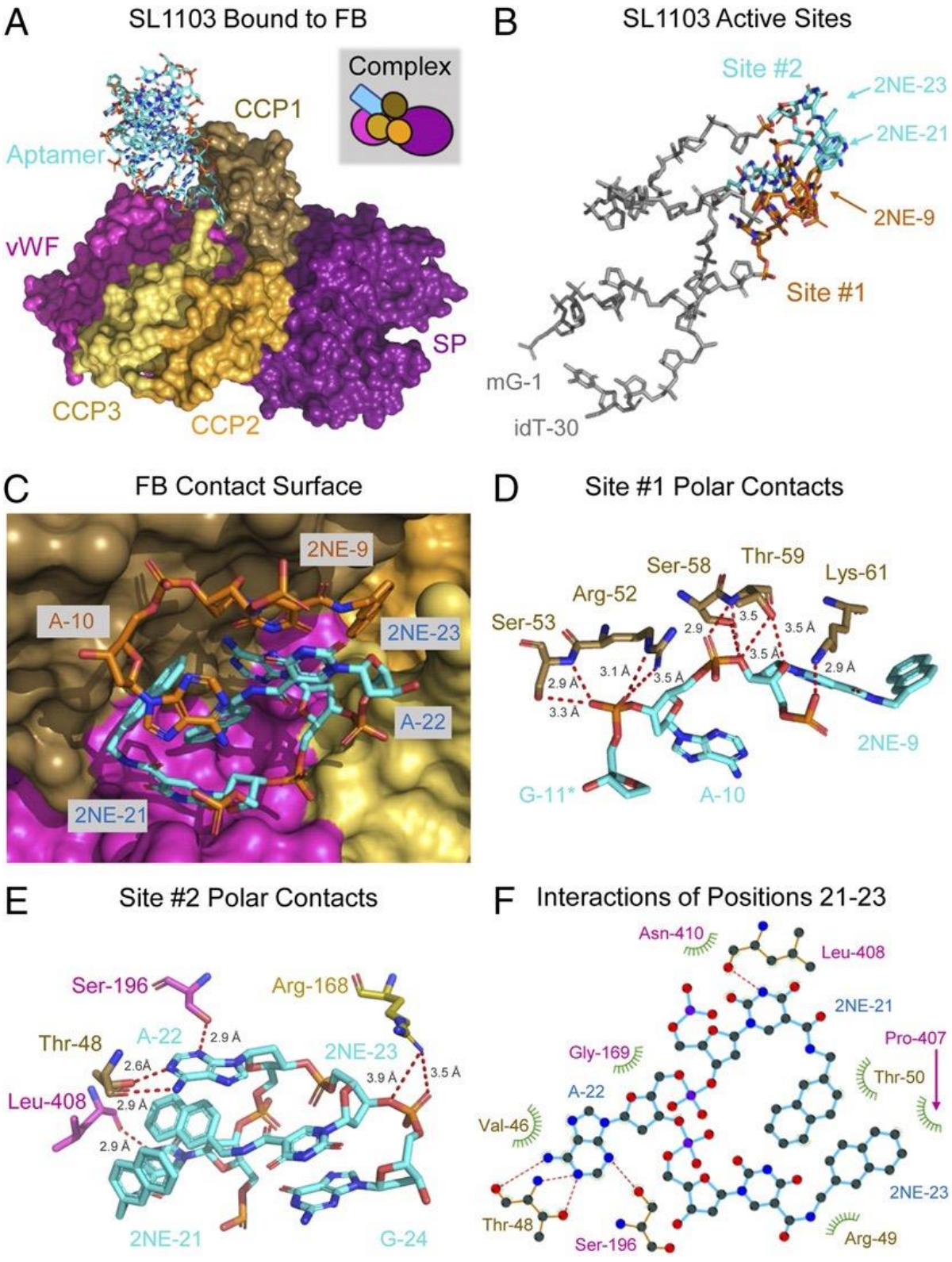

Figure 3.4. Structural Analysis of SL1103 Bound to FB.

(A) Structure of the SL1103/FB complex at 3.1 Å limiting resolution, as represented by Chains A and B in the PDB deposition 7JTN. SL1103 is drawn in ball-and-stick convention with carbon atoms in cyan, oxygen atoms in red, and phosphorous atoms in orange. FB is depicted as a molecular surface, where each domain is colored differently. A cartoon representation of the complex is shown in the grey box, similarly to **Figure 3.6**. (B) Location of the FB-binding sites in SL1103. The SOMAmer is drawn in ball-and-stick convention where the sugar-phosphate atoms of the backbone are shown for all residues, while the nitrogenous bases are also shown for FB-binding Site #1 (carbon atoms in orange) and Site #2 (carbon atoms in cyan). The locations of selected positions in SL1103 are indicated. (C) Closeup representation of the FB contact surface in SL1103. FB is depicted identically to panel A, while the positions from FB-binding Site #1 (carbon atoms in orange) and Site #2 (carbon atoms in cyan) are shown in ball-and-stick convention. (D) Polar contacts in FB-binding Site #1 of SL1103. Residues in FB are shown in ball-and-stick convention with the same coloring scheme as panel A, while positions from SL1103 are shown with carbon atoms colored cyan. Likely hydrogen bonds are represented by red dashes, along with their respective distances in Angstroms (Å). Note that the nitrogenous base of G-11 is hidden for the sake of clarity. (E) Polar contacts in FB-binding Site #2 of SL1103. Representations and coloring schemes are identical to those in panel D. (F) Schematic representation of the packing interactions between FB-binding Site #2 of SL1103 and FB. Positions 21-23 of the SOMAmer are drawn with their carbon atoms in blue, while groups from FB are depicted according to the color scheme of panel A. Hydrophobic/packing interactions are represented by green arcs, while residues that participate in polar interactions are shown in ball-and-stick convention. Likely hydrogen bonds are represented by red dashes.

SL1102 and SL1103 Bind FB at the Juncture of its CCP1, CCP3, and vWF Domains

We sought structural information to better understand the physical basis for inhibition of the AP by these FB-binding SOMAmers. To that end, we crystallized SL1102 and SL1103 bound to human FB, collected X-ray diffraction data, and solved each structure by molecular replacement using a structure of Factor B as an initial search model (23). Since the diffraction data for the SL1103/FB crystal extended to 3.1 Å limiting resolution while that from the SL1102/FB crystal extended to only 3.5 Å (Table 3.2), we completed the SL1103/FB structure first then used the refined model for the SL1103 SOMAmer (29-bases) as starting model for the SL1102 SOMAmer (31-bases). The final models for SL1103/FB and SL1102/FB had R_{work} and R_{free} values of 20.8/24.1% and 22.7/25.7%, respectively (Table 3.2). Each model contains two copies of the SOMAmer/FB complex in the asymmetric unit that are related by non-crystallographic symmetry

(Figure 3.5). Aside from the presence of an additional base-pair formed by extension of the 5' and 3' ends in SL1102 when compared to SL1103 (Table 3.1, Figure 3.5), the individual SOMAmer/FB complexes are practically indistinguishable from one another as judged by structural superposition (*Data Not Shown*). Consequently, we restricted subsequent analyses to the complex represented by Chains A and B in the SL1103/FB structure.

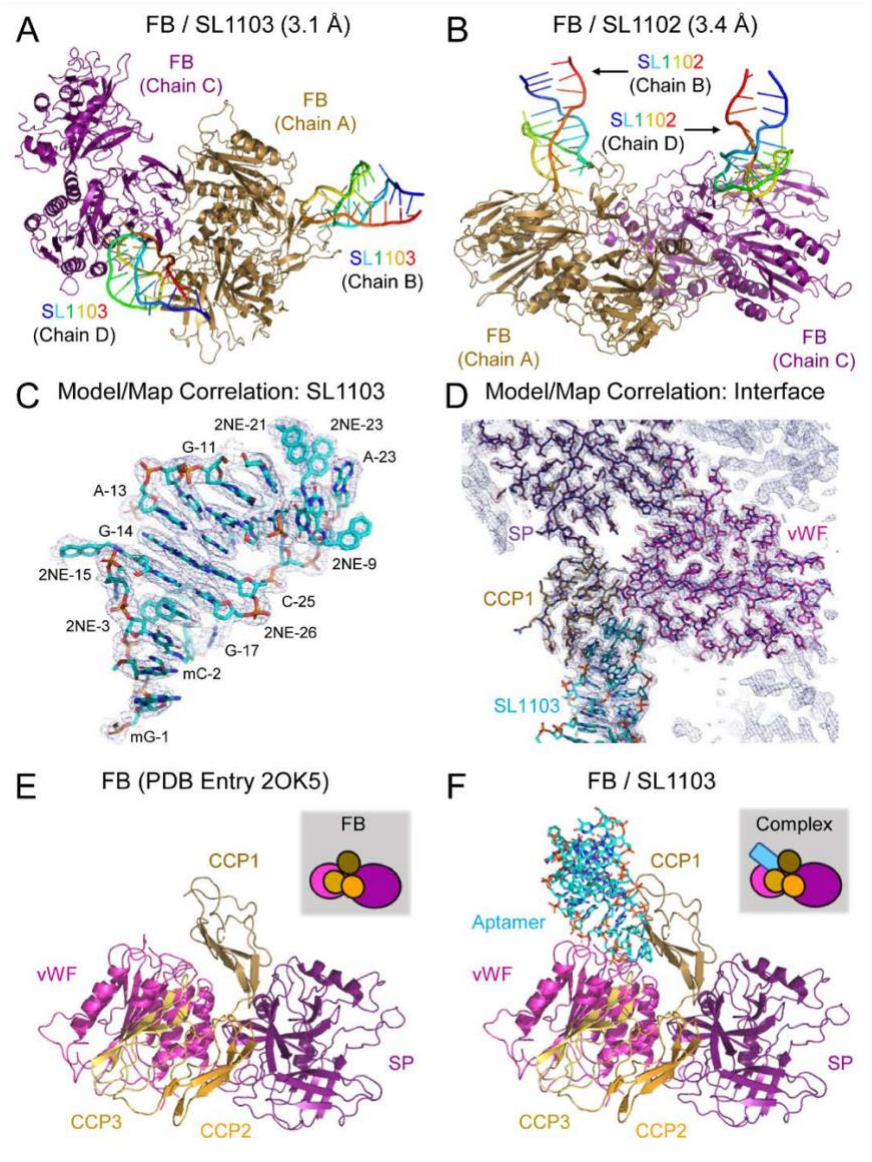

Figure 3.5. Supporting Data Pertaining to the SL1103/FB and SL1102/FB Crystal Structures.

(A) Final model of the SL1103/FB crystal structure determined at 3.1 Å limiting resolution. The asymmetric unit contains two copies of the SL1103/FB complex, represented by chains A and B and chains C and D, respectively. SOMAmers are shown as ribbon diagrams with their 5'-ends in blue and their 3'-ends in red. (B) Final model of the SL1102/FB crystal structure determined at 3.4 Å limiting resolution. The asymmetric unit contains two copies of the SL1103/FB complex, represented by chains A and B and chains C and D, respectively. SOMAmers are shown as ribbon diagrams with their 5'-ends in blue and their 3'-ends in red. (C) Representative model/map correlation for the SL1103 SOMAmer. Chain B is depicted in ball-and-stick convention (carbon atoms in cyan) along with the corresponding $2F_o$-F_c electron density map contoured at 1.3σ (grey cage). Selected positions of SL1103 are labeled. (D) Representative model/map correlation at the interface between FB and SL1103. Macromolecules are depicted in ball-and-stick convention using the color scheme from **Figure 3.4**. $2F_o$-F_c electron density map contoured at 1.3σ is shown as a grey cage. (E) Structure of FB in the unbound state, as rendered from the PDB entry 2OK5 (23). FB is shown as a ribbon diagram using a color scheme identical to **Figure 3.4**. A schematic representation in shown in the grey box. (F) Structure of SL1103/FB shown in an identical orientation to panel E. A schematic representation of the complex is shown in the grey box.

Table 3.2. X-ray Diffraction Data Collection and Refinement Statistics.

	SL1103 / FB (7JTN)	**SL1102 / FB (7JTQ)**
Data Collection		
Space group	*P* 2_1	*P* 2_1
Cell dimensions		
a, *b*, *c* (Å)	87.13 144.41 87.19	87.04 145.75 87.06
α, β, γ (°)	90.00 109.46 90.00	90.00 109.62 90.00
Resolution (Å)	50.00-3.10 (3.21-3.10)	50.00-3.50 (3.63-3.50)
Completeness (%)	99.4 (96.0)	97.3 (93.6)
$I / \sigma I$	7.2 (1.4)	4.1 (1.2)
R_{pim}	0.101 (0.461)	0.147 (0.461)
$CC_{1/2}$	0.917 (0.573)	0.931 (0.590)
Redundancy	5.7 (4.1)	3.4 (3.0)
Refinement		
R_{work} / R_{free} (%)	20.8 / 24.1	22.7 / 25.7
No. of atoms	12,542	12,610
Protein	11,080	11,098
Aptamer	1,462	1,512
Ramachandran Plot		
Favored / Allowed (%)	93.6 / 6.4	93.0 / 7.0
B-Factors		
Protein	16.86–185.84 (61.18)	32.99–194.27 (82.16)
Aptamer	23.22–172.75 (58.69)	50.29–187.98 (84.46)
Root mean square deviations		
Bond lengths (Å)	0.013	0.009
Bond angles (°)	1.62	1.33

*Values in parentheses are for highest-resolution shell.

The SL1103 molecule adopts a compact, cylinder-like fold that is approximately 50 Å in length and 20 Å in diameter. SL1103 resembles a spiral staircase when viewed as a ribbon diagram, where the railing is comprised of the SOMAmer sugar-phosphate backbone (Figure 3.6A). Position mG-17 in SL1103 (mG-18 per the numbering convention used in Figure 3.1C) represents the second pivot point in this SL1103 staircase (Figure 3.6A); its guanine base does not pack within the core of the SOMAmer, but instead is solvent exposed. Not surprisingly, mG-17 is the only non-terminal position permissive of substitution with a C3-spacer (Figure 3.1C). Aside from this, the core of the SL1103 molecule is held together by extensive base-stacking and base-pairing interactions (Figure 3.5C). The most noteworthy of these are a series of triplex-like structures formed by coplanar arrangements of C-25, G-6, and G-14 as well as A5 and the uracil-like moieties of 2NEdU-26 and 2NEdU-15 (Figure 3.6B). The existence of these unconventional interactions is supported by appropriate hydrogen bond distances (i.e. 2.7-3.4 Å), unambiguous $2F_o$-F_c electron density at reasonably high contour levels (e.g. 1.3σ), and strong model-to-map correlations in these areas (Figure 3.5C, D).

The seven modified 2NEdU bases also feature prominently in the SL1103 structure (Figure 3.6). The first cluster of four 2NEdU is found near the middle of the SL1103 molecule and is comprised of positions 3, 15, 26, and 27. In an earlier experiment, we determined that dT substitution at positions 3 and 15 had relatively mild effects on SOMAmer function, but loss of the 2NEdU at positions 26 and 27 essentially abolished SOMAmer activity (Figure 3.1C). Consistent with these observations, the 2NEdU sidechains from positions 26 and 27 appear to participate in base stacking interactions in the middle of the SOMAmer that may be required for proper folding of the nucleic acid chain (Figure 3.1D). The second cluster of three 2NEdU is comprised of positions 9, 21, and 23, and lies at the end of the SOMAmer structure opposite the

5’- and 3’-termini. Interestingly, we also found in an earlier experiment that substitution of positions 21 and 23 by dT abolished SOMAmer function (Figure 3.1C). While it is unclear if these positions are required for structural stability of the SOMAmer molecule, they do form a knot-like structure that contributes significantly to the FB-binding surface of SL1103, as described below.

SL1103 binds FB at groove-like surface lying at the juncture of the CCP1 and CCP3 domains from Ba and the vWF domain from Bb (Figure 3.4A, Figure 3.5E, F). Approximately half of the buried surface area in the SL1103-binding site is derived from CCP1, with the remainder equally portioned from CCP3 and vWF. CCP1 also participates in 12 of the 16 intermolecular hydrogen bonds found in the SL1103/FB complex. Together, these lines of evidence suggest that CCP1 is the primary recognition site for SL1103. Within SL1103, the FB-binding site assembles from two sets of non-contiguous bases (Figure 3.4B, Figure 3.6E, F) that are found in proximity to one another in the folded SOMAmer (Figure 3.4C). The first of these (hereafter “Site #1) is comprised of positions 8 through 11 and includes a single 2NEdU modification at position 9. Site #1 accounts for ~454 $Å^2$ of buried surface area from the SOMAmer and appears to form 10 hydrogen bonds with groups found within CCP1 of FB (Figure 3.4D, Figure 3.4E, F). Five of these hydrogen bonds involve atoms from the sugar-phosphate backbone of 2NEdU-9. The second site (hereafter “Site #2) is comprised of positions 21 through 24 and includes two 2NEdU modifications at positions 21 and 23. Site #2 accounts for ~637 $Å^2$ of buried surface area from the SOMAmer and appears to form 6 hydrogen bonds with groups found within the CCP1, CCP3, and vWF domains of FB (Figure 3.4E, Figure 3.6E, F). The defining features of Site #2 include 3 hydrogen bonds between the adenine base of A-22 and Thr-48 and Ser-196 of FB, as well as extensive packing interactions between these positions and nearby surfaces derived from FB (Figure 3.4F). It is interesting to note that the sidechain modifications of 2NEdU-21 and -23 adopt

conformations whereby their napthyl groups are nearly stacked upon another and form a platform to display the adenine base from position 22, which forms 3 hydrogen bonds with FB. This peculiar structural arrangement resembles a molecular knot and is difficult to envisage absent the 2NEdU modifications (Figure 3.4E, F). Indeed, our previous experiments showed that dT or C3-spacer substitution at any of these positions abolished function and argue for an essential role for Site #2 in SOMAmer activity (Figure 3.1C).

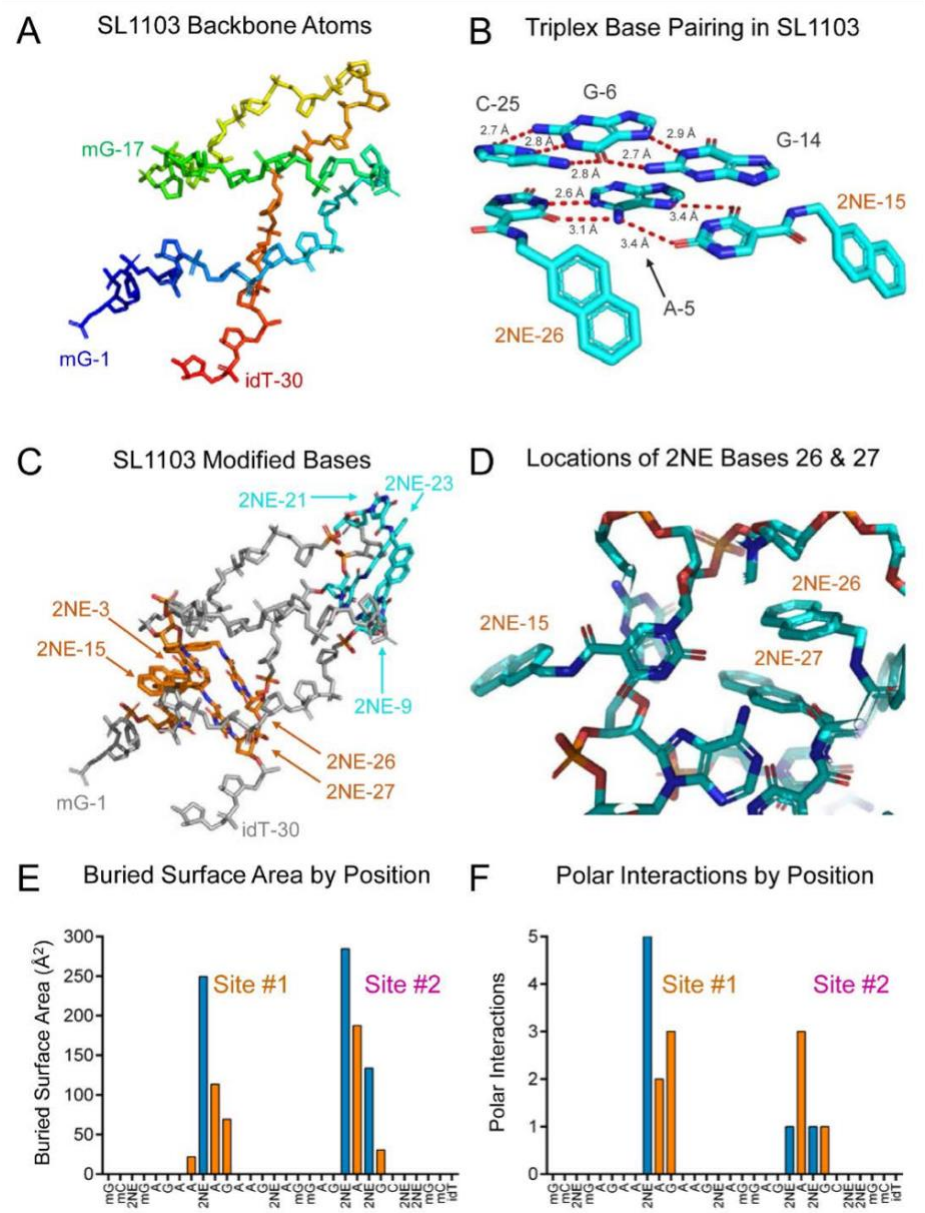

Figure 3.6. Supporting Data Pertaining to the SL1103 SOMAmer Structure.

(A) Backbone atoms of SL1103 shown in ball-and-stick convention. The 5'-end is colored blue, while the 3'-end, represented by the 3'-3' idT cap, is colored red. The location of position mG-17, which is not essential for SL1103 function, is indicated. (B) Examples of triplex base pairing in the SL1103 structure. Only the nitrogenous bases are shown (carbon atoms in cyan). Likely hydrogen bonds are shown as red dashes, along with their corresponding distances. (C) Backbone atoms of SL1103 shown in ball-and-stick convention. The locations of 2NEdU positions are indicated and their nitrogenous bases are also shown. 2NEdU positions with carbon atoms in orange do not contact FB, while those with carbon atoms in cyan are found at the FB interface. (D) Closeup view of SL1103 illustrating the base-stacking orientation of 2NE positions 26 and 27. (E) Buried surface area as a function of sequence position in SL1103. Values were plotted according to whether the base at that position was conventional (orange bars) or a 2NEdU modification (blue bars). Buried surface areas were calculated using EBI-PISA (40). (F) Polar interactions formed as a function of sequence position in SL1103. Values were plotted according to whether the base at that position was conventional (orange bars) or a 2NEdU modification (blue bars). Apparent polar interactions were identified using EBI-PISA (40).

Factor B-Binding SOMAmers Inhibit the AP by Blocking Formation of the Pro-C3 Convertase

Whereas biochemical studies of FB binding to C3b have revealed two mechanistically distinct steps that are dependent on Ba and Bb, respectively (17,22,24,25), the physical basis for these interacations is most readily appreciated by examining the crystal structure of FB bound to C3b (25) (Figure 3.7A). In this regard, this structure of the so-called "Pro-C3 Convertase" shows that CCP1 of the Ba fragment and the vWF domain of the Bb fragment each from close associations with the C345c domain of C3b (Figure 3.7B). Given the location of the SOMAmer binding site at the juncture of the CCP1, CCP3, and vWF domains (Figure 3.4), we hypothesized that SOMAmer binding to FB would block FB/C3b binding through the mechanism of steric hindrance (Figure 3.7C). Blocking formation of the Pro-C3 Convertase in this manner would prevent formation of the active C3 Convertase (Figure 3.7D), and therefore explain the potent inhibitory effects of these SOMAmers on the AP (Figure 3.3).

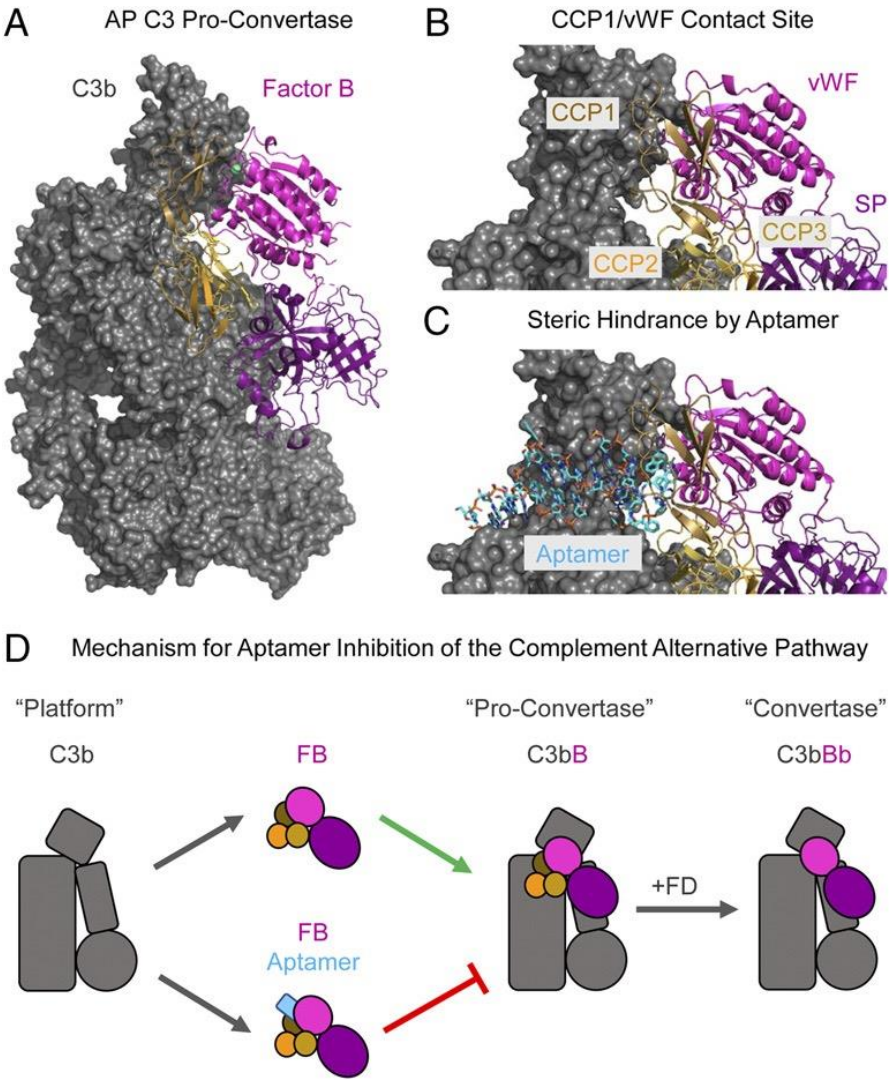

Figure 3.7. Proposed Mechanism for AP Inhibition by FB-Binding SOMAmers.

(A) Structure of the AP Pro-C3 Convertase, as rendered from the PDB entry 2XWJ (25). C3b is depicted as a molecular surface, while FB is drawn in cartoon convention according to the color scheme used in **Figure 3.4**. The Ni^{++}-ion found at the interface between the vWF domain of FB and the C345c domain of C3b is shown as a green sphere. (B) Closeup representation of the FB/C3b complex as drawn in panel A. The locations of individual domains within FB are highlighted. (C) Identical representation to panel B, but also showing SL1103 as inferred from the SL1103/FB crystal structure. By binding tightly to this site on FB, SL1103 would be expected to sterically occlude interaction of FB domains CCP1 and vWF with the C345c domain of C3b. (D) Schematic portraying a proposed mechanism for AP inhibition by FB-binding SOMAmers. The top pathway shows the normal sequence of events, where FB binds to C3b to generate the Pro-C3 Convertase that can be cleaved by FD to yield to the active C3 Convertase (i.e. C3bBb). The bottom pathway shows inhibition of Pro-C3 Convertase formation due to the presence of the FB-binding SOMAmer. This sequence of events would block subsequent formation of the active C3 Convertase, thereby resulting in potent inhibition of AP activity.

To test this hypothesis directly, we employed a competition-style assay that was derived from an established surface plasmon resonance method for monitoring FB binding to site-specifically immobilized C3b (17,19,25,44). As expected, we found that injection of increasing concentrations of FB over a C3b surface yielded a strong, dose-dependent binding response that could be fit to a two-step association model (17,25) (Figure 3.8A). However, when we repeated this experiment using analyte solutions that contained increasing concentration ratios of SL1103 in addition to FB, we observed that the FB binding response decreased dramatically (Figure 3.8B-D). We detected no binding at all when equal concentrations of FB and SL1103 were injected over the C3b surface (Figure 3.8E). When we examined the SPR response immediately prior to injection stop, we found that increasing concentrations SL1103 resulted in progressively greater inhibition of FB-binding across all injection points used (Figure 3.8F). Together these experiments showed that inclusion of SL1103 had the overall effect of reducing the effective concentration of FB present. Therefore, they demonstrate that these FB-binding SOMAmers inhibit formation of the AP Pro-C3 Convertase in a purified setting.

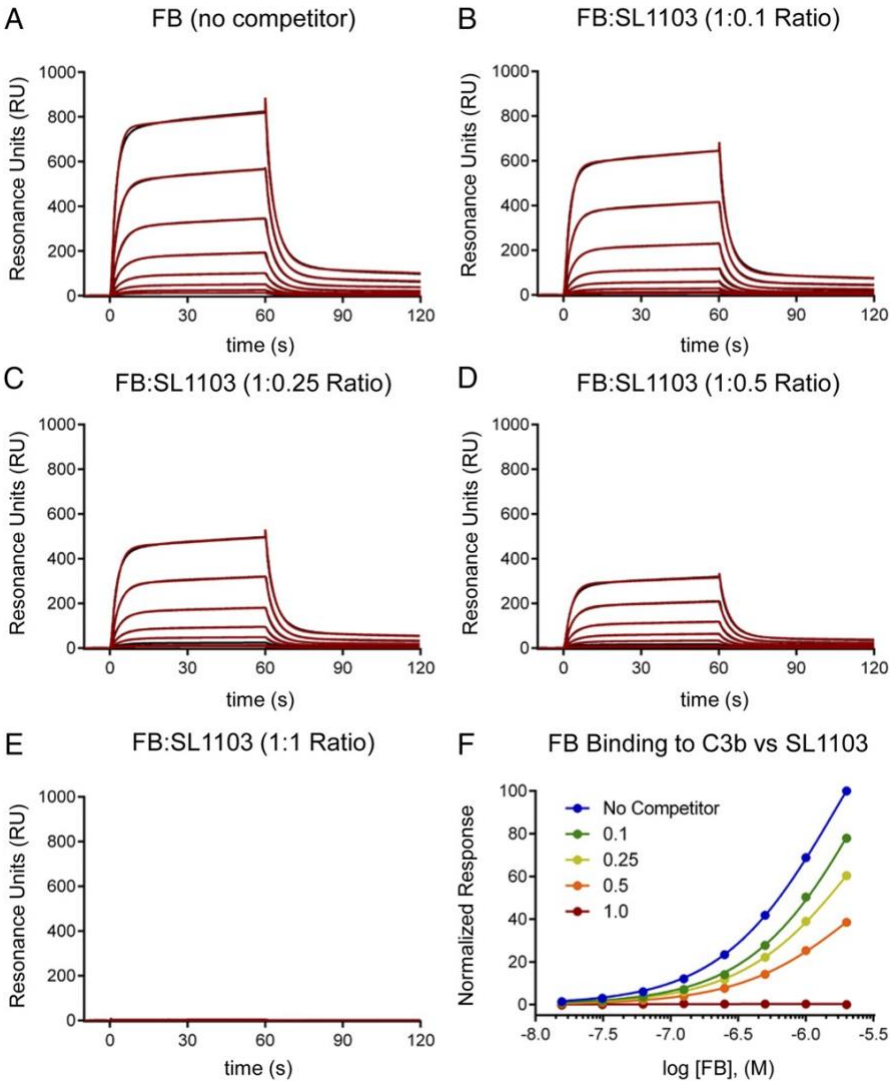

Figure 3.8. FB-Binding SOMAmers Reagents Inhibit Formation of the AP Pro-C3 Convertase.

An SPR sensor surface consisting of site-specifically immobilized C3b was used to investigate binding of FB either alone or in the presence of increasing concentrations of SL1103. A two-fold dilution series of FB spanning eight different concentrations from 15.625 nM to 2 µM was injected over the surface and the reference-corrected sensorgrams (black traces) were fit to a two-state reaction model (red traces). (A) Binding of FB in the absence of any SL1103. (B) Binding of FB in the presence 0.1 molar equivalents of SL1103. (C) Binding to FB in the presence of 0.25 molar equivalents of SL1103. (D) Binding of FB in the presence of 0.5 molar equivalents of SL1103. (E) Binding of FB in the presence of equimolar SL1103. (F) Comparison of the normalized SPR response obtained immediately prior to injection stop for each concentration of FB, either in the absence or presence of various levels of SL1103 (legend is inset). Note that increasing levels of SL1103 diminished FB-binding to the surface at each FB concentration examined.

As a final test of the functional consequences of this competitive effect, we examined whether members of this SOMAmer family could block formation of the active AP C3 Convertase (Figure 3.9). When we incubated purified FB and C3b at equimolar concentrations then added catalytic quantities of FD, we observed the generation of two species indicative of FB cleavage into its Ba and Bb fragments. However, when we repeated this experiment in the presence of increasing concentrations of SL1102, we observed a dose-dependent decrease in the extent of FB cleavage into Ba and Bb. We also noted that when SL1102 was included at a concentration roughly half that of FB, the level of FB cleavage was likewise roughly half that of the uninhibited reaction. This finding was consistent with the long-standing observation that FD cannot cleave FB unless it is bound to C3b (or a closely related molecule like Cobra Venom Factor) (45). It also ruled out the possibility that SOMAmer binding might have somehow altered this property and led to consumptive cleavage of FB. Consequently, this experiment demonstrated that FB binding by this family of SOMAmers inhibits formation of the active AP C3 Convertase in addition to inhibiting formation of the AP Pro-C3 Convertase (Figure 3.10).

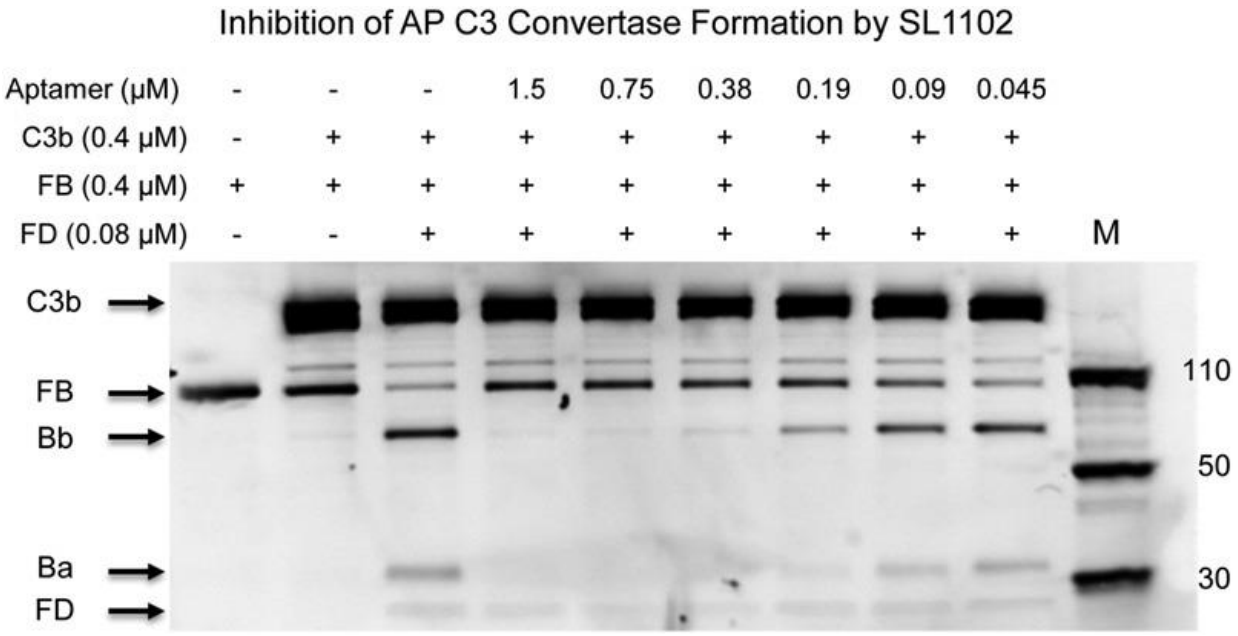

Figure 3.9. FB-Binding SOMAmers Reagents Inhibit Formation of the AP C3 Convertase.

Formation of the AP C3 Convertase was monitored by an SDS-PAGE based method. The appearance of the FB proteolytic cleavage products, Ba and Bb, was only seen when FB is incubated with C3b in the presence of FD. Inclusion of increasing concentrations of the FB-binding SOMAmer, SL1102, inhibited FB cleavage in a dose-dependent manner, even though all other required components were present. Significantly, convertase formation was blocked at an approximately equimolar ratio between FB and SL1102. Positions of C3b, FB, Bb, Ba and FD are indicated with arrows. Mass of the protein molecular weight markers (M) are given in kilodaltons. (Experiments done by Somalogic, Inc.)

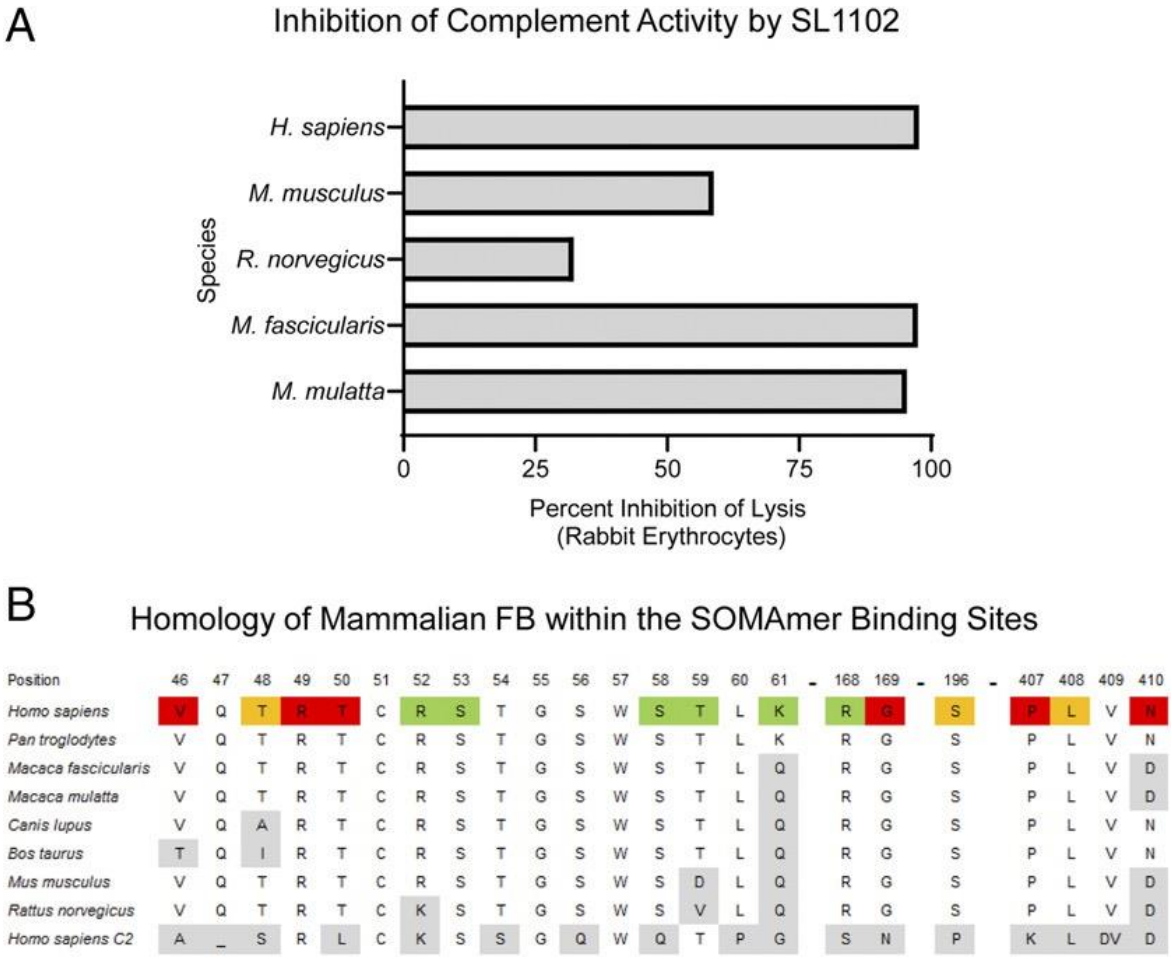

Figure 3.10. Cross Species Reactivity of FB-Binding SOMAmers Reagents.

(A) Percent inhibition of rabbit erythrocyte hemolysis by 1 µM SL1102 (2 µM for mouse) in the presence of 15% (v/v) normal sera (30% (v/v) for mouse). (B) Homology between human FB and representative mammalian species for the amino acids forming major contacts with the FB-binding SOMAmers. Polar contacts are highlighted in green, those that form packing interactions are highlighted in red, while those residues that make both packing and polar contacts are highlighted in orange. Residues that differ from human FB are highlighted in gray. Note that Site #1 of the SOMAmer primarily contacts FB residues 52-61, while Site #2 contacts FB residues outside that region (see **Figure 3.4**). (Experiments done by Somalogic, Inc.)

Discussion

In this report, we have described the identification, structure, and functional characterization of a family of DNA aptamers that bind FB with picomolar affinity and inhibit the complement AP. Unlike conventional aptamers, these so-called SOMAmers incorporate chemical modifications of the sugar phosphate backbone, such as 2'-*O*-methylation and a 3'-3' inverse deoxythymidine cap, to improve their stability against degradation by nucleases. They also make use of the unconventional nucleotide, 2NEdU, in place of deoxythymidine (30). This latter modification imparts unique structural and functional properties to SOMAmers and results in significantly increased affinities for their targets (29,31). Indeed, the FB-binding affinities observed for the SOMAmer family described here ranged from 10-100 pM (Figure 3.1). Subsequent crystal structure determinations for two such SOMAmers (i.e. SL1102 and SL1103) bound to FB revealed that several of the 2NEdU modifications were found at the two contact sites between the macromolecules (Figure 3.4, Figure 3.5, and Figure 3.6) and contributed significantly to the surface area buried at each contact site (Figure 3.4 and Figure 3.6). Consequently, these crystal structures confirmed previous substitution scanning data, which showed that alteration of the 2NEdU positions essentially abolished the FB-binding properties of the SOMAmers (Figure 3.1). By binding tightly to a site on FB that lies at the juncture of its CCP1, CCP3, and vWF domains (Figure 3.7), this family of SOMAmers prevents FB binding to C3b and subsequent formation the AP C3 convertase (Figure 3.8, and Figure 3.9). Ultimately, this results in potent inhibition of the AP (Figure 3.3).

The structures of SL1102 and SL1103 bound to FB are characterized by numerous polar interactions, as well as what appears to be an exceptional level of shape complementary between the SOMAmers and FB (Figure 3.4, Figure 3.5, and Figure 3.6). These attributes were the outcome

of a multi-layered SELEX process, which utilized human FB as the target molecule for *in vitro* evolution of these ligands. Although the family of SOMAmers described in this work binds with picomolar affinity to human FB and potently inhibits human complement, we suspected that the highly optimized nature of their interactions with human FB might also limit the activity of these molecules against the FB from more distantly related mammalian species. Indeed, whereas SL1102 blocked hemolysis of rabbit erythrocytes by sera obtained from macaques to essentially the same extent as it did human serum, SL1102 was noticeably less effective in inhibiting hemolysis by rodent sera (Figure 3.10A). Given this observation, evaluation of these SOMAmers in various experimental rodent models of complement-mediated diseases might not be appropriate.

We compared the sequences of FB from various mammalian species to the SOMAmer/FB crystal structures (Figure 3.4 and Figure 3.5) to arrive at structural explanation for this divergence in function. Even though these FB homologs shared greater than 80% sequence identity, we identified several positions within the SOMAmer/FB binding site that contained substitutions. Most significantly, Thr-59 in primate FB was changed to Asp and Val in mouse and rat FB, respectively (Figure 3.10B). While it is worth noting that Thr-59 forms several backbone and sidechain-mediated polar interactions with FB-binding Site #1 of the SOMAmers (Figure 3.4D), it is unclear at the present time if changes at residue 59 alone could be responsible for failure of these SOMAmers to fully inhibit rodent complement. In the future, this limitation might be circumvented by attempting to reverse-engineer these SOMAmers to gain binding activity toward rodent FB. Alternatively, the SELEX procedure could be redone entirely using rodent FB as the target molecule. Presumably, this would allow identification of analogous family of FB-binding SOMAmers that can inhibit rodent complement with comparable potency as molecules like SL1102 and SL1103 inhibit the primate complement system. Such work would have the added

benefit of allowing for directly comparing the efficacy of a similar inhibitory concept across different model systems.

Though it was long suspected in past, work from throughout the last two decades has now firmly established the complement AP as a driving force in many human inflammatory diseases (Reviewed in (3,5,6,46)). This has led to considerable interest in developing inhibitors that target the various proteins required for proper AP function as therapeutics (Reviewed in (4,8)). Since the AP C3 convertase is the enzyme underlying the self-amplifying activation of C3 via the AP, it presents perhaps the most attractive target for inhibitor development. Nevertheless, the AP C3 convertase itself is comprised of two large molecules in C3b and Bb. It also cleaves one of the most abundant proteins in the blood as its substrate (i.e. C3). These considerations have raised important questions regarding the most effective strategy for blocking convertase activity. In this regard, various monoclonal antibodies (15,47), peptidomimetics (8,48), and even small-molecule inhibitors (39) of C3/C3b function have been described. Several Compstatin-class peptidomimetics within this category are now in clinical trials for indications such as periodontal disease, paroxysmal nocturnal hemoglobinuria (PNH), and C3 glomerulopathy (C3G) (8). But in spite of this progress, targeting FB remains an equally intriguing and complementary approach. To that end, a small-molecule FB inhibitor that appears to reversibly bind the Bb active site and inhibit its enzymatic activity has recently been described (49). This molecule, known as LNP023, has been investigated in rodent models of arthritis and membranous nephropathy and is currently in clinical trials for treatment of PNH and C3G (49). Other inhibitors, including two separate FB-binding monoclonal antibodies have also been reported and successfully investigated in various disease models (50,51). These molecules block the AP by inhibiting pro-convertase formation, which is also a defining characteristic of the FB-binding SOMAmers described here (Figure 3.8).

Although none of these inhibitors have progressed to clinical trials, we believe further investigation is warranted as each of them interferes with an event farther upstream in the AP than does LNP023.

The high affinity and conformational selectivity with which antibodies recognize their targets make them valuable assets for therapeutic manipulation of physiological systems. Although SOMAmers and other aptamer-like molecules do not possess any of the downstream effector functions of antibodies (e.g. opsonization, triggering the CP, etc.), they maintain the ability to bind their cognate ligands with high affinity and potency in a much smaller package (e.g. ~10 kDa). In addition to this, chemical modifications of the sugar-phosphate backbone (e.g. 2-*O*-methylation) and the inclusion of non-standard nitrogenous bases provide SOMAmers with significant improvements in nuclease sensitivity and serum stability (Figure 3.2). This enhanced pharmacological profile, along with their low-cost of synthesis compared to production of proteins like antibodies, raises the possibility that SOMAmers could be powerful tools for inhibiting the function of serum-resident or otherwise extracellular proteins. The generalizable nature of the SELEX process has already enabled identification of SOMAmers that bind over 1,000 different human proteins (29). Many of these SOMAmers could be potent inhibitors of complex biochemical networks (e.g. complement, coagulation, etc) or various signaling axes that control cellular responses (e.g. cytokines, chemokines, etc.). Consequently, SOMAmers and related molecules seem poised to find further applications in any number of human disease settings.

Acknowledgments

The authors thank Kasra Ramyar, Bret Freudenthal, and Amy Gelinas for helpful discussions throughout the course of this work. X-ray diffraction data were collected at Southeast

Regional Collaborative Access Team (SER-CAT) 22-ID beamline at the Advanced Photon Source, Argonne National Laboratory. A list of supporting institutions may be found at www.ser-cat.org/members.html. Use of the Advanced Photon Source was supported by the U.S. Department of Energy, Office of Science, Office of Basic Energy Sciences, under Contract No. W-31-109-Eng-38.

References

1. Hajishengallis, G., Reis, E. S., Mastellos, D. C., Ricklin, D., and Lambris, J. D. (2017) Novel Mechanisms and Functions of Complement. *Nat. Immunol* **18**, 1288-1298
2. Ricklin, D., Hajishengallis, G., Yang, K., and Lambris, J. D. (2010) Complement: a Key System for Immune Surveillance and Homeostasis. *Nat. Immunol* **11**, 785-797
3. Ricklin, D., Reis, E. S., and Lambris, J. D. (2016) Complement in Disease: a Defence System Turning Offensive. *Nat. Rev. Nephrol.* **2016**, 383-401
4. Ricklin, D., and Lambris, J. D. (2013) Complement in Immune and Inflammatory Disorders: Therapeutic Interventions. *J. Immunol.* **190**, 3839-3847
5. Ricklin, D., and Lambris, J. D. (2013) Compement in Immune and Inflammatory Disorders: Pathophysiological Mechanisms. *J. Immunol.* **190**, 3831-3838
6. Reis, E. S., Mastellos, D. C., Ricklin, D., Mantovani, A., and Lambris, J. D. (2018) Complement in Cancer: Untangling an Intricate Relationship. *Nat. Rev. Immunol.* **18**, 5-18
7. Morgan, B. P. (2018) Complement in the Pathogenesis of Alzheimer's Disease. *Semin. Immunopathol.* **40**, 113-124
8. Mastellos, D. C., Ricklin, D., and Lambris, J. D. (2019) Clinical Promise of Next-Generation Complement Therapeutics. *Nat. Rev. Drug Disc.* **18**, 707-729
9. Rawal, N., and Pangburn, M. K. (2003) Formation of High Affinity C5 Convertase of the Classical Pathway of Complement. *J. Biol. Chem.* **278**, 38476-38483
10. Rawal, N., and Pangburn, M. K. (2001) Formation of High-Affinity C5 Convertases of the Alternative Pathway of Complement. *J. Immunol.* **166**, 2635-2642
11. Harboe, M., Ulvund, G., Vien, L., Fung, M., and Mollnes, T.E. (2004) The Quantitative Role of Alternative Pathway Amplification in Classical Pathway Induced Terminal Complement Activation. *Clin. Exp. Immunol.* **138**, 439-446
12. Fromell, K., Adler, A., Aman, A., Manivel, V. A., Huang, S., Duhrkop, C., Sandholm, K., Ekdahl, K. N., and Nilsson, B. (2020) Assessemtn of the Role of C3(H_2O) in the Alternative Pathway. *Front. Immunol.* **11**, 530
13. Ricklin, D., Reis, E. S., Mastellos, D. C., Gros, P., and Lambris, J. D. (2016) Complement Component C3 - The "Swiss Army Knife" of Innate Immunity and Host Defense. *Immunol. Rev.* **274**, 33-58
14. Ferreira, V. P., Pangburn, M. K., and Cortes, C. (2010) Complement Control Protein Factor H: the Good, the Bad, and the Inadequate. *Mol. Immunol.* **47**, 2187-2197

15. Paixao-Cavalcante, D., Torreria, E., Lindorfer, M. A., Rodriguez de Cordoba, S., Morgan, B. P., Taylor, R. P., Llorca, O., and Harris, C. L. (2014) A Humanized Antibody that Regulates the Alternative Pathway Convertase: Potential for Therapy of Renal Disease Associated with Nephritic Factors. *J. Immunol.* **192**, 4844-4851
16. Hammel, M., Sfyroera, G., Ricklin, D., Magotti, P., Lambris, J. D., and Geisbrecht, B. V. (2007) A Structural Basis for Complement Inhibition by Staphylococcus aureus. *Nat. Immunol.* **8**, 430-437
17. Chen, H., Ricklin, D., Hammel, M., Garcia, B. L., McWhorter, W. J., Sfyroera, G., Wu, Y. Q., Tzekou, A., Li, S., Geisbrecht, B. V., Woods, V. L., Jr., and Lambris, J. D. (2010) Allosteric Inhibition of Complement Function by a Staphylococcal Immune Evasion Protein. *Proc. Natl. Acad. Sci. U.S.A.* **107**, 17621-17626
18. Hammel, M., Sfyroera, G., Pyrpassopoulos, S., Ricklin, D., Ramyar, K. X., Pop, M., Jin, Z., Lambris, J. D., and Geisbrecht, B. V. (2007) Characterization of Ehp: a Secreted Complement Inhibitory Protein from Staphylococcus aureus. *J. Biol. Chem.* **202**, 30051-30061
19. Ricklin, D., Tzekou, A., Garcia, B. L., Hammel, M., McWhorter, W. J., Sfyroera, G., Wu, Y.-Q., Holers, V. M., Herbert, A. P., Barlow, P. N., Geisbrecht, B. V., and Lambris, J. D. (2009) A Molecular Insight into Complement Evasion by the Staphylococcal Complement Inhibitor Protein Family. *J. Immunol.* **183**, 2565-2574
20. Garcia, B. L., Summers, B. J., Zhuoer, L., Ramyar, K. X., Ricklin, D., Fu, Z.-Q., Lambris, J. D., and Geisbrecht, B. V. (2012) Diversity in the C3b Contact Residues and Tertiary Structures of the Staphylococcal Complement Inhibitor (SCIN) Protein Family. *J. Biol. Chem.* **287**, 628-640
21. Garcia, B. L., Ramyar, K. X., Tzekou, A., Ricklin, D., McWhorter, W. J., Lambris, J. D., and Geisbrecht, B. V. (2010) Molecular Basis for Complement Recognition and Inhibition Determined by Crystallographic Studies of the Staphylococcal Complement Inhibitor (SCIN) Bound to C3c and C3b *J. Mol. Biol.* **402**, 17-29
22. Rooijakkers, S. H., Wu, J., Ruyken, M., van Domselaar, R., Planken, K. L., Tzekou, A., Ricklin, D., Lambris, J. D., Janssen, B. J., van Strijp, J. A., and Gros, P. (2009) Structural and Functional Implications of the Alternative Complement Pathway C3 Convertase Stabilized by a Staphylococcal Inhibitor. *Nat. Immunol* **10**, 721-727
23. Milder, F. J., Gomes, L., Schouten, A., Janssen, B. J., Huizinga, E. G., Romijn, R. A., Hemrika, W., Roos, A., Daha, M. R., and Gros, P. (2007) Factor B Structure Provides Insights into Activation of the Central Protease of the Complement System. *Nat. Struct. Mol. Biol.* **14**, 224-228
24. Pryzdial, E. L., and Isenman, D. E. (1987) Alternative Complement Pathway Activation Fragment Ba Binds to C3b. Evidence that Formation of the Factor B-C3b Complex Invovles Two Discrete Points of Contact. *J. Biol. Chem.* **262**, 1519-1525
25. Forneris, F., Ricklin, D., Wu, J., Tzekou, A., Wallace, R. S., Lambris, J. D., and Gros, P. (2010) Structures of C3b in Complex with Factors B and D Give Insight into Complement Convertase Formation. *Science* **330**, 1816-1820
26. Bunka, D. H., and Stockley, P. G. (2006) Aptamers Come of Age - at Last. *Nat. Rev. Microbiol.* **4**, 588-596
27. Tuerk, C., and Gold, L. (1990) Systematic Evolution of Ligands by Exponential Enrichment: RNA Ligands to Bacteriophage T4 DNA Polymerase. *Science* **249**, 505-510

28. Ellington, A. D., and Szostak, J. W. (1990) *In vitro* Selection of RNA Molecules that Bind Specific Ligands. *Nature* **346**, 818-822
29. Gold, L., Ayers, D., Bertino, J., Bock, C., Bock, A., Brody, A., Brody, E. N., Carter, J., Dalby, A. B., Eaton, B. E., Fitzwater, T., Flather, D., Forbes, A., Foreman, T., Fowler, C., Gawande, B., Goss, M., Gunn, M., Gupta, S., Halladay, D., Heil, J., Heilig, J., Hicke, B., Husar, G., Janjic, N., Jarvis, T., Jennings, S., Katilius, E., Kenney, T. R., Kim, N., Koch, T. H., Kraemer, S., Kroiss, L., Le, N., Levine, D., Lindsey, W., Lollo, B., Mayfield, W., Mehan, M., Mehler, R., Nelson, S. K., Nelson, M., Nieuwlandt, D., Nikrad, M., Ochsner, U., Ostroff, R. M., Otis, M., Parker, T., Pietrasiewicz, S., Resnicow, D. I., Rohloff, J., Sanders, G., Sattin, S., Schneider, D., Singer, B., Stanton, M., Sterkel, A., Stewart, A., Stratford, S., Vaught, J. D., Vrkljan, M., Walker, J. J., Watrobka, M., Waugh, S., Weiss, A., Wilcox, S. K., Wolfson, A., Wolk, S. K., Zhang, C., and Zichi, D. (2010) Aptamer-Based Multiplexed Proteomic Technology for Biomarker Discovery. *PloS One* **5**, e15004
30. Vaught, J. D., Bock, C., Carter, J., Fitzwater, T., Otis, M., Schneider, D., Rolando, J., Waugh, S., Wilcox, S. K., and Eaton, B. E. (2010) Expanding the Chemistry of DNA for *In vitro* Selection. *J. Am. Chem. Soc.* **132**, 4141-4151
31. Davies, D. R., Gelinas, A. D., Zhang, C., Rohloff, J. C., Carter, J. D., O'Connell, D., Waugh, S. M., Wolk, S. K., Mayfield, W. S., Burgin, A. B., Edwards, T. E., Stewart, L. J., Gold, L., Janjic, N., and Jarvis, T. C. (2012) Unique Motifs and Hydrophobic Interactions Shape the Binding of Modified DNA Ligands to Protein Targets. *Proc. Natl. Acad. Sci. U.S.A.* **109**, 19971-19976
32. Caruthers, M. H., Barone, A. D., Beaucage, S. L., Dodds, D. R., Fisher, E. F., McBride, L. J., Matteucci, M., Stabinsky, Z., and Tang, J. Y. (1987) Chemical Synthesis of Deoxyoligonucleotides by the Phosphoramidite Method. *Methods Enzymol.* **154**, 287-313
33. Rohloff, J. C., Gelinas, A. D., Jarvis, T. C., Ochsner, U. A., Schneider, D. J., Gold, L., and Janjic, N. (2014) Nucleic Acid Ligands With Protein-like Side Chains: Modified Aptamers and Their Use as Diagnostic and Therapeutic Agents. *Mol. Ther. Nucleic Acids* **3**, e201
34. Gupta, S., Hirota, M., Waugh, S. M., Murakami, I., Suzuki, T., Muraguchi, M., Shibamori, M., Ishikawa, Y., Jarvis, T. C., Carter, J. D., Zhang, C., Gawande, B., Vrkljan, M., Janjic, N., and Schneider, D. J. (2014) Chemically Modified DNA Aptamers Bind Interleukin-6 with High Affinity and Inhibit Signaling by Blocking its Interaction with Interleukin-6 Receptor. *J. Biol. Chem.* **289**, 8706-8719
35. Otwinowski, Z., and Minor, W. (1997) Processing of X-ray Diffraction Data Collected in Oscillation Mode. *Methods Enzymol.* **276**, 307-326
36. McCoy, A. J., Grosse-Kunstleve, R. W., Adams, P. D., Winn, M. D., Storoni, L. C., and Read, R. J. (2007) Phaser Crystallographic Software. *J. Appl. Cryst.* **40**, 658-674
37. Adams, P. D., Grosse-Kunstleve, R. W., Hung, L.-W., Ioerger, T. R., McCoy, A. J., Moriarty, N. W., Read, R. J., Sacchettini, J. C., Sauter, N. K., and Terwilliger, T. C. (2002) PHENIX: Building New Software for Automated Crystallographic Structure Determination. *Acta Cryst.* **D58**, 1948-1954
38. Adams, P. D., Afonine, P. V., Bunkoczi, G., Chen, V. B., Davis, I. W., Echols, N., Headd, J. J., Hung, L. W., Kapral, G. J., Grosse-Kunstleve, R. W., McCoy, A. J., Moriarty, M. W., Oeffner, R., Read, R. J., Richardson, D. C., Richardson, J. S., Terwilliger, T. C., and Zwart, P. H. (2010) PHENIX: a Comprehensive Python-Based System for Macromolecular Structure Solution. *Acta. Cryst. D Biol. Crystallogr.* **66**, 213-221

39. Garcia, B. L., Skaff, D. A., Chatterjee, A., Hanning, A., Walker, J. K., Wyckoff, G. J., and Geisbrecht, B. V. (2017) Identification of C3b-Binding Small-Molecule Complement Inhibitors Using Cheminformatics. *J. Immunol.* **198**, 3705-3718
40. Krissinel, E., and Henrick, K. (2007) Inference of Macromolecular Assemblies from Crystalline State. *J. Mol. Biol.* **372**, 774-797
41. Wallace, A. C., Laskowski, R. A., and Thornton, J. M. (1996) LIGPLOT: a Program to Generate Schematic Diagrams of Protein-Ligand Interactions. *Protein Eng.* **8**, 127-134
42. Gawande, B. N., Rohloff, J. C., Carter, J. D., von Carlowitz, I., Zhang, C., Schneider, D. J., and Janjic, N. (2017) Selection of DNA Aptamers with Two Modified Bases. *Proc. Natl. Acad. Sci. U.S.A.* **114**, 2898-2903
43. Drolet, D. W., Green, L. S., Gold, L., and Janjic, N. (2016) Fit for the Eye: Aptamers in Ocular Disorders. *Nucleic acid therapeutics* **26**, 127-146
44. de Jong, N. W. M., Vrieling, M., Garcia, B. L., Koop, G., Brettmann, M., Aerts, P. C., Ruyken, M., van Strijp, J. A. G., Holmes, M., Harrison, E. M., Geisbrecht, B. V., and Rooijakkers, S. H. M. (2018) Identification of a Staphylococcal Complement Inhibitor with Broad Host Specificity in Equid Staphylococcus aureus Strains. *J. Biol. Chem.* **293**, 4468-4477
45. Volanakis, J. E., Barnum, S. R., and Kilpatrick, J. M. (1993) Purification and Properties of Human Factor D. *Methods Enzymol.* **222**, 82-97
46. Thurman, J. M., and Holers, V.M. (2006) The Central Role of the Alternative Complement Pathway in Human Disease. *J. Immunol.* **176**, 1305-1310
47. Alsenz, J., Becherer, J.D., Nilsson, B., and Lambris, J.D. (1989) Structural and Functional Analysis of C3 Using Monoclonal Antibodies. . *Curr. Top. Microbiol. Immunol.* **153**, 235-248
48. Qu, H., Ricklin, D., Bai, H., Chen, H., Reis, E. S., Maciejewski, M., Tzekou, A., DeAngelis, R. A., Resuello, R. R., Lupu, F., Barlow, P. N., and Lambris, J. D. (2013) New Analogs of the Clinical Complement Inhibitor Compstatin with Subnanomolar Affinity and Enhanced Pharmacokinetic Properties. *Immunobiology* **218**, 496-505
49. Schubart, A., Anderson, K., Mainolfi, N., Sellner, H., Ehara, T., Adams, C. M., Sweeney, A. M., Liao, S.-M., Crowley, M., Littlewood-Evans, A., Sarret, S., Wieczorek, G., Perrot, L., Dubost, V., Flandre, T., Zhang, Y., Smith, R. J. H., Risitano, A. M., Karki, R. G., Zhang, C., Valeur, E., Sirockin, F., Gerhartz, B., Erbel, P., Hughes, N., Smith, T. M., Cumin, F., Argikar, U. A., Haraldsson, B., Mogi, M., Sedrani, R., Wiesmann, C., Jaffee, B., Maibaum, J., Flohr, S., Harrison, R., and Eder, J. (2019) Small-Molecule Factor B Inhibitor for the Treatment of Complement-Mediated Diseases. *Proc. Natl. Acad. Sci. U.S.A.* **116**, 7926-7931
50. Thurman, J. M., Kraus, D. M., Girardi, G., Hourcade, D., Kang, H. J., Royer, P. A., Mitchell, L. M., Giclas, P. C., Salmon, J., Gilkeson, G., and Holers, V. M. (2005) A Novel Inhibitor of the Alternative Complement Pathway Prevents Antiphospholipid Antibody-Induced Pregnancy Loss in Mice. *Mol. Immunol.* **42**, 87-97
51. Subias, M., Tortajada, A., Gastoldi, S., Galbusera, M., Perrote-Lopez, A., de Juana Lopez, L., Gonzalez-Fernandez, F. A., Villegas-Martinez, A., Dominguez, M., Llorca, O., Noris, M., Morgan, B. P., and Rodriguez de Cordoba, S. (2014) A Novel Antibody against Human Factor B that Blocks Formation of the C3bB Proconvertase and Inhibits Complement Activation in Disease Models. *J. Immunol.* **193**, 5567-5575

Chapter 4 - Group B *Streptococcus* Surface Protein β: Structural Characterization of a Novel Complement Factor H-binding Motif and its Contribution to Immune Evasion

This chapter supposed to be published as a journal article.

Xin Xu*, Alexander L. Lewis Marffy †, Andrew Keightley#, Alex J. McCarthy†, & Brian V. Geisbrecht*

*Department of Biochemistry & Molecular Biophysics, Kansas State University; Manhattan, KS U.S.A.

†Department of Infectious Diseases, Section of Molecular Microbiology, MRC Centre for Molecular Bacteriology & Infection, Imperial College London; London, U.K.

#Department of Ophthalmology, School of Medicine, University of Missouri-Kansas City; Kansas City, MO U.S.A.

Abstract

The β antigen from Group B *Streptococcus* (GBS) is a ~125 kDa, cell-surface exposed protein that binds to multiple host-derived ligands, including complement factor H (FH). Many details regarding this interaction and its significance to immune evasion by GBS remain unclear. Here we identified a novel three-helix bundle domain within the C-terminal half of the B75KN region of β as the major FH-binding determinant and determined its crystal structure at 2.5 Å resolution. Analysis of this structure suggested a role in FH binding for a loop region connecting helices α1 and α2, which we confirmed by mutagenesis and direct binding studies. Using a combination of protein crosslinking and mass spectrometry, we observed that B75KN bound to CCP3 and CCP4 domains of FH. Although this binding site lies within a complement regulatory region of FH, we determined that FH bound by β retained its decay acceleration and cofactor activities. Heterologous expression of β by *L. lactis* resulted in recruitment of FH to the bacterial surface and a significant reduction of C3b deposition following exposure to human serum. Surprisingly, we found that FH-binding by β was not required for bacterial resistance to phagocytosis by neutrophils or killing of bacteria by whole human blood. However, loss of the B75KN region significantly diminished bacterial survival in both assays. While our results show that FH recruited to the bacterial surface through a high-affinity interaction maintains key complement regulatory functions, they raise questions about the importance of FH-binding to immune evasion by GBS as a whole.

Introduction

Streptococcus agalactiae, also known as Group B *Streptococcus* (GBS), is an opportunistic pathogen that is a major cause of morbidity or mortality in newborns globally (1-5). This Gram-positive bacterium asymptomatically colonizes the gastrointestinal and vaginal epithelium in up to 30% of women and can be transmitted vertically from mother to child, potentially resulting in invasive neonatal diseases including pneumonia, sepsis and meningitis (6-8). GBS is commonly classified into 10 antigenically distinct serotypes, of which serotypes Ia, Ib, II, III and V are more commonly associated with invasive disease worldwide (9). Alarmingly, the incidence of GBS disease in neonates and adults are on the rise (10-12) and no vaccine is currently available. The major host defense mechanisms that protect against invasive GBS infections require the deposition of complement C3b onto the microbial surface via the alternative pathway (AP) or classical pathway (CP) of the complement system. C3b marks microbes for opsonophagocytic killing by phagocytes including neutrophils and for lysis via formation of the membrane attack complex (MAC). Importantly, bacterial pathogens including GBS have evolved mechanisms to suppress complement deposition, and these are often correlated with resistance to osponophagocytic killing (13,14).

Factor H (FH) is a principal negative regulator of the complement AP (15). It is a soluble, ~150 kDa protein composed of 20 complement control protein (CCP) modules (also known as short consensus repeat (SCR) domains). Cells marked with FH are protected against the AP by competing with factor B (FB) for interaction with C3b, acting as a cofactor for C3b cleavage to iC3b by factor I (FI) and promoting decay of the C3 convertase (C3bBb) (15). FH is deposited on host cells by recognition of polyanion markers, including sialic acids and glycosaminoglycans

(GAGs), through CCP7, CCP19 and/or CCP20. The inhibition activities of FH are mediated by the CCP1–4 domains that harbors a C3b-binding site (16). The properties of these domains allow FH to restrict complement activation on host cells and non-cellular surfaces lacking membrane complement regulators (17-19). In contrast, microbes that do not express polyanion markers are not recognized by FH and are susceptible to C3b deposition.

Pathogen cells can recruit FH through modifying their surface to mimic host cells or by expressing specific molecules that act as FH receptors. Examples of this phenomenon are widespread, and are found in bacterial, viral, protozoan, fungal and helminth pathogens (20,21). Binding of FH to the pathogen surface has been shown to suppress C3b deposition, to induce degradation of C3b to iC3b, and/or to accelerate the decay of C3 and C5 convertases (22-27). However, the impact of FH recruitment on resistance to opsonophagocytic killing remains unclear (28,29). GBS appears to have several mechanisms to sequester FH. The first of these is production of capsular polysaccharide containing α2,3-linked N-acetylneuraminic acid (Neu5Ac), which is identical to the sialic acid found on human cells. Capsule has been associated with reduced C3b deposition and enhanced resistance to opsonophagocytosis (30), presumably through FH recruitment. The second is expression of two surface-localized *Streptococcal* histidine triad proteins called Sht and ShtII. These molecules are found in 96.8% and 100% of GBS strains, respectively, and directly bind FH (25,31). The third and final mechanism is direct binding of FH by the surface localized β protein (32), which is commonly expressed by serotype Ia, Ib, II and V strains (33). Despite the characterization of multiple FH ligands in GBS, the molecular details of these individual interactions and their functional consequences remain poorly understood.

Expression of β protein by GBS strain A909 cells (capsular type 1A) results in recruitment of FH from human serum, and promotes bacterial resistance to opsonophagocytosis and

enhancement of survival in human blood (32,34). Unfortunately, interpretations of these data are not straightforward since GBS strain A909 cells also produce capsule and express the FH-binding proteins Sht and ShtII (32). Further complications arise from the fact that the ~125 kDa β protein binds several other ligands within the human immune system, including soluble IgA and the cell-surface receptors Siglec-5, Siglec-7, Siglec-14, CEACAM1 and CEACAM5 (32,34-37). Whether and how any of these protein-protein interactions influence one another remains unclear at this time. Though the binding site of most β protein ligands has been mapped to a distinct domain (Figure 4.1A), the FH-binding activity has only been tentatively localized to a region spanning roughly the C-terminal half of β (i.e. B75KN-XPZ-B75KC) (32). Here, we aimed to define the role of β protein and FH interactions for GBS immune evasion using structural and functional analyses. Understanding how β protein and FH interact, and how these interactions influence the function of the host immune system, is critical for better understanding and treatment of invasive GBS diseases.

Materials and Methods

Protein Samples

Codon-optimized DNA fragments encoding truncated and/or site-directed mutant forms of the Group B *Streptococcus* β protein were subcloned into the *Bam*HI and *Not*I sites of the prokaryotic expression vector pT7HMT (38). The corresponding plasmids were transformed into *E. coli* BL21 (DE3) cells for routine protein production work or *E. coli* B834 (DE3) cells for generating Seleno-L-methionine-labeled protein for X-ray crystallography studies. General methods for recombinant protein expression, purification by immobilized metal-ion affinity chromatography, and site-specific cleavage by TEV protease to remove affinity tags have been

previously described (39,40). Following removal of the affinity tag, all recombinant proteins were subjected to final purification by gel filtration chromatography using either a Superdex 75 26/60 or a Superdex 200 26/60 column (Cytiva Life Sciences) that had been previously equilibrated in phosphate buffered saline (PBS; 10 mM Na/K-phosphate (pH 7.4), 137 mM NaCl, 3 mM KCl). Fractions containing proteins of interest (as judged by SDS-PAGE) were pooled, concentrated by ultrafiltration, and stored at -80 °C for further use.

Samples of complement factor B (FB), factor H (FH), factor I (FI), and C3b purified from pooled human serum were purchased from Complement Technology, Inc. (Tyler, TX, USA). Commercial sources of various antibodies and antibody conjugates are provided within the appropriate subsections below.

Limiting Proteolytic Digestion of β-B75KN and Characterization by Mass Spectrometry

Limiting proteolytic digestion was used to identify new stable subdomains within the β-B75KN region. Briefly, trypsin and subtilisin were first obtained from Promega (WI, USA) and reconstituted to a concentration of 1 mg/mL. A dilution series of each protease was prepared to yield final ratios of protease to target protein of 1:15, 1:45, 1:150, 1:450, 1:1500, 1:4500, and 1:15,000. Reactions were begun by combining the protease and target protein in each tube, followed by quickly vortexing and collecting the contents in the bottom of each tube by centrifugation. Reactions were allowed to proceed for 30 min at 25 °C, after which time proteolysis was terminated by adding 5 µL of non-reducing SDS-PAGE sample buffer and placing the sample in a boiling water bath for 5 min. The reaction contents were separated by SDS-PAGE and detected by Coomassie Brilliant Blue staining. Gel bands of interest were reduced, alkylated, processed for in-gel trypsin digestion, and characterized by tandem mass spectrometry according to the general methods described previously (41).

Surface Plasmon Resonance Analysis of β Protein Interactions with FH

Direct binding of recombinant β proteins to purified human FH was assessed by Surface Plasmon Resonance (SPR). All experiments were performed at 25 °C on a Biacore T-200 instrument (Cytiva Life Sciences) using a running buffer of HBS-T (20 mM HEPES (pH 7.4), 140 mM NaCl, and 0.005% (v/v) Tween-20) and a flowrate of 30 μL/min. Standard amine coupling chemistry (Amine Coupling Kit; Cytiva Life Sciences) was used according to the manufacturer's suggestions to create experimental and reference surfaces on separate flow cells of a CMD-200 sensor chip (Xantec Bioanalytics GmbH; Dusseldorf, Germany). The experimental surface was prepared by immobilizing FH (50 μg/mL in 10 mM sodium acetate (pH 4.5)) to a final density of 1967 RU, while the reference surface was prepared by activation followed by quenching with 1 M ethanolamine (pH 9.5). Recombinant β proteins were injected over the biosensor surface in reference subtraction mode using a two-fold series of increasing concentrations ranging from 19.5 nM to 10 μM. Each experimental cycle consisted of an association phase of 2 min followed by a dissociation phase of 3 min. Regeneration of the biosensor surface was achieved by two injections of 0.1 M glycine (pH 10.0), 2 M NaCl for 30 sec. Sensorgram series were analyzed according to different mathematical models using Biacore T-200 Evaluation software v3.2 (Cytiva Life Sciences). Initially, data were fit globally to a simple affinity (dose/response) model to derive an apparent K_D without regard to kinetic parameters. Thereafter, two separate kinetic models that accounted for either a signal binding event (one association and dissociation rate constant, one apparent K_D) or ligand heterogeneity with two independent binding events (two association and dissociation rate constants giving two apparent K_D values) were used. All parameters presented in Table 1 represent the mean and standard deviation of two independent determinations.

Protein Structure Determination by X-ray Crystallography and Structural Analysis

Purified seleno-L-methionine-labeled β-B75KN-CTD was exchanged into 10 mM HEPES (pH 7.5), 50 mM NaCl using 3 kDa molecular weight cut-off ultrafiltration units and concentrated to ~20 mg/mLl as judged by OD_{280} using the theoretical extinction coefficient. Fusiform crystals were obtained by vapor diffusion of hanging drops prepared by mixing 1 µL of protein with 1 µL of a precipitant solution consisting of 2 M ammonium sulfate, 5% (v/v) 2-propanol and equilibrating over 500 µL of precipitant solution at 20 ºC after roughly 10-14 days. Samples were cryopreserved by soaking crystals in their respective precipitant solutions supplemented with an additional 30% (w/v) glucose prior to flash-cooling in liquid N_2.

X-ray diffraction data were collected from a single SeMet-labeled β-B75KN-CTD crystal at 100 K using beamline 22-ID of the Advance Photon Source, Argonne National Laboratory and radiation at a Selenium remote wavelength (λ=0.9724 Å). Diffraction data were integrated, scaled, and reduced using the HKL2000 software suite (42). Experimental phase information was obtained by AutoSol (43) as implemented in the PHENIX (44) software suite. This allowed identification and refinement of a total of 6 Se sites within the asymmetric unit of the $P3_121$ unit cell. Iterative cycles of manual rebuilding building in Coot (45) and refinement using PHENIX.REFINE were used to complete the final model. A quantitative description of the cell constants, diffraction data quality, and properties of the final model can be found in Table 2.

The final model consists of two copies of the β-B75KN-CTD protein arranged as an antiparallel dimer. The two copies superimpose with an RMSD of 0.311 Å across 69 Cα positions. Chain A consists of 85 amino acids which correspond to residues 736-763 and 769-825 of the β protein. Chain B consists of 82 amino acids which correspond to residues 735-762 and 771-824 of the β protein. Residues at the N-terminus of the β-B75KN-CTD fragment, which correspond to positions 724-734 of the β protein, are not visible in either copy. Similarly, the loop region that

connects helices α1 and α2 is poorly ordered such that positions 764-768 are not modeled in either copy. The refined coordinates and structure factors have been deposited in the PDB using the accession code 7S0R. All representations of protein structures were generated and rendered by PyMol (www.pymol.org/).

Mapping Interactions between β-B75KN and FH by Crosslinking and Mass Spectrometry

The binding site for β-B75KN was mapped onto human FH by crosslinking the two proteins and characterizing the adducts by mass spectrometry (CovalX AG; Zurich, Switzerland). Initially, high-mass MALDI analysis was performed on samples of β-B75KN and FH individually as a control for both their integrity and aggregation state. A two-fold dilution series of each protein spanning a concentration range of ~1.0 mg/mL to 10 μg/mL was prepared, mixed with an equal volume of sinapinic acid matrix (10 mg/ml) dissolved in acetonitrile/water (1:1, v/v), 0.1% (v/v) trifluoracetic acid, and spotted on a MALDI plate. An analogous set of experiments was performed by incubating the same dilution series (9 μL) with the amine-reactive crosslinker disuccinimidyl suberate (DSS; 1 μL at 2 mg/mL) for 180 min at room temperature to detect the presence of non-covalent complexes. High-mass MALDI-TOF mass spectra from 0 to 2000 kDa were obtained using a Bruker Autoflex II ToF-ToF mass spectrometer equipped with a CovalX HM4 interaction module. Neither β-B75KN nor FH showed evidence of aggregation or significant deviations from the expected molecular weight. A similar approach was used to characterize the β-B75KN/FH complex, with the exception that a sample consisting of 1.1 μM β-B75KN and 1.7 μM FH was prepared and analyzed both with and without DSS crosslinking as described above. All analyses were repeated in triplicate.

Next, a peptide mass fingerprint was obtained for FH by proteolytic digestion followed by characterization of the products using nanoscale liquid chromatography coupled to tandem mass

spectrometry. Samples of FH that had been reduced and alkylated using standard approaches were digested overnight with either trypsin, chymotrypsin, ASP-N, elastase, or thermolysin. Following acidification by adding formic acid to 1% (v/v) final concentration, the reaction contents were separated on an UltiMate 3000-RSLC nano-LC system equipped with a C_{18} PepMapRSLC column and analyzed in-line using an LTQ-Orbitrap MS/MS mass spectrometer (ThermoFisher Scientific). A total of 89.68% of the 1231 residue FH sequence was covered by combining the individual digests maps of trypsin (69 peptides covering 60.92%), chymotrypsin (78 peptides covering 62.22%), ASP-N (2 peptides covering 1.78%), elastase (56 peptides covering 41.83%), and thermolysin (84 peptides covering 60.35%).

Finally, to define the β-B75KN binding site on FH, a sample containing both proteins was crosslinked and characterized. β-B75KN/FH (20 μL prepared as described above) was incubated with an isotopically defined mixture of DSS (2 μL of a 2 mg/mL solution containing equal quantities of d_0/d_{12}) for 180 min at room temperature. Following reduction and alkylation, the sample was proteolyzed as described above, acidified, and processed by nanoLC-MS/MS. Crosslinked peptides were identified in the resulting mass spectra using the Xquest v2.0 (46) and Stavrox v3.6 (47) software packages.

Parental Bacterial Strains and Construction of Heterologous Expression Vectors

The organisms used in this study are previously described isogenic GBS A909 strains (wildtype, Δ*bac* and Δ*bac* + pLZ.*bac*) (32) and isogenic *L. lactis* MG1363 strains constructed in this study as described below. GBS were cultured at 37 ºC in Todd-Hewitt Broth (TH), which was supplemented with 70 μg/mL spectinomycin for growth of the A909Δ*bac* + pLZ.*bac* strain. *L. lactis* were cultured at 30 ºC in M17 Broth supplemented with 0.5% (w/v) glucose and 0.5% (w/v)

lactose (GM17), additionally supplemented with 5 μg/mL erythromycin for growth of strains carrying pOri23 vectors.

Derivatives of the pOri23 *E. coli* - *L. lactis* shuttle vector were constructed and used for heterologous expression of β protein in *L. lactis* (48). PCR was used to amplify the *bac* gene from GBS strain A909 using the specific primers (containing a restriction site, *bac* specific sequence) BamHI-*bac*-F (5'- TATGAATGACAATGATGTTGGATCCATGTTTAAATCTAATTATG-3') and SalI-*bac*-R (5'-ATCGATAAGCTTGGCTGCAGGTCGACTCATGATTTTCTTCTTTTCATTGC-3') and Phusion High-Fidelity DNA polymerase (ThermoFisher). Standard protocol reaction mixtures were utilized with thermocycling conditions of 2 min at 98 °C, 35 cycles of 15 sec at 98 °C, 30 sec at 62 °C, and 3 min at 72°C, followed by 5 min at 72 °C. DNA of an amplicon of expected size (3.4 kb) was purified from a 1% (w/v) agarose using GeneJET Gel Extraction Kit (ThermoFisher), digested with *BamH*I and *Sal*I (New England Biolabs) and ligated into *BamH*I/*Sal*I linearized pOri23 vector following manufacturer's protocols. The product was transformed into *E. coli* DH5α cells and transformants were selected for by growth at 37 °C on LB agar supplemented with 500 μg/mL erythromycin. Transformants carrying pOri23 vectors containing the *bac* gene were screened by colony PCR using DreamTaq Green PCR master mix 2X (ThermoFisher) and primers amplifying across the *bac* insert of pOri23.

The wild-type pOri23.*bac* vector was used as the template for inverse PCR to construct (i) pOri23.*bac*ΔB75KN, a vector encoding β protein with an in-frame deletion of the B75KN domain (residues 504 to 788), using primers specific to the IgI3 (5'-GATCCGCGGCCGCTTGTTTCTCCTCTTTCTTTTGC-3') and XPZ (5'-GATCGCGGCCGCGACGCCAGAAACTCCAGATACACCG-3') domains and containing *Not*I

restriction sites, and (ii) pOri23.*bac*ΔFHBD, a vector encoding β protein with an in-frame mutation of the FH-binding QHLQKKN loop (FHBD; residues 223-QHLQKKN-229 to GAPG), using primers specific to the upstream (5'-AAGGTTTTAGATGGAGTTCATGGCGCGCCGGGCGATC-3') and downstream (5'-GATCGCCCGGCGCGCCATGAACTCCATCTAAAACCTT-3') sequence of the FHBD and containing *Asc*I restriction sites. Standard protocol reaction mixtures of Phusion High-Fidelity DNA polymerase (ThermoFisher) were utilized with thermocycling conditions of 2 min at 98 °C, 25 cycles of 15 sec at 98 °C, 30 sec at 62 °C, and 5 min at 72 °C, followed by a final cycle of 5 min at 72 °C. The resultant linearized PCR product was digested with *Dpn*I (Promega) following standard protocols and transformed into *E. coli* DH5α cells. Transformants carrying pOri23 vectors containing the *bac* gene inserts were screened by colony PCR using DreamTaq Green PCR master mix 2X (ThermoFisher).

Generation and Characterization of Heterologous Expression Strains of L. lactis

For heterologous expression experiments, competent *L. lactis* were produced by culturing bacteria in GM17 media (M17 media, 0.5% (w/v) glucose, 0.5% (w/v) lactose) supplemented with 0.5 M sucrose at 30 °C until mid-log phase (OD_{600} = 0.7). Bacteria were incubated at 4 °C for 10 min then centrifuged at 4000 rpm for 15 min, washed 3 times by resuspending in 3 mL Electroporation Buffer (0.5 M sucrose, 10% (v/v) glycerol), centrifuging at 4000 rpm for 15 min, and removing the supernatant. *L. lactis* was transformed with pOri23 vectors by electroporation using a 1 mm-gap electroporation cuvette at 1.2 kV and recovered by growth in M17 medium + 0.5 M sucrose + 0.5% (w/v) glucose + 20 mM $MgCl_2$ + 2 mM $CaCl_2$ at 30 °C for 2 h. Transformants were selected by growth at 30 °C on GM17 agar plates supplemented with 5 μg/mL erythromycin.

Heterologous expression of β protein by *L. lactis* stains was examined by a combination of gel electrophoresis and flow cytometry analysis. For electrophoresis studies, 1 mL of bacteria that had been cultured overnight were pelleted, resuspended in 100 μL of Sample Buffer, and heated to 95 ^{o}C for 10 min. Proteins were separated on a 12.5% SDS-PAGE gel, washed in ddH_2O, stained with Biosafe Coomassie Blue stain (BioRad) and de-stained with ddH_2O to allow for visualization of polypeptide bands. Surface expression of β protein by the same strains was also examined by flow cytometry using a previously described rabbit anti-β serum (49). Mid-logarithmic phase bacteria were incubated at room temperature for 45 min with either 0.1% (v/v) rabbit anti-β serum or normal rabbit serum as a control. The samples were washed in PBS + 0.5% (w/v) BSA and incubated at room temperature for 45 min with a 1:1000 dilution of FITC-conjugated goat anti-rabbit-IgG prior to detection (Life Technologies). Fluorescence of bacteria was measured by flow cytometry after washing in PBS + 0.5% (w/v) BSA and fixation in 1% (w/v) PFA.

Flow Cytometry Measurements of FH, C3b, and iC3b on the Surface of L. lactis

The FH-binding properties of *L. lactis* strains expressing either wild-type or mutant β proteins was examined by flow cytometry. FITC-labelled FH was prepared as previously described (50). Mid-logarithmic phase cells representing each strain were then incubated at room temperature for 45 min with either 5 μg/mL FH-FITC or buffer as a control. Fluorescence of bacteria was measured by flow cytometry after washing in PBS + 0.5% (w/v) BSA and fixation in 1% (w/v) PFA.

Levels of C3b deposition on *L. lactis* cells following exposure to human serum were measured by flow cytometry. Cells of stationary phase *L. lactis* strains were incubated at 37 ^{o}C for 30 min with either 3% (v/v) pooled human serum (AS) or heat-inactivated pooled serum (HIS). Bacteria were washed by adding 100 μL of PBS, followed by centrifugation at 4000 rpm for 5

min, and removal of the supernatant. Cells were then stained with a 1:2000 dilution of goat anti-C3b-FITC pAb (MP Biomedical) at 4 ^{o}C for 60 min. Bacteria were washed with PBS before fixing in 1% (w/v) PFA. Fluorescence of bacteria was measured by flow cytometry. The results of each trial were expressed as the geometric mean of the fluorescence signal.

Levels of iC3b deposition on *L. lactis* cells were likewise measured by flow cytometry. Stationary phase *L. lactis* cells were incubated at 37 ^{o}C for 45 min with either 3% (v/v) AS or HIS as a control. Bacteria were washed in PBS and stained by incubating on ice for 45 min with either 5 μg/mL mouse anti-iC3b-neoantigen-IgG pAb (BioRad), 5 μg/mL mouse isotype control (eBiosciences), or goat anti-C3b-FITC (MP Biomedical). PE-conjugated goat anti-mouse-IgG (1:1000, Life Technologies) was used for detection of mouse antibodies. All samples were washed in PBS and fixed in 1% (w/v) PFA prior to measurement of fluorescent signals by flow cytometry.

Measurements of C3b Deposition on L. lactis by Western Blot

Stationary phase cells from various *L. lactis* strains were incubated with 30% (v/v) AS for indicated time periods. Bacteria were washed 5 times by addition of 100 μL PBS, centrifuged at 4000 rpm for 5 min, and the supernatant was removed. Cell pellets were resuspended in Sample Buffer, boiled, and separated by SDS-PAGE. Separated proteins were blotted onto a nitrocellulose membrane, blocked in 5% (w/v) non-fat dry milk, washed in TBS-T buffer (20 mM Tris, 150 mM NaCl, 0.1% (v/v) Tween-20, pH 7.4), and stained with a 1:10,000 dilution of goat anti-C3 mAb (Complement Technology) at 37 ^{o}C for 1 h. Following this, the membrane was washed in TBS-T buffer, stained with a 1:10,000 dilution of HRP-conjugated donkey anti-goat-IgG (Jackson Laboratory) at 37 ^{o}C for 1 h, and washed with TBS-T buffer. Chemiluminescent signals were detected using ECL Western Blot Substrate (Promega).

SPR Measurements of C3 Convertase Formation and Decay

The convertase decay accelerating activity of FH was assessed by an SPR method as previously described (16,51). Site-specifically biotinylated C3b (52) was captured on three different experimental flow cells of an SA sensor chip (Cytiva Life Sciences) at final ligand densities of 1275, 1480, and 1055 RU, while a reference flow cell was prepared by capturing biotin alone. All experiments were performed at 25 °C on a Biacore T-200 instrument (Cytiva Life Sciences) using a running buffer of HBS-T supplemented with 5 mM $MgCl_2$ and a flowrate of 10 μL/min. Each experiment consisted of two separate injection events: the first injection occurred for 2 min followed by a 1 min dissociation phase and a brief stabilization period, while the second injection occurred for 2 min followed by a 3 min dissociation phase. All individual analytes or mixtures thereof were used at a final concentration of 500 nM. Regeneration of the surface was achieved by a 30 sec pulse of 2 M NaCl + 10 mM EDTA, followed by two consecutive pulses of 0.1 M sodium acetate (pH 4.0). Estimates for the apparent rate constant of convertase decay were obtained by fitting the 150 sec period following the second injection stop to a one-phase exponential decay curve in GraphPad Prism v9.2.0.

Interactions of site-specifically immobilized C3b with either FH alone or pre-formed B75KN/FH or B6C-IgI3-B74KN/FH complexes were assessed using the same sensor chip and buffer system described above, but with a flow rate of 20 μL/min. Each experimental cycle consisted of a 2 min injection followed by a 3 min dissociation phase and used the same regeneration sequence outlined above. Analytes were injected over the biosensor surface in reference subtraction mode using a two-fold series of increasing concentrations ranging from 15.6 nM to 500 nM. Sensorgram series were analyzed with a simple affinity (dose/response) model to derive an apparent K_D without regard to kinetic parameters using Biacore T-200 Evaluation software v3.2 (Cytiva Life Sciences).

Analysis of FH Cofactor Activity for FI-mediated Degradation of C3b

The purity of C3b, FI and FH (Complement Technology) was assessed by separation on a 12.5% SDS-PAGE gel under non-reducing conditions. 250 μL of stationary phase bacteria (washed and resuspended to an absorbance of OD_{600}=2.0) were pelleted in a 1.5 mL Eppendorf tube and incubated at 37 ºC for 60 min in either 100 μL of HBS^{+++} buffer (20 mM HEPES (pH 7.4), 140 mM NaCl, 5 mM $CaCl_2$, 2.5 mM $MgCl_2$ and 0.5% (w/v) BSA) or HBS^{+++} buffer supplemented with 10 μg/mL of purified FH. Bacteria were washed 5 times by addition of 1 mL HBS^{+++} buffer, followed by centrifugation at 4000 rpm for 5 min and removal of the supernatant. Resuspended bacteria were transferred to sterile 1.5 mL Eppendorf tubes after each washing step. Bacterial pellets were resuspended in 50 μL of HBS^{+++} containing 10 μg/mL C3b and 10 μg/mL FI and incubated at 37 ºC for 30 min. Bacteria were pelleted by centrifugation at 4000 rpm for 5 min. The supernatant was transferred to a sterile 1.5 mL Eppendorf tube. For control samples, 50 μL of HBS^{+++} containing 10 μg/mL C3b and 10 μg/mL FI supplemented with or without 10 μg/mL FH was incubated at 37 ºC for 30 min. Samples were mixed with Sample Buffer containing β-mercaptoethanol and processed for anti-C3 immunoblot as described above. Densitometry analysis was performed using the open-source image processing package FIJI to determine the mean density of β band and α'45 fragment band.

Functional Assays of Immune Evasion

Three independent assays were used to assess the role of FH-binding by β in promoting resistance to the innate immune system. Direct killing by complement was assessed by measuring the survival of various *L. lactis* strains following exposure to human serum. 50 μL of mid-logarithmic phase bacteria (resuspended to 1 $x10^6$ CFU/mL in HBS^{++} buffer (20 mM HEPES (pH 7.4), 140 mM NaCl, 5 mM $CaCl_2$, 2.5 mM $MgCl_2$) and 85 μL of HBS^{++} were combined with either

15 μL of 100% pooled human serum (AS) or 100% heat-inactivated pooled human serum (HIS). Reactions were then mixed and incubated at 37ºC. Samples were collected at designated time points, serially diluted in sterile PBS, plated onto M17 agar plates, and cultured at 37 ºC overnight to allow for colony development. The results of each trial were expressed as CFU normalized to a control group.

Resistance of various *L. lactis* strains to phagocytosis by neutrophils was also measured. To begin, FITC-labelled *L. lactis* cells were generated by incubating stationary phase bacteria with 1 mg/mL FITC (Sigma Aldrich) for 30 min. The cells were washed 5 times with PBS to remove excess dye, and the FITC-labeled bacteria were opsonized by incubation with 3% (v/v) AS at 37 ºC for 30 min. Neutrophils were isolated from human blood as previously described (53), pursuant to an ethical approval for draw and use of human blood obtained from the Regional Ethics Committee and Imperial NHS Trust Tissue Bank (REC approval no. 17/WA/0161, ICHTB HTA license no. 12275, ICREC no. 19IC5166). Freshly isolated neutrophils were then incubated with serum opsonized, FITC-labelled *L. lactis* cells at a MOI 10 at 37 ºC for 30 min with shaking. Following the incubation interval, neutrophils were washed with PBS and fixed in 1% (w/v) PFA. Residual extracellular FITC-labeled bacteria were quenched by addition of 250 μg/mL trypan blue dissolved in ice-cold 0.1 M citrate buffer (pH 4.0). Neutrophil fluorescence was then measured by flow cytometry. The results of each trial were expressed as the geometric mean normalized to a control group.

Finally, survival of various *L. lactis* strains was assessed in whole human blood. In these experiments, 150 μL of whole blood and 50 μL of bacteria (Mid-logarithmic phase bacteria resuspended to 1 x10^7 CFU/mL in HBS^{++} buffer) were mixed in a sterile 1.5 mL Eppendorf tube and incubated at 37 ºC with rotation. Samples were withdrawn at designated time points, serially

diluted into sterile PBS, plated onto GM17 agar plates, and cultured at 30 ºC overnight to allow for colony development. The results were expressed as CFU normalized to a control group.

Results

A Novel Domain within the B75KN Region of GBS β Harbors a Binding Site for Factor H

Previous studies have shown that β binds to human FH (32,54), but the biochemical parameters that define this interaction have not been fully investigated through rigorous quantitative approaches. Owing to its large size (~132 kDa) and difficulty with producing the full-length β molecule recombinantly in *E. coli*, we employed a panel of domain deletion fragments of β that are more amenable to structure/function studies (Figure 4.1A). We overexpressed and purified fragments of β consisting of domains B6C-IgI3-B75KN (residues 221-789), B6C (residues 221-389), and B75KN (residues 504-789) as reported in previous publications (37,55). We then immobilized purified human FH on a biosensor surface and injected increasing concentrations of each truncated β protein (up to a maximum of 10 μM) to define the minimal FH-binding site of β and to describe the affinity and kinetics of this interaction.

Consistent with previous reports, we observed that B6C-IgI3-B75KN bound tightly to human FH (Figure 4.1B) (54). Fitting the experimental data from two independent sensorgram series to an approach to equilibrium (i.e. steady state) model resulted in an apparent K_D of 342±10 nM (Table 4.1). Interestingly, we also found that the reference-corrected sensorgram series did not fit well to a simple kinetic model (i.e. 1:1 binding), but rather required a more complex mechanism to explain the data. Incorporation of a separate set of association and dissociation rate constants to account for heterogeneity of FH on the biosensor surface resulted in the highest quality fit of the data to the model. This yielded two independent equilibrium dissociations constants of 279±49

nM and 7.01±1.29 nM (Table 4.1), the former of which was well matched to the K_D derived from the approach to equilibrium model described above.

Since B6C-IgI3-B75KN bound FH with high affinity, we hypothesized that a defined region within this ~66 kDa fragment might be responsible for its FH binding activity. We therefore injected B6C (Figure 4.1C) and B75KN (Figure 4.1D) over the FH surface and found that only the latter fragment retained FH binding activity. Fitting these experimental data to an approach to equilibrium model resulted in an apparent K_D of 595±8.7 nM (Table 4.1); nevertheless, as with B6C-IgI3-B75KN, we found that a ligand heterogeneity model best described the B75KN/FH binding data when analysed for kinetic parameters. Interestingly, the first dissociation constant of 306±4.1 nM corresponded well to that of B6C-IgI3-B75KN, while the second dissociation constant was approximately five-fold weaker at 33.6±0.18 nM (Table 4.1). This indicated that the B75KN region retained high-affinity binding to FH.

Although many classes of FH-binding immune evasion proteins have been described (Reviewed in (21)), certain molecules, including CpbA from *S. pneumoniae* (56) and OspE from *B. burgdorferi* (57), contain defined FH-binding domains of ~150 residues or less. Since the B75KN region of β is over 280 residues in length, we wondered whether it could be truncated further into a discrete FH-binding domain. We therefore used a substoichiometric dilution series of either trypsin or subtilisin to digest B75KN (58), separated the reaction products by SDS-PAGE, and identified various polypeptide species that appeared resistant to further proteolytic degradation (59) (Figure 4.1E). We found that B75KN could be truncated by either trypsin or subtilisin into fragments corresponding to a N-terminal domain (residues 504-687, hereafter B75KN-NTD) and a C-terminal domain (residues 688-789, hereafter B75KN-CTD). Thus, we prepared these two novel fragments of the β protein for characterization.

When we injected these proteins over the FH surface, we observed that B75KN-NTD lacked FH-binding activity (Figure 4.1E) but that B75KN-CTD retained this function (Figure 4.1F). Fitting these data to an approach to equilibrium model yielded an apparent K_D of 864±3 nM (Table 4.1), which was comparable to that of B75KN (595±8.7). Further kinetic analysis of the data using a ligand heterogeneity model revealed two independent equilibrium dissociation constants of 394±35.9 nM and 2160±788 nM (Table 4.1). Whereas the first of these K_D values corresponded well to the same parameter for B6C-IgI3-B75KN (279±44 nM) and B75KN (306±4.1 nM), the second K_D value for B75KN-CTD was greatly diminished when compared to its larger counterparts (7.01±1.29 and 33.6±0.18 nM, respectively). This suggested that the FH-binding site within B75KN-CTD was described by the first set of constants (Table 4.1), while removal of regions N-terminal to B75KN-CTD essentially eliminated the FH-binding site described by the second set of constants. In fact, we found the B75KN-CTD/FH binding data could be well fit to a simple kinetic model, which yielded a K_D value of 458±30 nM (Table 4.1); this value was in good agreement with the K_D from first set of constants derived from fitting to the ligand heterogeneity model. Thus, while the interaction between β and FH is complex and seems to involve two unique binding sites, the B75KN-CTD domain identified here is a major determinant of FH binding to β.

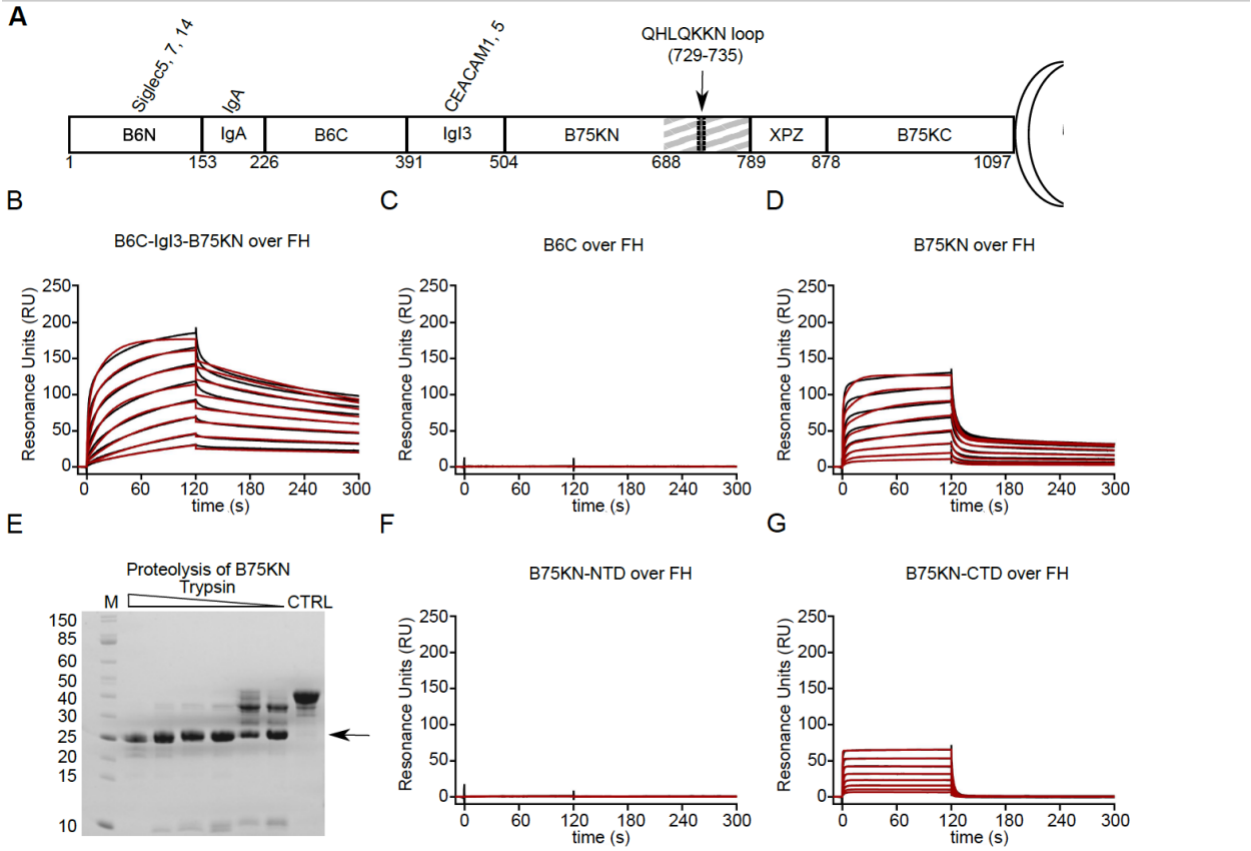

Figure 4.1. A Protease-Stable Domain within the B75KN Region of GBS β Harbors a Binding Site for Factor H.

(A) Schematic representation of the β protein showing location of key domains. The shaded area indicates the minimal binding site of human factor H (FH) located in the C-terminal region of B75KN. The arrow indicates the location of the putative factor H binding loop of the sequence QHLQKKN. (B) SPR series for binding of the B6C-IgI3-B75KN fragment to immobilized FH showing both the experimental data (black traces) and the fit to a ligand heterogeneity model (red traces). (C) SPR series for binding of the B6C fragment to immobilized FH showing both the experimental data (black traces) and the fit to a ligand heterogeneity model (red traces). (D) SPR series for binding of the B75KN fragment to immobilized FH showing both the experimental data (black traces) and the fit to a ligand heterogeneity model (red traces). (E) Limiting proteolysis of B75KN by trypsin. A fixed concentration of the purified B75KN fragment (ctrl) was incubated with increasing concentrations of trypsin for 30 min prior to separating the reaction products by SDS-PAGE. The polypeptide species at ~25 kDa indicated by the arrow was characterized by tryptic-peptide mass fingerprinting. Molecular size standards (M) are shown at the left of the gel image. (F) SPR series for binding of the B75KN-NTD fragment to immobilized FH showing both the experimental data (black traces) and the fit to a ligand heterogeneity model (red traces). (G) SPR series for binding of the B75KN-CTD fragment to immobilized FH showing both the experimental data (black traces) and the fit to a ligand heterogeneity model (red traces). The parameters derived from analysis of various SPR series are found in **Table 4.1**.

Table 4.1. Interaction Parameters for Various β Fragments with Immobilized Human FH[a]

Analyte	Model	k_{a-1} (10^4 $M^{-1}s^{-1}$)	k_{d-1} (10^{-3} s^{-1})	K_{D-1} (nM)	k_{a-2} (10^4 $M^{-1}s^{-1}$)	k_{d-2} (10^{-3} s^{-1})	K_{D-2} (nM)
β-B6C-IgI3-B75KN	Affinity[b]	-	-	342±10	-	-	-
	Simple Kinetic[c]	6.19±0.16	2.42±0.05	39.1±1.8	-	-	-
	Ligand Heterogeneity[d]	1.50±0.11	4.17±0.34	279±44	17.00±0.06	1.19±0.22	7.01±1.29
β-B75KN	Affinity	-	-	595±8.7	-	-	-
	Simple Kinetic	5.18±0.04	3.74±0.01	72.1±0.7	-	-	-
	Ligand Heterogeneity	57.4±1.03	176±0.78	306±4.1	4.35±0.04	1.46±0.06	33.6±0.18
β-B75KN-CTD	Affinity	-	-	864±3.0	-	-	-
	Simple Kinetic	70.9±3.01	324±7.50	458±30	-	-	-
	Ligand Heterogeneity	100±8.04	394±4.38	394±35.9	0.17±0.07	4.00±2.86	2160±788

[a]All values are presented at their mean ± standard deviation obtained for two replicate injections over the biosensor surface.
[b]Model accounts for observed binding response as a function of analyte concentration alone.
[c]Model accounts for a single binding site between the analyte and ligand described by one association and dissociation rate constant.
[d]Model accounts for two analyte binding sites on the ligand each described by a set of association and dissociation rate constants.

Crystal Structure of the B75KN-CTD Reveals a Helical Bundle Motif Common to Bacterial Innate Immune Evasion Proteins

Although the experiments described above defined B75KN-CTD as the minimal FH-binding fragment of β, high resolution structural information is only available for the so-called IgI3 domain that corresponds to residues 392-507 (Figure 4.1A) (37). Consequently, we pursued structural studies of B75KN-CTD to provide further insight into the physical features underlying FH binding by β. We crystallized a Seleno-L-methionine-labeled form of the B75KN-CTD, collected single-wavelength anomalous diffraction data using a synchrotron X-ray source, and solved its structure to 2.5 Å limiting resolution (Table 4.2). Following a combination of automated building and manual rebuilding, we refined our model to R_{work} and R_{free} values of 24.3% and 29.1%, respectively (Table 4.2).

The asymmetric unit of the B75KN-CTD crystal contains two copies of the protein related by a non-crystallographic symmetry axis (Figure 4.2A, B). In general terms, the final model of each polypeptide consists of residues 736-824 of β with the exception that positions 764-768 could

not be modelled due to weak electron density in this area (Figure 4.2A, B). The structure of B75KN-CTD is defined by a three α-helix bundle fold. Variations on this motif are especially common among innate immune evasion proteins from Gram-positive bacteria, including the staphylococcal peroxidase inhibitor, SPIN (60,61), the staphylococcal complement evasion proteins Efb (62), Ehp/Ecb (63), SCIN-A (64), and SCIN-B (52), and the FH-binding protein CbpA/PspC from *S. pneumoniae* (56). In this particular case, the long axes of the secondary structure elements helix α1 (appox. Ser-737 to Leu-758), helix α2 (approx. Ile-773 to Asn-793), and helix α3 (approx. Glu-797 to Leu-822) are found in a nearly perfect anti-parallel arrangement with one another (Figure 4.2B). The hydrophobic sidechains found at the interfaces between these helices are also highly complementary to one another and appear to serve as a molecular zipper that holds the helical bundle together. Together, this imparts a compact, cylindrical shape to B75KN-CTD with overall dimensions of approximately 50 Å in length and 20 Å in diameter.

A QHLQKKN-containing Loop in B75KN-CTD Mediates Binding of FH to β

B75KN-CTD shares relatively weak amino acid similarity to known FH-binding proteins, which precluded use of sequence relationships to help us define its FH binding site. Moreover, visualization of the B75KN-CTD structure as a molecular surface revealed that it was essentially devoid of prominent grooves or electrostatic features that might suggest a clear role in FH binding. Consequently, we turned our attention to the loop consisting of residues 763-769, which connects helices α1 and α2 (Figure 4.2B). Although this loop contains several positions (i.e. 764-768) that could not be modelled in the B75KN-CTD structure, our premise was that its sequence, QHLQKKN, was rich in hydrogen bond donors/acceptors that might facilitate protein-protein interactions and that it may also be highly dynamic in the absence of a binding partner.

To test whether the QHLQKKN loop played a role in FH binding, we constructed site-directed mutants of two β fragments that otherwise bound FH with high affinity (Table 4.1). We replaced all seven of the QHLQKKN residues with a tetra-glycine linker sequence to remove all sidechain-derived chemical groups in both B75KN (hereafter B75KN-ΔG_4) and B75KN-CTD (hereafter B75KN-CTD-ΔG_4) (Figure 4.2C, D). Following expression and purification of each mutant, we observed that both B75KN-ΔG_4 and B75KN-CTD-ΔG_4 were significantly impaired in their ability to bind immobilized FH in an SPR assay. Whereas the apparent K_D of B75KN-ΔG_4 was 13.8±0.8 μM and was diminished by greater than 20-fold when compared wild-type B75KN (Figure 4.2E and Table 4.1), we found that the smaller fragment B75KN-CTD-ΔG_4 failed bind immobilized FH at all (Figure 4.2F). Together, these data revealed that the residues found within the QHKQKKN loop that connects helices α1 and α2 of β-B75KN-CTD are a major determinant of GBS β FH binding activity.

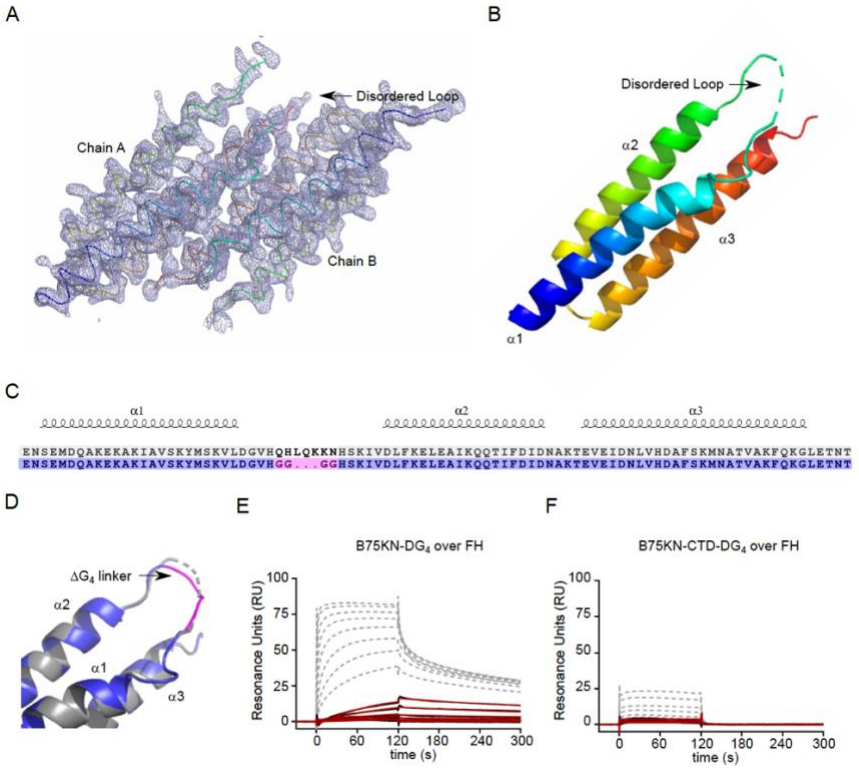

Figure 4.2. Structural Analysis of B75KN-CTD and Identification of its FH-binding Site.

(A) Representation of the asymmetric unit for the B75KN-CTD crystal structure determined at 2.5 Å limiting resolution and refined to an Rfree value of 29.1% showing the correlation of the final 2Fo-Fc electron density map contoured at 1.3σ (blue mesh) with the model containing two copies of the B75KN-CTD protein (colored wire). Individual polypeptides are depicted with their N-terminus in blue and their C-terminus in red. Note the location of the disordered loop in each copy that could not be modelled due to weak electron density in that region. (B) Representation of B75KN-CTD as a cartoon diagram with its N-terminus in blue and its C-terminus in red. The locations of the secondary structure elements and the disordered loop are labelled. This image was drawn from Chain A of the final model. (C) Sequence/structure alignment comparing the N-through C-terminus of the B75KN-CTD model (top) with the B75KN-CTD-ΔG4 loop deletion mutant (bottom). Residues matching wild type are highlighted purple in the bottom sequence, while the residues changed as highlighted pink. The location of secondary structure elements is presented at the top of the panel. (D) Structural superposition of the wild-type B75KN-CTD protein (grey cartoon) with an energy minimized model of the B75KN-CTD-ΔG4 mutant (purple cartoon). The glycine residues introduced in the mutant protein are colored pink. (E) SPR series for binding of the B75KN-ΔG4 mutant to immobilized FH showing both the experimental data (black traces) and the fit to a ligand heterogeneity model (red traces). An equivalent SPR series for binding of wild-type B75KN is shown for comparison (dotted grey traces). (F) SPR series for binding of the B75KN-CTD-ΔG4 mutant to immobilized FH showing both the experimental data (black traces) and the fit to a ligand heterogeneity model (red traces). An equivalent SPR series for binding of wild-type B75KN-CTD is shown for comparison (dotted grey traces).

Table 4.2. X-ray Diffraction Data Collection and Refinement Statistics

	β–B75KN-CTD (7S0R)
Data Collection	
Space group	*P* 3_1 2 1
Cell dimensions	
a, *b*, *c* (Å)	56.84 56.84 137.41
Resolution (Å)	50.00-2.50 (2.59-2.50) *
Completeness (%)	99.8 (99.8)
$I / \sigma I$	11.8 (3.4)
R_{pim}	0.053 (0.424)
$CC_{1/2}$	0.983 (0.847)
Redundancy	14.3 (9.5)
Phase Calculation	
Figure of Merit	0.30
No. Sites	6
Refinement	
Resolution (Å)	33.53-2.50
No. reflections	9,290
R_{work} / R_{free} (%)	24.3 / 29.1
No. atoms	1,320
Ramachandran Plot	
Favored / Allowed (%)	95.6 / 4.4
B-Factors	
Range & Mean (Å^2)	49.21-143.18 (75.96)
R.M.S. Deviations	
Bond lengths (Å)	0.008
Bond angles (°)	0.87

*Values in parentheses are for highest-resolution shell.

The B75KN Fragment Binds FH at a Key Regulatory Site within its CCP3 and CCP4 Domains

Whereas our previous experiments identified the FH-binding site within B75KN-CTD, they did not provide any insight into the location of the B75KN binding site within FH. Indeed, FH is comprised of 20 tandem CCP4/SCR repeats and numerous unique evasion protein binding sites have been mapped to either individual CCP4/SCR domains or adjacent combinations thereof (summarized in (21)). In light of the many possibilities, we opted against a candidate screening approach and instead used protein crosslinking followed by characterization of the crosslink sites to define the β binding site within FH. We employed the B75KN fragment and serum-purified

human FH for this purpose since the apparent affinity of this interaction (Table 4.1) was well-matched to the concentrations of proteins used to generate the crosslinked complex for subsequent analysis (*see Materials & Methods*).

We began by obtaining high-mass MALDI-TOF spectra of B75KN and FH to control for the presence of aggregates or other non-uniform behavior in the samples. We found that the main peak in the spectra of both B75KN (34.138 kDa_{obs} vs 33.759 kDa_{exp}) and FH (154.222 kDa_{obs} vs 137.025 kDa_{exp}) corresponded well to the expected mass of each protein (Figure 4.4A, D), not accounting for any post-translational modifications such as N-linked glycans in FH. Furthermore, when we repeated this analysis for both proteins individually following incubation with bifunctional amine reactive crosslinker, DSS, we observed that neither protein was prone to formation of higher molecular weight species (Figure 4.3A, D & Figure 4.4B-C, E-F). This demonstrated that B75KN and FH on their own behaved as monomers under the experimental conditions used for cross-linking. However, when we incubated a mixture of B75KN and FH in the presence of DSS, we observed the formation of a single higher molecular weight peak (195.218 kDa_{obs}) that was consistent with a binary complex of B75KN/FH (Figure 4.3C). This indicated that a defined crosslinked species could be generated and further characterized through analytical methods.

To characterize the B75KN/FH binary complex in greater detail, we next generated a peptide mass fingerprint of FH using multi-enzyme proteolysis coupled to nanoscale LC-MS/MS analysis. Digestion of FH alone with either trypsin, chymotrypsin, ASP-N, elastase, or thermolysin, resulted in identification of 289 overlapping peptides (*see Materials & Methods*). Only two segments of greater than 20 residues, spanning positions 796-826 (domains 13-14) and 1092-1125 (domains 18-19), were absent from the FH coverage map. There was also no coverage

of positions 529, 1029, and 1095, all of which are Asn residues predicted to be modified by N-linked glycans (65). Nevertheless, the composite coverage map represented ~90% of the FH sequence and included portions of all 20 domains of FH (*Data Not Shown*).

Using this information to guide localization of B75KN/FH interfaces, we then incubated a sample containing both proteins with an isotopically-defined mixture of DSS reagent that allows for rapid identification of cross-linked species in protease digested samples (46,47). In this manner, we identified a total of six crosslinked peptides with amino acids derived from both B75KN and FH (Table 4.3). Although we used the entire B75KN fragment for this set of experiments, we only detected crosslinks within residues from its B75KN-CTD domain. Visualization of these peptides within the B75KN-CTD structure revealed that they corresponded to four unique segments, one of which overlaps with the C terminal-most positions in the QHLQKKN loop required for FH binding (Figure 4.4G & Table 4.3). Thus, our crosslinking analysis was internally consistent with the mutagenesis data above (Figure 4.2E, F).

When we examined the locations of the FH-derived peptides, however, we made the surprising observation that they corresponded to FH domains 3 and 4 (Table 4.3). Visualization of these peptides within the FH(1-4) crystal structure (66) revealed that they corresponded to four unique segments which accounted for nearly half of the residues in domains 3 and 4 (Figure 4.3D, upper). Although FH(1-4) represents only ~20% of the full-length FH protein (Figure 4.3D, lower), it constitutes a major complement regulatory region of this molecule (15,66). The purported lariat-like structure of full-length FH, along with two separate polyanion binding sites found in domains 7 and domains 19 and 20, is believed to display domains 1-4 away from FH-bound surfaces (67); this favorable C3b-binding orientation allows the convertase decay and FI-cofactor activities of FH(1-4) to be most fully realized at surfaces susceptible to complement attack (67). In this regard,

the B75KN binding site appears to be entirely accessible in crystal structures of FH(1-4)/C3b (Figure 4.3E & Figure 4.4H; (66)) and mini-FH/C3b/FI (Figure 4.3F & Figure 4.4I; (68)). This strongly suggested that FH recruited to the GBS surface by β would retain its complement regulatory activities and benefit bacterial complement evasion. Indeed, previous reports have also shown that FH maintains its function as a negative regulator of complement activation, albeit when sequestered by pathogens other than GBS (69,70).

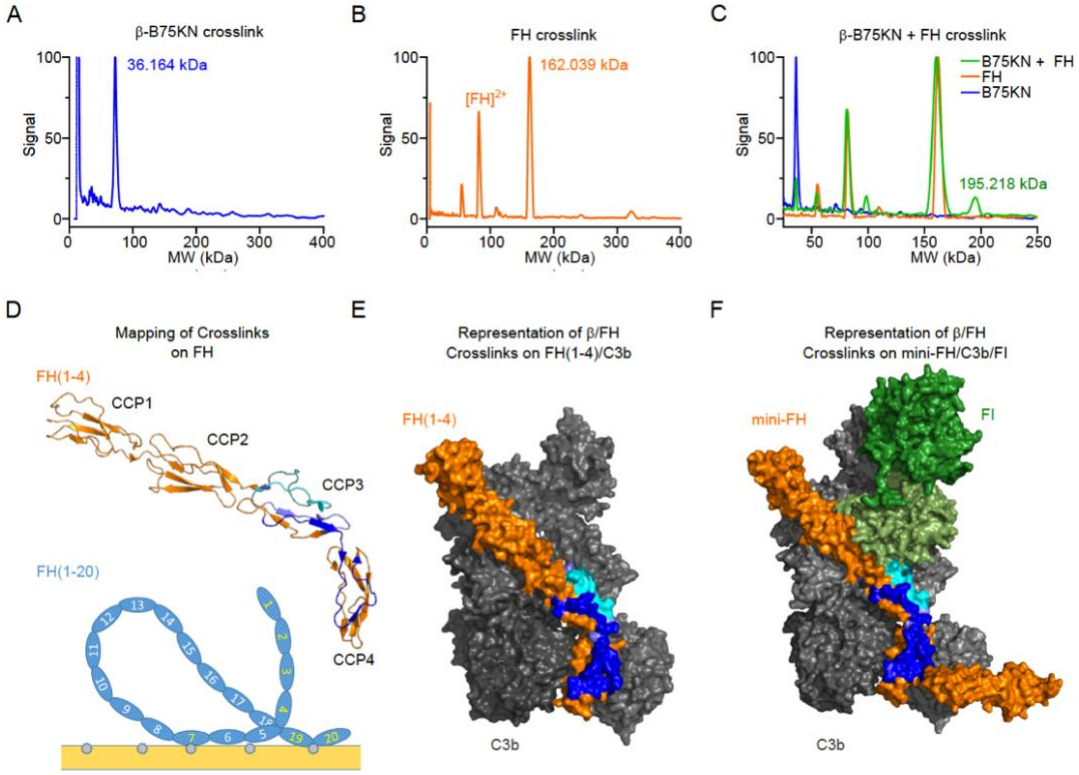

Figure 4.3. The B75KN Region of β protein Binds FH in the CCP3 and CCP4 Modules.

(A) High-mass MALDI-TOF spectrum of a sample of B75KN following treatment with the bifunctional amine-reactive crosslinker DSS. (B) High-mass MALDI-TOF spectrum of a sample of FH following treatment with the bifunctional amine-reactive crosslinker DSS. The peak corresponding to a doubly charged species is labelled. (C) Comparison of high-mass MALDI-TOF spectra for a sample of either crosslinked B75KN plus factor H (FH; green) with that of either B75KN (blue) or FH (orange) alone. The peak corresponding to the B75KN/FH complex is labelled. (D) Representation of the site of B75KN crosslinks within FH. The structure of FH (1-4) is shown as a cartoon diagram (orange) with the locations of B75KN-crosslinked peptides

highlighted (blue). A model of the lariat-like structure for full-length FH adsorbed to a sialic acid (grey) bearing surface (orange) is shown at the bottom left. The individual domains are numbered highlighting domains 1-4 as a complement regulatory region and domains 7 and 19-20 as polyanion binding sites (15). (E) Representation of the site of B75KN crosslinks with FH in the context of the FH(1-4/)C3b complex (66). FH (1-4) (orange) and C3b (grey) are rendered as molecular surfaces with the cross-linked peptides highlighted (blue). Note that the crosslinked peptides are solvent accessible in this complex. (F) A similar image to panel E, but within the context of the mini-FH/C3b/FI complex (68). Mini-FH (orange), C3b (grey), and FH green) are rendered as molecular surfaces with the cross-linked peptides highlighted (blue). Note that the presence of FI does not appear to change the solvent accessibility of the crosslinked peptides. (A-C were done by CovalX, Inc.)

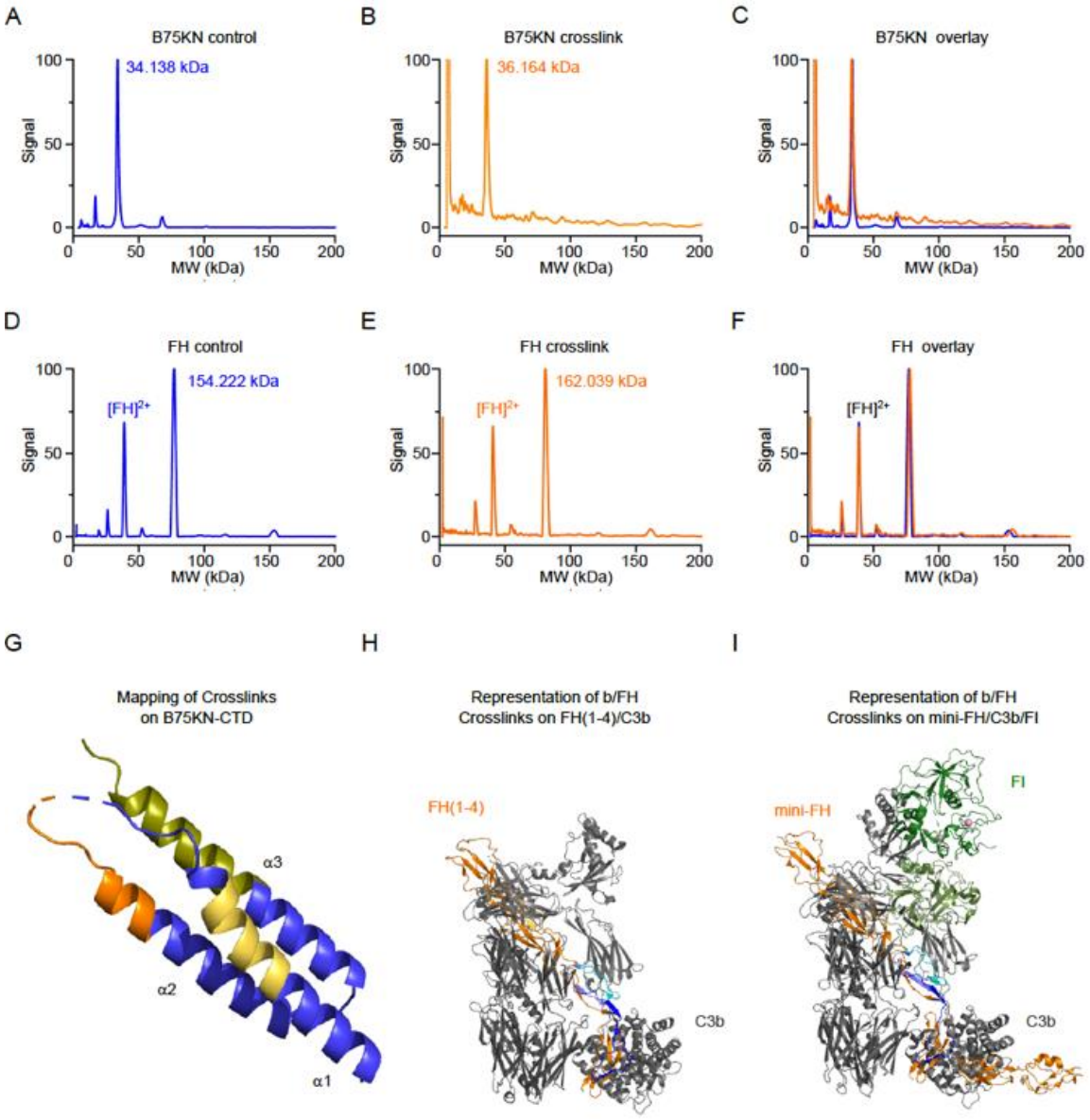

Figure 4.4. Supporting Information for the B75KN/FH Crosslinking Study.

(A) High-mass MALDI-TOF spectrum for a sample of B75KN protein. (B) Same as panel A, with the exception that the B75KN sample had been treated with the bifunctional amine-reactive crosslinker DSS. (C) Spectral overlay of the untreated (blue) and DSS-treated (orange) samples of B75KN. (D) High-mass MALDI-TOF spectrum for a sample of FH. The peak corresponding to the doubly charged species is labelled. (E) Same as panel D, with the exception that the FH sample had been treated with the bifunctional amine-reactive crosslinker DSS. The peak corresponding to the doubled charged species is labelled. (F) Spectral overlay of the untreated (blue) and DSS-treated (orange) samples of FH. (G) Representation of the sites of FH crosslinks within the B75KN-CTD structure. The structure of B75KN-CTD is shown as a cartoon diagram (blue) with the locations of FH-crosslinked peptides highlighted (gold, yellow, and orange). The disordered loop, which contains FH-crosslinked residues, is shown at the top left-hand corner of the image. (H) Representation of the site of B75KN crosslinks with FH in the context of the FH (1-4)/C3b complex. FH (1-4) (orange) and C3b (grey) are rendered as cartoons with the cross-linked peptides highlighted (blue). (I) A similar image to panel H, but within the context of the mini-FH/C3b/FI complex. Mini-FH (orange), C3b (grey), and FH green) are rendered as cartoons with the cross-linked peptides highlighted (blue). (A-F were done by CovalX, Inc.)

Table 4.3. Identities of Peptide Crosslinks Between the B75KN Region of β and Human FH

Enzyme	β Peptide[a]	FH Peptide[b]	FH Location	Sequence of Crosslinked Peptides[c]
Tryp	768-778	146-156	CCP3	β: KNHS(K)IVDLFK FH: CLPV(T)APENGK
Tryp	818-826	146-156	CCP3	β: FQ(K)GLETNT FH: CLPV(T)APENGK
Tryp	748-756	157-166	CCP3	β: IAV(S)KYMSK FH: IVS(S)AMEPDR
Tryp	768-772	167-183	CCP3	β: KN(H)SK FH: E(Y)HFGQAVRFVCNSGYK
Chym	809-818	199-227	CCP3&4	β: SKMNA(T)VAKF FH: SKEKPKCVEISCKSPDVING(S)PISQKIIY
Chym	809-818	199-227	CCP3&4	β: SKMNA(T)VAKF FH: SKEKPKCVEISCKSPDVINGSPISQ(K)IIY

[a]β numbering corresponds to the reference sequence BAE45252.1 in the GenBank Database
[b]FH numbering corresponds to the reference sequence P08603.4 in the UniProtKB Database
[c]The chemically modified residue in each sequence is designated inside parentheses.
(Experimentswere done by CovalX, Inc.)

FH Binding to β Protein Reduces C3b Deposition on Bacterial Surfaces.

Although previous investigations of intact GBS bacteria have established that cell surface β protein can specifically absorb FH from human serum (32), the implications of the crosslinking data presented above (Figure 4.3& Figure 4.41) prompted us to test directly whether FH bound to β protein maintained its functional activity. Since the majority of GBS strains also express the FH-

binding proteins Sht and ShtII (25,31), we chose to utilize *Lactococcus lactis* as a heterologous expression system to ensure that our functional characterization of β/FH interactions was not confounded by other FH ligands. We cloned the *bac* gene of GBS strain A909 into the pOri23 *E. coli-L. lactis* shuttle vector and used transformed *L. lactis* cells (48) to serve as a wild-type surrogate. However, to study the function of FH-bound by cell surface β protein, we used site-directed mutagenesis to construct pOri23.*bac* derivative vectors with either the entire B75KN domain or the FH-binding QHLQKKN loop (FHBD) mutated. To generate a vector for expression of βΔB75KN, we performed inverse PCR of pOri23.*bac* using primers designed against the B75KN-flanking domains IgI3 and XPZ (Figure 4.1A) to create an in-frame deletion of the B75KN domain. To generate a vector for expression of β protein with mutation of the QHLQKKN loop, we performed inverse PCR of pOri23.*bac* using primers designed upstream and downstream of the FHBD that altered the QHLQKKN sequence to GAPG. We then compared β protein levels of the wild-type and mutant-expressing strains using a combination of electrophoresis and flow cytometry. SDS-PAGE of bacterial lysates revealed that the *L. lactis* strains carrying pOri23.*bac*ΔB75KN and pOri23.*bac*ΔFHBD expressed β protein forms at slightly lower molecular weights than wild-type (Figure 4.5A). Flow cytometry analysis following incubation with antisera raised against β protein likewise confirmed surface expression of β across all experimental *L. lactis* strains (Figure 4.5B). Importantly, both approaches indicated that all three strains showed similar levels of β protein expression to one another.

To assess whether the engineered *L. lactis* strains interacted with human FH as expected, we next used flow cytometry to test each strain for its capacity to bind FITC-labelled FH (Figure 4.5C). We found that FITC-labelled FH bound the wild-type β-expressing strain, which confirmed that β protein can recruit FH to the surface of *L. lactis*. This was consistent with previous

observations using intact GBS bacteria (32). By contrast, we found that the *L. lactis* strains expressing either βΔB75KN or βΔFHBD failed to bind FH. Together, these results showed that β protein binds FH to the surface of *L. lactis* and that this activity is dependent on the FHBD loop within the B75KN domain.

To investigate the functional consequences of FH binding to β protein, we then used flow cytometry to measure C3b deposition onto the surface of *L. lactis* strains following incubation with human serum (Figure 4.5D). We found that expression of wild type β protein led to a significant reduction in total C3b deposition on the surface of *L. lactis* when compared to the control strain ($p<0.01$). By contrast, we observed that *L. lactis* strains expressing either βΔB75KN or βΔFHBD showed a trend toward greater levels of total C3b deposition when compared with the wild-type strain; although loss of the FH-binding loop did not result in differences in C3b levels with wild-type that met the threshold for statistical significance ($p>0.05$), removal of the entire B75KN domain did so ($p<0.01$). In this regard, we noted that β binds to numerous ligands found in the bloodstream (32,34-37), including IgA (35). Thus, recruitment of other molecules by β could have diminished C3b deposition independently of FH binding. Nevertheless, these results showed that β expression suppresses opsonization of the bacterial surface by C3b.

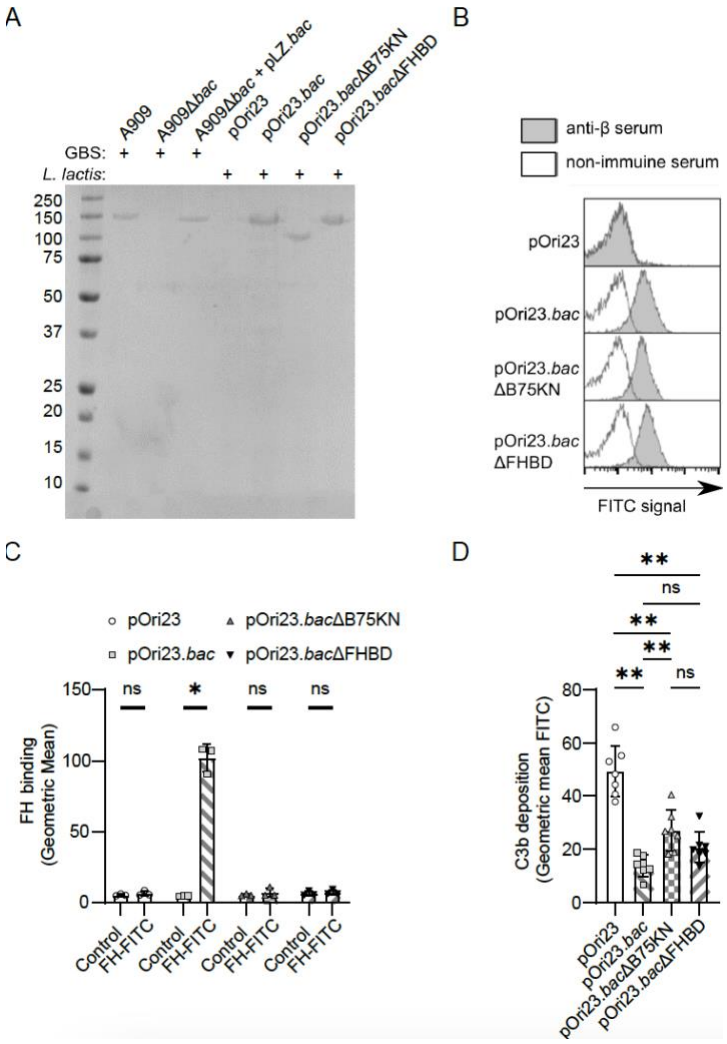

Figure 4.5. β Protein Expression Suppresses C3b Deposition onto the Bacterial Surface.

(A) Expression of β protein by *L. lactis* strains measured by SDS-PAGE analysis. Lysates of stationary phase GBS strains or *L. lactis* strains carrying pOri23, pOri23.bac, pOri23.bacΔB75KN, and pOri23.bacΔFHBD vectors were boiled in sample buffer, separated by SDS-PAGE and stained. (B) Surface expression of β protein by *L. lactis* strains measured by flow cytometry analysis. Mid-log phase *L. lactis* strains were incubated with 0.1% rabbit anti-β serum or normal rabbit serum, washed, stained with FITC-goat anti-rabbit IgG (1:1000) then fixed in 1% PFA. Representative flow cytometry plots of n = 3 replicates are shown. (C) Binding of FITC-labelled FH to the surface of *L. lactis* strains measured by flow cytometry. Mean and standard deviation of n = 3 replicates are shown. (D) Total C3b deposition on the surface of *L. lactis* strains after incubation in human serum. Stationary phase *L. lactis* strains were incubated in 3% human active serum (AS) or heat-inactivated serum (HIS) at 37ºC for 30 min, washed, stained with goat anti-C3-FITC pAb (1:1,000), washed, and fixed in 1% PFA. Total C3b deposition of AS relative to HIS was quantified. Mean and standard deviation of n = 6 replicates are shown. ANOVA was performed to determine statistical significance. (*$p<0.05$, **$p<0.01$). (Experiments were done by Dr. McCarthy's Lab)

FH Bound to β Protein Retains its Complement Regulatory Activities

The structural observations presented above suggested that β-bound FH might retain its canonical complement regulatory activities (Figure 4.3). This assertion was further supported by heterologous expression studies in *L. lactis*, which showed that wild type β recruited FH to the bacterial surface and reduced serum deposition of C3b (Figure 4.5). However, since the β-binding site was unusual insofar as it mapped to key functional region of FH, we sought additional information and investigated the complement regulatory activities of β-bound FH in two established assays. To assess the feasibility of examining the impact of β on FH-mediated convertase decay, we initially captured human C3b that had been site-specifically biotinylated at its thioester cysteine on a streptavidin sensor chip. We then characterized its affinity for full-length FH alone, as well as for preformed B75KN/FH and B6C-IgI3-B75KN/FH complexes. Although we found that B75KN/FH (K_D=221±21 nM) and B6C-IgI3-B75KN/FH (K_D=268±34 nM) had apparent affinities for C3b slightly reduced when compared to that of FH alone (K_D=157±14 nM), they nevertheless exhibited nanomolar affinity (Figure 4.7). This demonstrated that β-binding did not disrupt the ability of FH to interact with C3b.

We then used an SPR-based method that monitors formation and decay of the AP C3 convertase in real-time (16,51). In this experiment, two separate injection phases are employed such that the first phase allows for formation and initial decay of the convertase while the second phase introduces an exogenous molecule/complex into the system that might alter the overall convertase decay rate. As a control, we first injected a fixed concentration (i.e. 500 nM) of B75KN, FH, or pre-formed B75KN/FH complex over the C3b surface to gauge both the magnitude and decay rate of the SPR signal that resulted (Figure 4.6A). In addition, this showed that B75KN

alone did not bind to C3b. We then injected either FB or a premixed solution of FB/FD to generate the AP C3 convertase on the immobilized C3b, and followed this by injection of either B75KN, FH, or a preformed B75KN/FH complex in various combinations (Figure 4.6B). Whereas FB on its own dissociated relatively quickly, the convertase complex (i.e. C3bBb) exhibited a slower decay rate. Consistent with the inability of B75KN to bind C3b directly, we found that the decay rate of the convertase was not altered by the presence of B75KN on its own. By contrast, we observed that injection of FH over a convertase-bearing surface resulted in an initial increase in the SPR signal that returned to an equilibrium level, followed by rapid decay upon injection stop. This result was consistent with decay accelerating activity attributable to FH (Figure 4.6C). When we carried out an analogous experiment with a preformed B75KN/FH as the second analyte, however, we not only observed a correspondingly larger initial increase and equilibrium level, but we also found rapid decay upon injection stop. These results were consistent with binding of a complex (i.e. B75KN/FH) larger than FH alone to the convertase-bearing surface, and also showed evidence of decay accelerating activity attributable to the B75KN/FH complex. We obtained a qualitatively similar set of results when this entire suite of experiments was performed with the much larger β fragment B6C-IgI3-B75KN in place of B75KN (Figure 4.7). Therefore, the presence of β did not dramatically alter the decay accelerating activity of FH.

In addition to its role in promoting convertase decay, FH also serves as a co-factor for FI-mediated proteolytic cleavage of C3b to iC3b. However, since iC3b cannot serve as a platform for further formation of C3 convertases, maintenance of cofactor activity by bound FH would benefit bacterial complement evasion. We therefore investigated whether FH bound to β protein maintained its co-factor activity for FI mediated inactivation of C3b to iC3b. The cofactor activity of β-bound FH was assessed in an assay utilizing purified C3b, FI and FH (Figure 4.6D)

(25,27,32). Briefly, we incubated *L. lactis* strains with purified FH, performed extensive washes, and then incubated the *L. lactis* strains with purified C3b and FI. After removing the *L. lactis* cells by centrifugation, we analyzed the supernatants for cleavage of C3b to iC3b by Western blot analysis using an anti-C3 antibody (Figure 4.6E).

As expected, we found that C3b was not degraded to detectable levels of iC3b when FH was omitted from the assay. This indicated that *L. lactis* cells do not possess inherent surface-anchored molecules with cofactor activities similar to FH. By contrast, we found that *L. lactis* cells expressing wild type β degraded C3b to iC3b in the presence, but not the absence, of FH. This degradation of C3b to iC3b was similar to that we observed for the control when purified C3b and FI were incubated in the presence but not absence of FH. We further found that *L. lactis* strains carrying pOri23, pOri23.*bac*ΔB75KN, or pOri23.*bac*ΔFHBD produced no detectable levels of iC3b, even after preincubation with FH. These results were consistent with our previous experiments (Figure 4.5C), which showed that only the wild-type β-expressing strain could recruit FH to the bacterial surface.

It was important to address whether our observations could be due to variations in C3b levels between individual assays. Since only the α chain is proteolyzed during conversions of C3 while its β chain remains constant, we used densitometry to compare the ratio of intensities between the α 45' and β chains across various experiments (Figure 4.6F). Using numbers calculated from four technical replicates, we estimated that approximately 18% of C3b was degraded to iC3b upon incubation of pOri23.*bac* cells with FH and FI. For comparison, we determined that 65% of C3b was degraded upon incubation with soluble FH and FI. Thus, these

results confirm that FH maintained its co-factor properties for FI when bound to β protein at the cell surface.

To understand the potential immune evasion implications of enhanced FH recruitment and subsequent stimulation of FI activity at the surface of β-expressing bacteria, we investigated whether the C3b deposited on *L. lactis* upon incubation with human serum was more effectively turned over to iC3b. We incubated β-expressing *L. lactis* strains with human serum, withdrew samples at 5, 15, 30, and 60 min, and assessed thereafter the both the levels and nature of C3-derived opsonins on the bacterial surface. Consistent with the flow cytometry studies discussed previously (Figure 4.5D), we observed that the wild type β-expressing cells had markedly reduced anti-C3 immunoreactivity when compared to the other cells across all time points examined (Figure 4.6G). The polyclonal anti-C3 antibody used in this study recognizes both the α and β chains of C3; this led to difficulty in interpreting immunoreactivity against the nearly co-migrating β and α 67' chains. Therefore, we probed serum treated *L. lactis* cells from each strain with a mAb selective for an iC3b neoantigen, measured the signal by flow cytometry, and normalized the signal relative to the observed levels of C3b deposition (Figure 4.6H), since C3b deposition levels vary between strains (Figure 4.5 & Figure 4.6G). Using numbers obtained from five technical replicates, we found no statistically significant differences in the iC3b/C3b ratio between these strains. These inconclusive results may be due to the use of a mAb that cannot detect low levels of iC3b. Alternatively, the results may also suggest that enhanced turnover of C3b to iC3b is not a major consequence of β protein expression at the bacterial surface. Thus, while expression of β protein clearly lowers bacterial opsonization by C3, its does not appear to significantly change the functional properties of FH upon binding.

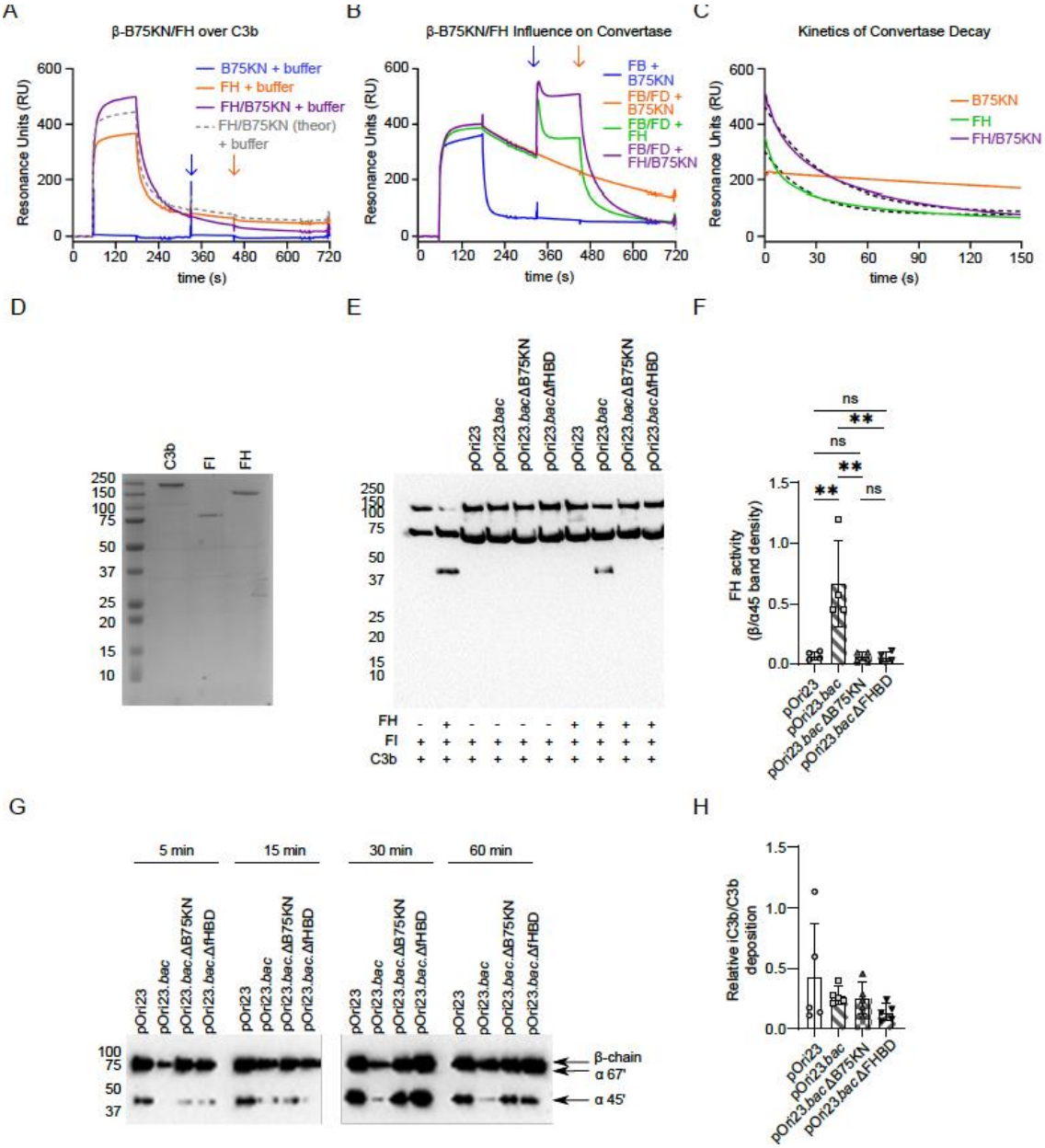

Figure 4.6. FH Bound by β Protein Retains its Complement Regulatory Activities.

(A) Site-specifically biotinylated C3b was captured on a streptavidin-coated biosensor and used to assess ligand binding by SPR. Representative reference-corrected sensorgrams for injections of 500 nM B75KN (blue trace), FH (orange trace), or pre-formed B75KN/FH complex (purple trace) are shown. The theoretical response for the B75KN/FH complex based upon the mass increase of the analyte relative to FH alone is also presented (grey dashed trace). Blue and orange arrows mark the start and stop of the second injection phase, respectively. (B) Representative reference-corrected sensorgrams illustrating the formation (first injection phase) and decay (second injection phase) of the AP C3 convertase on immobilized C3b are shown. Injections of FB alone followed by B75KN (blue trace) are presented along with injection of a FB/FD mixture followed by B75KN (orange trace). Injection of FB/FD followed by FH (green trace) highlights the decay-acceleration activity of FH. Injection of FB/FD followed by the B75KN/FH complex (purple) yielded a greater

increase in SPR response when compared to FH alone, but decay acceleration activity was still present. (C) Plot showing the rate of convertase decay for B75KN alone (orange trace; t1/2=287 sec), FH alone (green trace; t1/2=16.7 sec), or the B75KN/FH complex (purple trace; t1/2=24.2 sec) across the 150 sec time interval following second injection stop. Data were taken from the experiment shown in panel B. Dashed black lines represent the data fit to a single exponential decay function. The experiments shown in panels A-C are representative of n=3 replicates. (D) Purity of C3b, factor I (FI) and factor H (FH) assessed by SDS-PAGE analysis. (E) FH bound to β protein retains its co-factor activity for FI mediated inactivation of C3b. Stationary phase *L. lactis* strains were incubated with FH (10 μg/mL) or buffer control, vigorously washed, and resuspended in the presence of C3b (10 μg/mL) and FI (10μg/mL) at 37 ºC for 30 min. Proteins were boiled under reducing conditions, separated by SDS-PAGE, and analyzed by Western blot. The membrane was stained for total C3 using goat-anti-C3 mAb (1:5,000) and HRP-conjugated rabbit anti-goat-IgG (1:10,000). Image representative of n=4 replicates. (F) Densitometry analysis of data in panel E was performed using FIJI software to measure the intensity of β and α2 bands. (G) Total C3b deposition on *L. lactis* strains after incubation in human serum. Stationary phase *L. lactis* strains were incubated with 30% (v/v) human serum for indicated time periods, vigorously washed, and boiled in sample buffer. Proteins were separated by SDS-PAGE and analyzed by Western blot. The membrane was stained for total C3 using anti-C3.HRP polyclonal antibody (1:10,000). Data is representative of n=2 assays. (H) Deposition of iC3b and C3b on the surface of *L. lactis* strains measured by flow cytometry analysis. *L. lactis* strains were incubated with 3% (v/v) human serum, washed, stained with mouse polyclonal antibodies against the iC3b neoantigen (5 μg/mL), mouse isotype control (5 μg/mL), goat anti-C3b-FITC or buffer. PE-conjugated goat anti-mouse-IgG (1:1,000) was used for detection of mouse antibodies. All samples were fixed in 1% (v/v) PFA and analyzed by flow cytometry. The mean and standard deviation of n=5 replicates is shown. ANOVA was performed to assess levels of statistical significance. (*p<0.05, **p<0.01). (D-H were done by Dr. McCarthy's Lab.)

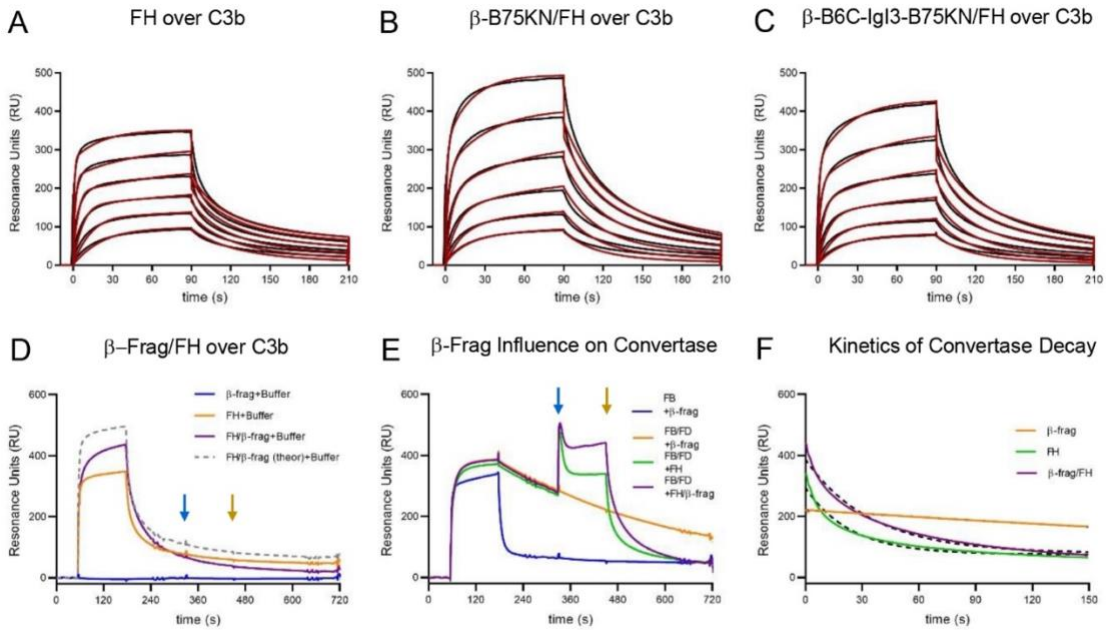

Figure 4.7 Supporting Information for the Convertase Decay Study.

(A) Representative reference-corrected sensorgram series for injection of FH over a surface of site-specifically immobilized C3b. Both the experimental data (black traces) and the fit to a ligand heterogeneity model (red traces) are shown. The apparent K_D for fitting to a simple affinity model (*Data Not Shown*) was 157±14 nM across a total of six technical replicates. (B) Representative reference-corrected sensorgram series for injection of B75KN/FH complex over site-specifically immobilized C3b. Both the experimental data (black traces) and the fit to a ligand heterogeneity model (red traces) are shown. The apparent K_D for fitting to a simple affinity model (*Data Not Shown*) was 221±21 nM across a total of three technical replicates. (C) Representative reference-corrected sensorgram series for injection of B6C-IgI3-B75KN/FH complex over site-specifically immobilized C3b. Both the experimental data (black traces) and the fit to a ligand heterogeneity model (red traces) are shown. The apparent K_D for fitting to a simple affinity model (*Data Not Shown*) was 268±34 nM across a total of three technical replicates. (D) Reference-corrected sensorgrams for injections of 500 nM B6C-IgI3-B75KN (blue trace), FH (orange trace), or pre-formed B6C-IgI3-B75KN/FH complex (purple trace) over site-specifically immobilized C3b. The theoretical response for the B6C-IgI3-B75KN/FH complex based upon the mass increase of the analyte relative to FH alone is also presented (grey dashed trace). Blue and orange arrows mark the start and stop of the second injection phase, respectively. (E) Reference-corrected sensorgrams illustrating the formation (first injection phase) and decay (second injection phase) of the AP C3 convertase on immobilized C3b are shown. Injections of FB alone followed by B6C-IgI3-B75KN (blue trace) are presented along with injection of a FB/FD mixture followed by B6C-IgI3-B75KN (orange trace). Injection of FB/FD followed by FH (green trace) highlights the decay-acceleration activity of FH. Injection of FB/FD followed by injection of a B6C-IgI3-B75KN/FH complex (purple) yielded a greater increase in SPR response when compared to FH alone, but decay acceleration activity was still evident. (F) Plot showing the rate of convertase decay for B6C-IgI3-B75KN alone (orange trace), FH alone (green trace), or the B6C-IgI3-B75KN/FH complex (purple trace) across the 150 sec time intervals following second injection stop. Data taken from the experiment shown in panel E. Dashed black lines represent the data fit to a single exponential decay function. Note that B6C-IgI3-B75KN is abbreviated as "β-frag" in the legend for the sake of simplicity. Data shown in panels D-F are representative of three technical replicates.

β Protein Does Not Enhance Resistance to Complement-mediated or Opsonophagocytic Killing Through FH Binding

Recruitment of FH and the resulting inhibition of C3b deposition at the bacterial surface has been proposed as a key aspect of innate immune evasion by pathogens (15). However, the immune evasion strategies of individual pathogens are often multifaceted and defining a direct contribution of any single evasion mechanism to killing resistance has been challenging. Although *L. lactis* is not known to possess any innate immune evasion mechanisms of its known, we found

that expression of β significantly reduced levels of C3b deposited on the *L. lactis* surface by human serum (Figure 4.5D & Figure 4.6G). Thus, we investigated whether expression of β by *L. lactis* would culminate in enhanced resistance to either complement-mediated killing, opsonophagocytosis by neutrophils, or killing by whole human blood.

We initially tested whether FH recruitment by β protein influences complement-mediated killing (Figure 4.8A). We measured the number of surviving bacteria after 2 h incubation with either active or heat-inactivated human serum by colony forming unit (CFU) quantification. We found no difference in bacterial survival among any of our *L. lactis* strains regardless of the serum used in the experiments. Although this was somewhat expected as Gram-positive bacteria like *L. lactis* are generally regarded as unsusceptible to the terminal complement complex (71), this result indicated that expression of β protein did not modify resistance to complement-mediated killing or bacterial growth in human serum.

We next tested whether β protein expression and capture of FH enhanced resistance to neutrophil-mediated opsonophagocytosis (Figure 4.8B). In this stepwise experiment, samples of FITC-labelled *L. lactis* strains were opsonized with human active serum for 30 min, incubated with human neutrophils for 30 min, washed to remove extracellular bacteria, and the fluorescence of the neutrophils was measured by flow cytometry. We found that neutrophils incubated with the *L. lactis* strain expressing wild type β showed an ~75%, statistically significant reduction ($p<0.01$) in FITC signal when compared those incubated with the control *L. lactis* strain. This demonstrated that β protein enhances resistance to neutrophil opsonophagocytosis and was consistent with a previous study using GBS bacteria (34). However, we also found that neutrophils incubated with *L. lactis* strains expressing either βΔFHBD or βΔB75KN also showed significant differences in fluorescence when compared to control ($p<0.01$). Since the strain that expressed wild-type β was

the only one that retained FH-binding activity (Figure 4.5C), these results suggested that inhibition of neutrophil-mediated opsonophagocytosis was not dependent upon β/FH interactions at the bacterial surface. Nevertheless, we noted that the βΔB75KN-expressing strain displayed an approximately two-fold, statistically significant increase ($p<0.05$) in susceptibility to opsonophagocytosis when compared to the wild-type strain. This implied that the B75KN domain of β makes an important functional contribution to bacterial evasion of opsonophagocytosis by neutrophils.

Finally, we investigated the effects of β protein expression and capture of FH by bacteria in a whole blood killing assay (Figure 4.8C). In this stepwise experiment, *L. lactis* strains were opsonized with human serum, incubated with whole human blood for defined time intervals, and the number of viable bacteria remaining were enumerated by CFU count following plating. Consistent with the experiment presented above, we found that all β-expressing strains of *L. lactis* exhibited a more than two-fold, statistically significant ($p<0.05$) resistance to killing when compared with the control *L. lactis* strain. Interestingly, while the *L. lactis* strain expressing βΔFHBD did not differ significantly from the strain expressing wild-type β in this assay, we again noted that the strain expressing βΔB75KN exhibited a trend toward increased killing susceptibility when compared to wild-type β expressing strain. However, this trend was not statistically significant. In conclusion, while this series of functional assays show that expression of β protein inhibits C3b deposition at the cell surface in a manner that significantly impedes both opsonophagocytosis by neutrophils and killing in whole blood, these effects appear to depend to a greater extent on the presence of the B75KN region than recruitment of FH *per se*.

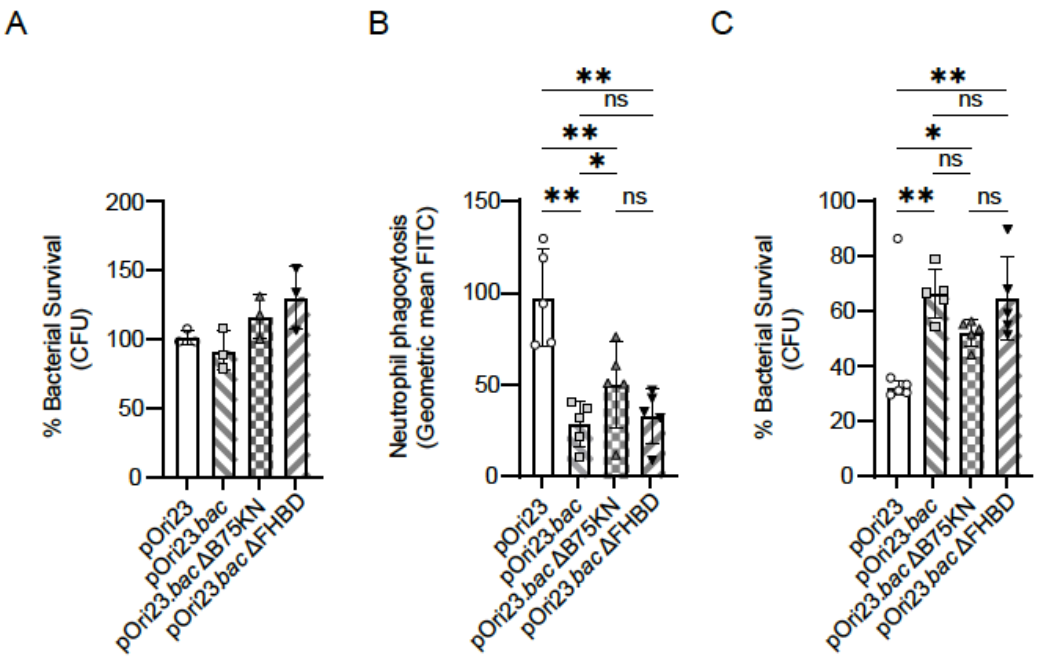

Figure 4.8. The B75KN Domain of β protein Suppresses Bacterial Phagocytic Killing Through a FH-Independent Mechanism.

(A) Survival of *L. lactis* strains in human active and heat-inactivated serum. Mid-logarithmic phase *L. lactis* strains were incubated with 10% serum or buffer at 37ºC for 120 mins. The number of colonies forming units (CFU) was quantified by serial dilution, plating and growth on GM17 agar plates. The % bacterial survival was determined by the CFU ratio of inoculum and samples. (B) Phagocytosis of FITC-labelled *L. lactis* strains by human neutrophils after opsonization in human serum. FITC-labelled stationary phase *L. lactis* strains incubated with human neutrophils at MOI 10 for 30 mins at 37ºC with shaking. Neutrophils were washed, and fluorescence measured by flow cytometry. Mean and standard deviation of n = 5 replicates is shown. (C) Survival of *L. lactis* strains in human whole blood. Mid-log phase *L. lactis* strains were inoculated into human whole blood and incubated at 37ºC with gentle rotation. CFU count was measured and % bacterial survival determined the same as (A). Mean and standard deviation of n = 5 replicates is shown. ANOVA was performed to determine statistical significance. (*p<0.05, **p<0.01). (Experiments were done by Dr. McCarthy's Lab.)

Discussion

The complement evasion strategies of various pathogens and parasites have been studied extensively (13,14). However, no single mechanism has received more attention than capture of the endogenous host regulator, FH (21). Considering both its abundance in human blood (~1.5 µM) and potent complement regulatory activities (15,72), recruitment of FH to the pathogen

surface would seem to provide a formidable barrier against complement attack. A recent inventory of pathogen and parasite FH-binding proteins identified nearly 100 different molecules from viruses, bacteria, fungi, protozoa, and helminths with purported roles in complement evasion (21). In spite of this remarkable diversity, unifying structure/function themes concerning the molecular interactions responsible for FH-recruitment have emerged (21). As typified by FHbp from *N. meningitidis* (73), the most well understood of these involves a type of molecular mimicry whereby the pathogen-derived protein displays a structure resembling features of host cell surface-exposed polyanion ligands for FH. Nevertheless, alternative interactions have also been identified. Among these, the *S. pneumoniae* FH-binding protein PspC is especially noteworthy as this molecule has been shown to bind tightly to FH, alter its conformation, and thereby enhance its intrinsic complement regulatory activities (22). Interestingly, the structure of the FH-binding region of PspC shows a three α-helix bundle fold (56) that shares significant structural homology to B75KN-CTD (RMSD of superposition 0.576 Å across 61 Cα positions) even though these two proteins share only ~30% sequence identity with one another.

Despite its structural similarities with PspC and other bacterial innate immune evasion molecules (52,60-64), our work here shows that the GBS β protein acts through a fundamentally different mechanism than other known FH-binding proteins (21). On one hand, the interaction of β with FH appears to be complex and involve two distinct sites within the larger β molecule (Figure 4.1 & Table 4.1). Although the novel B75KN-CTD is sufficient for FH-binding (Figure 4.1 & Figure 4.2), regions N-terminal to this domain appear necessary to manifest higher affinities (Table 4.1). While the experiments we present here do not offer any insight into how these N-terminally directed regions might contribute to FH binding, our results clearly show that loss of the residues connecting helices α1 and α2 in B75KN-CTD ablate its FH binding activity (Figure 4.2). These

contributions were confirmed independently through crosslinking mass spectrometry studies, which identified positions from this same region at the interface between B75KN and full-length FH (Figure 4.4 & Table 4.3). It is interesting to note that no points of contact between B75KN and FH were identified outside the B75KN-CTD. Although there are several potential explanations for this observation, one might be that the accessory contacts from regions N-terminal to B75KN-CTD are more like those ascribed to so-called fuzzy or transiently ordered complexes (74). On the other hand, the crosslinking mass spectrometry studies revealed that B75KN interacts with the domains CCP3 and CCP4 of FH (Figure 4.3 & Table 4.3). To the best of our knowledge, mapping of an immune evasion protein binding site to this region of FH is unprecedented (21). Since the CCP1-CCP4 region of FH is critical for its complement regulatory activities (15), we felt it essential to test whether β-binding was compatible with FH function even though existing crystal structures of FH/C3b complexes suggested that this should be the case (Figure 4.3 & Figure 4.4). Heterologous expression studies using *L. lactis* demonstrated that cell-surface exposed β both captured FH from serum and impaired opsonization of bacteria with C3b (Figure 4.5), while subsequent functional experiments showed that β-bound FH retained both its convertase decay acceleration and FI cofactor activities (Figure 4.6). Unlike the structurally-related PspC protein (22), however, β binding does not appear to augment the canonical complement regulatory activities of FH. Instead, β appears to simply serve as a high-affinity molecular tether for recruiting functional FH to the bacterial surface, presumably to facilitate complement evasion.

In some respects, the most significant outcome from our heterologous expression studies in *L. lactis* was the finding that β conferred resistance to opsonophagocytosis by neutrophils and killing by whole human blood (Figure 4.8). Although these observations were made using an intentionally reductionist system, they were conclusive and also consistent with a prior

investigation that employed strains of GBS bacteria (34). Nevertheless, the studies we present here also raise important questions regarding the biological signficance of FH-binding to β protein. We believe this paradox is powerfully illustrated by our finding that *L. lactis* cells which expressed βΔFHBD retained wild-type immune evasion properties (Figure 4.8) even though they lacked any FH binding activity (Figure 4.5). When taken at face value, these data argue that FH-binding to β protein cannot be responsible for bacterial resistance to opsonophagocytosis and subsequent killing by neutrophils. On the contrary, the simplest explanation for these observations is that β protein suppresses phagocytosis and killing through an FH-independent mechanism. In this regard, β protein also binds to IgA, as well as the inhibitory receptors CEACAM1, Siglec5 and/or Siglec7 (34,36,37) (Figure 4.1). It is possible that this network of interactions could work synergistically to promote the full immune evasion activities of β. Alternatively, these interactions may be sufficiently redundant so that β binding to any single target ligand might not play a strictly essential role for manifesting immune evasion activity. Although delineating the biological consequences of each β interaction to its overall immune suppressive properties will likely be difficult, we noted that *L. lactis* cells expressing βΔB75KN were diminished in their capacity to resist neutrophil phagocytosis and killing in whole blood (Figure 4.8). This strongly suggests that B75KN provides other properties aside from FH binding that are beneficial for immune evasion, possibly through interacting with as yet unknown components of the human innate immune system. Consequently, we believe further studies to identify additional binding partners of the B75KN domain are warranted, as it appears they may hold crucial information for understanding β function.

A large body of literature suggests that FH recruitment is a major innate immune evasion mechanism of diverse bacterial pathogens, including *N. meningitidis*, *B. burgdorferi*, *S. pneumoniae*, and *S. pyogenes*, among others (Reviewed in (13,14,20,21)). However, noteworthy

studies using animal infection models to compare the virulence of wild-type and FH-binding protein deficient strains of *Borrelia* have challenged this notion, as their negative results stand opposed to functional analyses performed *in vitro* (Reviewed in (21)). Analogous investigations of the FH-binding proteins from *S. pyogenes* are similarly contradictory, and led to questions regarding the *in vivo* relevance of various *in vitro* studies (Reviewed in (21). Some of these long-standing discrepancies could have arisen through incorrect assumptions. For example, evasion proteins from human pathogens do not always recognize components of the rodent innate immune system equally well, or even at all (e.g. (60,75,76)). In other cases, the presence of additional bacterial surface proteins that recognize the same host ligand (e.g. FH), or bacterial proteins that recognize multiple host-derived ligands (e.g. β) may yield confounding results in otherwise well-established assays of immune function. For these reasons, we pursued a functional comparison of the wild-type β protein with two precisely designed β mutants that ablated FH binding but retained interactions with other host ligands (Figure 4.1). By designing our study to assess the relevance of β/FH interactions vis-à-vis conferring immune evasion behaviour to the otherwise non-pathogenic *L. lactis*, we determined that FH-binding by β does not contribute to, or is not solely responsible for, bacterial resistance to opsonophagocytic killing (Figure 4.8). Recognizing the potential limitation of our own experiments as well as those described earlier in this paragraph, our findings contribute to an emerging theme that challenges the dogma that FH-binding is a major immune evasion strategy of bacterial pathogens.

It seems foolish to dismiss the nanomolar affinity interaction of β with FH as a biochemical curiosity. Yet if not, this begs the question that if FH-binding by a bacterial surface protein does not promote resistance to opsonophagocytic killing, what is its purpose? It has previously been reported that FH-binding enhances *in vitro* adhesion to and invasion of *S. pneumoniae* and *M.*

hyopneumoniae to epithelial and/or endothelial cells (77-80). How this adhesin-like activity of FH occurs at a structural and mechanistic level is not entirely clear. Although there is not a well-established literature on non-canonical roles of FH, one cannot escape the fact that FH is large host protein, replete with protein-protein interaction sites, and which is found in rather large abundance in human blood. Thus, it is tempting to speculate that binding of FH to β protein may contribute to immune evasion via mechanisms yet to be discovered and which may not be unique to GBS among bacterial pathogens.

Acknowledgements

The authors Brandon L. Garcia (East Carolina University) and John D. Lambris (University of Pennsylvania) for helpful discussions throughout the course of this work, as well as Jason Sumner, Alexis Nazabal, and Ryan Wenzel (CovalX AG) for sharing their technical expertise on the protein crosslinking mass and spectrometry studies. X-ray diffraction data were collected at Southeast Regional Collaborative Access Team (SER-CAT) 22-ID beamline at the Advanced Photon Source, Argonne National Laboratory. A list of supporting institutions may be found on the SER-CAT website. Use of the Advanced Photon Source was supported by the U.S. Department of Energy, Office of Science, Office of Basic Energy Sciences, under Contract No. W-31-109-Eng-38.

References

1. Thomas, L., and Cook, L. (2020) Two-component signal transduction systems in the human pathogen Streptococcus agalactiae. *Infection and immunity* **88**
2. Doran, K. S., and Nizet, V. (2004) Molecular Pathogenesis of Neonatal Group B Streptococcal Infection: No Longer in its Infancy. *Mol. Micro.* **54**, 23-31
3. Ruppen, C., Notter, J., Strahm, C., Sonderegger, B., and Sendi, P. (2018) Osteoarticular and skin and soft-tissue infections caused by Streptococcus agalactiae in elderly patients

are frequently associated with bacteremia. *Diagnostic microbiology and infectious disease* **90**, 55-57
4. Leclercq, S. Y., Sullivan, M. J., Ipe, D. S., Smith, J. P., Cripps, A. W., and Ulett, G. C. (2016) Pathogenesis of Streptococcus urinary tract infection depends on bacterial strain and β-hemolysin/cytolysin that mediates cytotoxicity, cytokine synthesis, inflammation and virulence. *Scientific reports* **6**, 1-14
5. Saad, E. J., Baenas, D. F., Boisseau, C. S., García, M. J., Núñez, S. A., Sanchez, P. E., Balderramo, D. C., Hernández, D., and Caeiro, J. P. (2018) Streptococcus agalactiae bacteremia in non-pregnant adult patients at two teaching hospitals. *Revista Argentina de microbiologia* **50**, 280-284
6. Durrant, J. D., and McCammon, J. A. (2011) NNScore 2.0: a neural-network receptor-ligand scoring function. *J Chem Inf Model* **51**, 2897-2903
7. Shabayek, S., and Spellerberg, B. (2018) Group B streptococcal colonization, molecular characteristics, and epidemiology. *Frontiers in microbiology* **9**, 437
8. Yadeta, T. A., Worku, A., Egata, G., Seyoum, B., Marami, D., and Berhane, Y. (2018) Vertical transmission of group B Streptococcus and associated factors among pregnant women: a cross-sectional study, Eastern Ethiopia. *Infection and drug resistance* **11**, 397
9. Edmond, K. M., Kortsalioudaki, C., Scott, S., Schrag, S. J., Zaidi, A. K. M., Cousens, S., and Heath, P. T. (2012) Group B streptococcal disease in infants aged younger than 3 months: systematic review and meta-analysis. *Lancet* **379**, 547-556
10. Watkins, L. K. F., McGee, L., Schrag, S. J., Beall, B., Hudson Jain, J., Pondo, T., Farley, M. M., Harrison, L. H., Zansky, S. M., Baumbach, J., Lynfield, R., Snippes Vagnone, P., Miller, L. A., Schaffner, W., Thomas, A. R., Watt, J. P., Petit, S., and Langley, G. E. (2019) Epidemiology of Invasive Group B Streptococcal Infections Among Nonpregnant Adults in the United States, 2008-2016. *JAMA Intern. Med.* **179**, 479-488
11. Jamrozy, D., Bijlsma, M. W., de Goffau, M. C., van de Beek, D., Kuijpers, T. W., Parkhill, J., van der Ende, A., and Bentley, S. D. (2020) Increasing incidence of group B streptococcus neonatal infections in the Netherlands is associated with clonal expansion of CC17 and CC23. *Sci. Rep.* **10**, 9539
12. O'Sullivan, C. P., Lamagni, T., Patel, D., Efstratiou, A., Cunney, R., Meehan, M., Ladhani, S., Reynolds, A. J., Campbell, R., Doherty, L., Boyle, M., Kapatai, G., Chalker, V., Lindsay, D., Smith, A., Davies, E., Jones, C. E., and Heath, P. T. (2019) Group B streptococcal disease in UK and Irish infants younger than 90 days, 2014-15: a prospective surveillance study. *Lancet Infect Dis.* **19**, 83-90
13. Lambris, J. D., Ricklin, D., and Geisbrecht, B. V. (2008) Complement Evasion by Human Pathogens. *Nat. Rev. Microbiol.* **6**, 132-142
14. Ermert, D., Ram, S., and Laabei, M. (2019) The hijackers guide to escaping complement: Lessons learned from pathogens. *Mol. Immunol.* **114**, 49-61
15. Ferreira, V. P., Pangburn, M. K., and Cortes, C. (2010) Complement Control Protein Factor H: the Good, the Bad, and the Inadequate. *Mol. Immunol.* **47**, 2187-2197
16. Ricklin, D., Tzekou, A., Garcia, B. L., Hammel, M., McWhorter, W. J., Sfyroera, G., Wu, Y.-Q., Holers, V. M., Herbert, A. P., Barlow, P. N., Geisbrecht, B. V., and Lambris, J. D. (2009) A Molecular Insight into Complement Evasion by the Staphylococcal Complement Inhibitor Protein Family. *J. Immunol.* **183**, 2565-2574
17. Kajander, T., Lehtinen, M. J., Hyvarinen, S., Bhattacharjee, A., Leung, E., Isenman, D. E., Meri, S., Goldman, A., and Jokiranta, T. S. (2011) Dual Interaction of Factor H with C3d

and Glycosaminoglycans in Host-Nonhost Discrimination by Complement. *Proc. Natl. Acad. Sci. U.S.A.* **108**, 2897-2902
18. Meri, S. (2016) Self-nonself discrimination by the complement system. *FEBS letters* **590**, 2418-2434
19. Morgan, H. P., Schmidt, C. Q., Guariento, M., Blaum, B. S., Gillespie, D., Herbert, A. P., Kavanagh, D., Mertens, H. D., Svergun, D. I., and Johansson, C. M. (2011) Structural basis for engagement by complement factor H of C3b on a self surface. *Nature structural & molecular biology* **18**, 463
20. Jozsi, M. (2017) Factor H Family Proteins in Complement Evasion of Microorganisms. *Front. Immunol.* **8**, 571
21. Moore, S. R., Menon, S. S., Cortes, C., and Ferreira, V. P. (2021) Hijacking Factor H for Complement Immune Evasion. *Front. Immunol.* **12**, 602277
22. Herbert, A. P., Makou, E., Chen, Z. A., Kerr, H., Richards, A., Rappsilber, J., and Barlow, P. N. (2015) Complement Evasion Mediated by Enhancement of Captured Factor H: Implications for Protection of Self-Surfaces from Complement. *J. Immunol.* **195**, 4986-4998
23. Amdahl, H., Jongerius, I., Meri, S., Pasanen, T., Hyvarinen, S., Haapasalo, K., van Strijp, J. A., Rooijakkers, S. H., and Jokiranta, T. S. (2013) Staphylococcal Ecb Protein and Host Complement Regulator Factor H Enhance Functions of Each Other in Bacterial Immune Evasion. *J. Immunol.* **191**, 1775-1784
24. Haupt, K., Reuter, M., van den Elsen, J. M., Burman, J. D., Halbich, S., Richter, J., Skerka, C., and Zipfel, P. F. (2008) The Staphylococcus aureus Protein Sbi Acts as a Complement Inhibitor and Forms a Tripartite Complex with Host Complement Factor H and C3b. *PLoS Pathog.* **4**, e1000250
25. Maruvada, R., Prasadarao, N. V., and Rubens, C. E. (2009) Acquisition of factor H by a novel surface protein on group B Streptococcus promotes complement degradation. *FASEB J.* **23**, 3967-3977
26. Caswell, C. C., Han, R., Hovis, K. M., Ciborowski, P., Douglas, R. K., Marconi, R. T., and Lukomski, S. (2008) The Scl1 protein of M6-type group A Streptococcus binds the human complement regulatory protein, factor H, and inhibits the alternative pathway of complement. *Mol. Microbiol.* **67**, 584-596
27. Jarva, H., Janulczyk, R., Hellwage, J., Zipfel, P. F., Bjorck, L., and Meri, S. (2002) Streptococcus pneumoniae evades complement attack and opsonophagocytosis by expressing the pspC locus-encoded Hic protein that binds to short consensus repeats 8-11 of factor H. *J. Immunol.* **168**, 1886-1894
28. Gustafsson, M. C. U., Lannergard, J., Nilsson, O. R., Kristensen, B. M., Olsen, J. E., Harris, C. L., Ufret-Vincenty, R. L., Stalhammar-Carlemalm, M., and Lindahl, G. (2013) Factor H binds to the hypervariable region of many Streptococcus pyogenes M proteins but does not promote phagocytosis resistance or acute virulence. *PLoS Pathog.* **9**, e1003323
29. Haapasalo, K., Vuopio, J., Syrjanen, J., Suvilehto, J., Massinen, S., Karppelin, M., Jarvela, I., Meri, S., Kere, J., and Jokiranta, T. S. (2012) Acquisition of complement factor H is important for pathogenesis of Streptococcus pyogenes infections: evidence from bacterial in vitro survival and human genetic association. *J. Immunol.* **188**, 426-435
30. Marques, M. B., Kasper, D. L., Pangburn, M. K., and Wessels, M. R. (1992) Prevention of C3 deposition by capsular polysaccharide is a virulence mechanism of type III group B streptococci. *Infect. Immun.* **60**, 3986-3993

31. Moulin, P., Rong, V., Silva, A. R. E., Pederick, V. G., Camiade, E., Mereghetti, L., McDevitt, C. A., and Hiron, A. (2019) Defining the Role of the Streptococcus agalactiae Sht-Family Proteins in Zinc Acquisition and Complement Evasion. *J. Bacteriol.* **201**, e00757-00718
32. Areschoug, T., Stalhammar-Carlemalm, M., Karlsson, I., and Lindahl, G. (2002) Streptococcal β Protein Has Separate Binding Sites for Human Factor H and IgA-Fc. *J. Biol. Chem.* **277**, 12642-12648
33. Lindahl, G., Stalhammar-Carlemalm, M., and Areschoug, T. (2005) Surface proteins of Streptococcus agalactiae and related proteins in other bacterial pathogens. *Clin. Microbiol. Rev.* **18**, 102-127
34. Carlin, A. F., Chang, Y.-C., Areschoug, T., Lindahl, G., Hurtado-Ziola, N., King, C. C., Varki, A., and Nizet, V. (2009) Group B Streptococcus suppression of phagocyte functions by protein-mediated engagement of human Siglec-5. *J. Exp. Med.* **206**, 1691-1699
35. Russell-Jones, G., Gotschlich, E., and Blake, M. S. (1984) A surface receptor specific for human IgA on group B streptococci possessing the Ibc protein antigen. *The Journal of experimental medicine* **160**, 1467-1475
36. Fong, J. J., Tsai, C.-M., Saha, S., Nizet, V., Varki, A., and Bui, J. D. (2018) Siglec-7 engagement by GBS β-protein suppresses pyroptotic cell death of natural killer cells. *Proc. Natl. Acad. Sci. USA* **115**, 10410-10415
37. van Sorge, N. M., Bonsor, D. A., Deng, L., Lindahl, E., Schmitt, V., Lyndin, M., Schmidt, A., Nilsson, O. R., Brizuela, J., Boero, E., Sundberg, E. J., van Strijp, J. A. G., Doran, K. S., Singer, B. B., Lindahl, G., and McCarthy, A. J. (2021) Bacterial protein domains with a novel Ig-like fold target human CEACAM receptors. *EMBO J.* **40**, e106103
38. Geisbrecht, B. V., Bouyain, S., and Pop, M. (2006) An Optimized System for the Expression and Purification of Secreted Bacterial Proteins. *Prot. Expr. Purif.* **46**, 23-32
39. de Jong, N. W. M., Ploscariu, N. T., Ramyar, K. X., Garcia, B. L., Herrera, A. I., Prakash, O., Katz, B. B., Leidal, K. G., Nauseef, W. M., van Kessel, K. P. M., van Strijp, J. A. G., and Geisbrecht, B. V. (2018) A Structurally Dynamic N-terminal Region Drives Function of the Staphylococcal Peroxidase Inhibitor (SPIN). *J. Biol. Chem.* **293**, 2260-2271
40. Bannantine, J. P., Lingle, C. K., Adam, P. R., Ramyar, K. X., McWhorter, W. J., Stable, J. R., Picking, W. D., and Geisbrecht, B. V. (2016) NlpC/P60 domain-containing proteins of Mycobacterium avium subspecies paratuberculosis that differentially bind and hydrolyze peptidoglycan. *Protein Sci.* **25**, 840-851
41. Keightley, J. A., Shang, L., and Kinter, M. (2004) Proteomic Analysis of Oxidative Stress-resistant Cells: a Specific Role for Aldose Reductase Overexpression in Cytoprotection. *Mol. Cell Proteomics* **3**, 167-175
42. Otwinowski, Z., and Minor, W. (1997) Processing of X-ray Diffraction Data Collected in Oscillation Mode. *Methods Enzymol.* **276**, 307-326
43. Terwilliger, T. C., Adams, P. D., Read, R. J., McCoy, A. J., Moriarty, N. W., Grosse-Kunstleve, R. W., Afonine, P. V., Zwart, P. H., and Hung, L.-W. (2009) Decision-making in structure solution using Bayesian estimates of map quality: the PHENIX AutoSol wizard. *Acta Crystallographica Section D: Biological Crystallography* **65**, 582-601
44. Adams, P. D., Grosse-Kunstleve, R. W., Hung, L.-W., Ioerger, T. R., McCoy, A. J., Moriarty, N. W., Read, R. J., Sacchettini, J. C., Sauter, N. K., and Terwilliger, T. C. (2002) PHENIX: Building New Software for Automated Crystallographic Structure Determination. *Acta Cryst.* **D58**, 1948-1954

45. Emsley, P., Lohkamp, B., Scott, W. G., and Cowtan, K. (2010) Features and Development of Coot. *Acta Cryst. D Biol. Crystallogr.* **66**, 486-501
46. Leitner, A., Walzthoeni, T., and Aebersold, R. (2014) Lysine-specific chemical cross-linking of protein complexes and identification of cross-linking sites using LC-MS/MS and the xQuest/xProphet software pipeline. *Nature Protocols* **9**, 120-137
47. Gotze, M., Pettelkau, J., Schaks, S., Bosse, K., Ihling, C. H., Krauth, F., Fritzsche, R., Kuhn, U., and Sinz, A. (2012) StavroX--a software for analyzing crosslinked products in protein interaction studies. *J. Am. Soc. Mass Spectrom.* **23**, 76-87
48. Que, Y. A., Haefliger, J. A., Francioli, P., and Moreillon, P. (2000) Expression of Staphylococcus aureus clumping factor A in Lactococcus lactis subsp. cremoris using a new shuttle vector. *Infect. Immun.* **68**, 3516-3522
49. Lindahl, G., Akerstrom, B., Vaerman, J. P., and Stenberg, L. (1990) Characterization of an IgA receptor from group B streptococci: specificity for serum IgA. *Eur. J. Immunol.* **20**, 2241-2247
50. Haapasalo, K., van Kessel, K., Nissila, E., Metso, J., Johansson, T., Miettinen, S., Varjosalo, M., Kirveskari, J., Kuusela, P., Chroni, A., Jauhiainen, M., van Strijp, J., and Jokiranta, T. S. (2015) Complement Factor H Binds to Human Serum Apolipoprotein E and Mediates Complement Regulation on High Density Lipoprotein Particles. *J. Biol. Chem.* **290**, 28977-28987
51. Garcia, B. L., Summers, B. J., Ramyar, K. X., Tzekou, A., Lin, Z., Ricklin, D., Lambris, J. D., Laity, J. H., and Geisbrecht, B. V. (2013) A Structurally Dynamic N-terminal Helix is a Key Functional Determinant in Staphylococcal Complement Inhibitor (SCIN) Proteins. *J. Biol. Chem.* **288**, 2870-2881
52. Garcia, B. L., Summers, B. J., Zhuoer, L., Ramyar, K. X., Ricklin, D., Fu, Z.-Q., Lambris, J. D., and Geisbrecht, B. V. (2012) Diversity in the C3b Contact Residues and Tertiary Structures of the Staphylococcal Complement Inhibitor (SCIN) Protein Family. *J. Biol. Chem.* **287**, 628-640
53. Zhao, Y., van Woudenbergh, E., Zhu, J., Heck, A. J. R., van Kessel, K. P. M., de Haas, C. J. C., Aerts, P. C., van Strijp, J. A. G., and McCarthy, A. J. (2020) The Orphan Immune Receptor LILRB3 Modulates Fc Receptor-Medicated Functions of Neutrophils. *J. Immunol.* **204**, 954-966
54. Jarva, H. (2004) Interactions of soluble complement regulators with pathogenic bacteria.
55. Nordstrom, T., Movert, E., Olin, A. I., Ali, S. R., Nizet, V., Varki, A., and Areschoug, T. (2011) Human Siglec-5 Inhibitory Receptor and Immunoglobulin A (IgA) Have Separate Binding Sites in Streptococcal β Protein. *J. Biol. Chem.* **286**, 33981-33991
56. Achila, D., Liu, A., Banerjee, R., Li, Y., Martinez-Hackert, E., Zhang, J.-R., and Yan, H. (2015) Structural determinants of host specificity of complement Factor H recruitment by Streptococcus pneumoniae. *Biochem. J.* **465**, 325-335
57. Bhattacharjee, A., Oeemig, J. S., Kolodziejczyk, R., Meri, T., Kajander, T., Lehtinen, M. J., Iwai, H., Jokiranta, T. S., and Goldman, A. (2013) Structural basis for complement evasion by Lyme disease pathogen Borrelia burgdorferi. *J. Biol. Chem.* **288**, 18685-18695
58. Yadav, B. S., Singh, S., Kumar, P., Mathur, D., Meena, R. K., Agrawal, R. K., and Mani, A. (2016) Bioinformatics-based study on prokaryotic, archaeal and eukaryotic nucleic acid-binding proteins for identification of low-complexity and intrinsically disordered regions. *Frontiers in Life Science* **9**, 2-16

59. Keightley, J. A., Shang, L., and Kinter, M. (2004) Proteomic Analysis of Oxidative Stress-resistant Cells. *Mol. Cell. Proteomics* **3**, 167-175
60. de Jong, N. W. M., Ramyar, K. X., Guerra, F. E., Nijland, R., Fevre, C., Voyich, J. M., McCarthy, A. J., Garcia, B. L., van Kessel, K. P. M., van Strijp, J. A. G., Geisbrecht, B. V., and Haas, P. A. (2017) Immune Evasion by a Staphylococcal Inhibitor of Myeloperoxidase. *Proc. Natl. Acad. Sci. U.S.A.* **114**, 9439-9444
61. Ploscariu, N. T., de Jong, N. W. M., van Kessel, K. P. M., van Strijp, J. A. G., and Geisbrecht, B. V. (2018) Identification and Structural Characterization of a Novel Myeloperoxidase Inhibitor from Staphylococcus delphini. *Arch. Biochem. Biophys.* **645**, 1-11
62. Hammel, M., Sfyroera, G., Ricklin, D., Magotti, P., Lambris, J. D., and Geisbrecht, B. V. (2007) A Structural Basis for Complement Inhibition by Staphylococcus aureus. *Nat. Immunol.* **8**, 430-437
63. Hammel, M., Sfyroera, G., Pyrpassopoulos, S., Ricklin, D., Ramyar, K. X., Pop, M., Jin, Z., Lambris, J. D., and Geisbrecht, B. V. (2007) Characterization of Ehp: a Secreted Complement Inhibitory Protein from Staphylococcus aureus. *J. Biol. Chem.* **202**, 30051-30061
64. Rooijakkers, S. H. M., Milder, F. J., Bardoel, B. W., Ruyken, M., van Strijp, J. A. G., and Gros, P. (2007) Staphylococcal Complement Inhibitor: Structure and Active Sites. *J. Immunol.* **179**, 2989-2998
65. Gupta, R., and Brunak, S. (2002) Prediction of glycosylation across the human proteome and the correlation to protein function. *Pac. Symp. Biocomput.*, 310-322
66. Wu, J., Wu, Y. Q., Ricklin, D., Janssen, B. J., Lambris, J. D., and Gros, P. (2009) Structure of Complement Fragment C3b-factor H and Implications for Host Protection by Complement Regulators. *Nat. Immunol* **10**, 728-733
67. Schmidt, C. Q., Bai, H., Lin, Z., Risitano, A. M., Barlow, P. N., Ricklin, D., and Lambris, J. D. (2013) Rational engineering of a minimized immune inhibitor with unique triple-targeting properties. *J. Immunol.* **190**, 5712-5721
68. Xue, X., Wu, J., Ricklin, D., Forneris, F., Di Crescenzio, P., Schmidt, C. Q., Granneman, J., Sharp, T. H., Lambris, J. D., and Gros, P. (2017) Regulator-Dependent Mechanisms of C3b Processing by Factor I Allow Differentiation of Immune Responses. *Nat. Struct. Mol. Biol.* **24**
69. Pathak, A., Bergstrand, J., Sender, V., Spelmink, L., Aschtgen, M.-S., Muschiol, S., Widengren, J., and Henriques-Normark, B. (2018) Factor H binding proteins protect division septa on encapsulated Streptococcus pneumoniae against complement C3b deposition and amplification. *Nat. Commun.* **9**, 3398
70. Horstmann, R. D., Sievertsen, H. J., Knobloch, J., and Fischetti, V. A. (1988) Antiphagocytic activity of streptococcal M protein: selective binding of complement control protein factor H. *Proc. Natl. Acad. Sci. USA* **85**, 1657-1661
71. Berends, E. T. M., Dekkers, J. F., Nijland, R., Kuipers, A., Soppe, J. A., van Strijp, J. A. G., and Rooijakkers, S. H. M. (2013) Distinct localization of the Complement C5b-9 complex on Gram-positive bacteria. *Cell. Microbiol.* **15**, 1955-1968
72. Cserhalmi, M., Papp, A., Brandus, B., Uzonyi, B., and Jozsi, M. (2019) Regulation of regulators: Role of the complement factor H-related proteins. *Semin. Immunol.* **45**, 101341
73. Schneider, M. C., Prosser, B. E., Caesar, J. J. E., Kugelberg, E., Li, S., Zhang, Q., Quoraishi, S., Lovett, J. E., Deane, J. E., Sim, R. B., Roversi, P., Johnson, S., Tang, C. M.,

and Lea, S. M. (2009) Neisseria meningitidis Recruits Factor H using Protein Mimicry of Host Carbohydrates. *Nature* **458**, 890-895
74. Arbesu, M., Iruela, G., Fuentes, H., Teixeira, J. M. C., and Pons, M. (2018) Intramolecular Fuzzy Interactions Involving Intrinsically Disordered Domains. *Front. Mol. Biosci.* **5**, 39
75. de Jong, N. W. M., Vrieling, M., Garcia, B. L., Koop, G., Brettmann, M., Aerts, P. C., Ruyken, M., van Strijp, J. A. G., Holmes, M., Harrison, E. M., Geisbrecht, B. V., and Rooijakkers, S. H. M. (2018) Identification of a Staphylococcal Complement Inhibitor with Broad Host Specificity in Equid Staphylococcus aureus Strains. *J. Biol. Chem.* **293**, 4468-4477
76. Jongerius, I., Köhl, J., Pandey, M. K., Ruyken, M., van Kessel, K. P., van Strijp, J. A., and Rooijakkers, S. H. (2007) Staphylococcal Complement Evasion by Various Convertase-blocking Molecules *J. Exp. Med.* **204**, 2461-2471
77. Hammerschmidt, S., Agarwal, V., Kunert, A., Haelbich, S., Skerka, C., and Zipfel, P. F. (2007) The Host Immune Regulator Factor H Interacts via Two Contact Sites with the PspC Protein of Streptococcus pneumoniae and Mediates Adhesion to Host Epithelial Cells. *J. Immunol.* **178**, 5848-5858
78. Quin, L. R., Onwubiko, C., Moore, Q. C., Fujioka Mills, M., McDaniel, L. S., and Carmicle, S. (2007) Factor H Binding to PspC of Streptococcus pneumoniae Increases Adherence to Human Cell Lines In Vitro and Enhances Invasion of Mouse Lungs In Vivo. *Infect. Immun.* **75**, 4082-4087
79. Agarwal, V., Asmat, T. M., Luo, S., Jensch, I., Zipfel, P. F., and Hammerschmidt, S. (2010) Complement regulator Factor H mediates a two-step uptake of Streptococcus pneumoniae by human cells. *J. Biol. Chem.* **285**, 23486-23495
80. Yu, Y., Wang, J., Han, R., Wang, L., Zhang, L., Zhang, A. Y., Xin, J., Li, S., Zeng, Y., Shao, G., Feng, Z., and Xiong, Q. (2020) Mycoplasma hyopneumoniae evades complement activation by binding to factor H via elongation factor thermo unstable (EF-Tu). *Virulence* **11**, 1059-1074

Chapter 5 - Conclusion

The work described in this dissertation focuses on characterizing interactions between complement molecules and their binding partners, which gives us new thoughts on complement binding proteins and complement inhibitors.

The human complement system consists of a series of soluble and cell-surface proteins that serve numerous roles in innate immunity and homeostasis. However, the structure of large molecules is still hard to obtain due to the flexibility of the protein or the limitation of current technologies. Our study generated stable transfected CHO cell lines that secreted a relatively high amount of C3 analog in a conditioned culture medium. The conformations and activities of our C3 and C3c analogs were assessed by measuring their binding profiles to known C3/b/c ligands by SPR experiments and demonstrated the feasibility of producing a C3 analog that can be site-specifically activated by an exogenous proteolytic enzyme TEV. A similar strategy could also be used in other large molecules such as C4. It is convincible that other complement component analogs could be designed and purified so that site-specific digestion by an exogenous enzyme like TEV protease would produce various fragments and targeted deletion mutants thereof.

We also identified and characterized structurally two sequences related SOMAmers that bound to human FB and potently inhibited functional assays specific for the AP. The two SOMAmers, SL1102 and SL1103, bound to FB with K_D values of picomolar affinity. These SOMAmers inhibited the activation of the central molecule C3 of the human complement system and lysis of rabbit erythrocytes under conditions specific for the AP. We showed that these SOMAmers recognized a site comprised primarily of domain CCP1 within FB by solving co-crystal structures of SL1102 and SL1103 bound to FB. With their unique and physiochemically diverse structures, SOMAmers have attracted increasing attention for uses in biomarker discovery,

diagnostics, and therapeutics (1). In the future, to the study of SOMAmers that target other complement molecules would be valuable for revealing new aspects of the structure and function of complement components of therapeutic interest.

Moreover, the selected FH binding region of β protein (B75KN) that was reported previously (2), was confirmed in this study. We also constructed new truncations of B75KN (N and C-terminal B75KN). Quantitative affinity measurements using SPR with recombinant truncated proteins indicated that the C-terminal B75KN truncation bound to FH. Surprisingly, when we mutated the structurally disordered loop with a Glycine linker, both B75KN and C-terminal B75KN showed their binding to FH was abolished. These results suggested that C-terminal B75KN was necessary for FH binding. Consistent with the FH binding properties of recombinant C-terminal B75KN, β protein expressed at the surface of *L.lactis* showed binding to FH, but *L.lactis* expressing β protein with the B75KN domain deleted (bΔB75KN) lost the ability to bind FH. Based on the result that *L.lactis* expressing mutated β (bΔFHBD) failed to recruit FH when incubated with normal human serum, our results showed that the sequence QHLQKKN in the B75KN disordered loop was a main determinant in FH binding. Moreover, our crosslinking experiments followed by high-mass MALDI-TOF characterization revealed that FH harbored a binding site for β protein within SCR 3-4. We utilized a heterologous expression in *L.lactis* approach and found that FH-binding did not contribute to, or was not solely responsible for, defining the capacity of β protein to resist opsonophagocytosis or killing. Similarly, the binding of FH to M protein, Sht, or ShtII does not enhance resistance to opsonophagocytic killing (3,4). Therefore, our findings contribute to an emerging theme that challenges the dogma that FH-binding is a major immune evasion strategy of bacterial pathogens. If FH-binding by these bacterial ligands does not promote resistance to opsonophagocytic killing, what is the function of

FH recruitment? It has previously been reported that FH-binding enhances *in vitro* adhesion and invasion of *S. pneumoniae* and *M. hyopneumoniae* to epithelial or endothelial cells (5-7). It is plausible that the binding of FH to β protein may contribute to bacterial virulence via mechanisms yet to be assessed.

Further investigations of this interaction are of interest for analyzing other potential binding sites within FH, and the analysis of pathogenetic mechanisms in infections caused by β expressing GBS. Studies of the interaction between β protein and FH could provide information on vaccine development because the β protein is found to have the ability to elicit protective immunity and has been used for the preparation of a protein-polysaccharide conjugate intended for use as a human vaccine (8). Above all, this study promotes our understanding of the β protein in the pathogenesis of streptococcal diseases.

We believe our work should facilitate structure/function understanding of the complement components in binding with their ligands and ultimately provides a more complete understanding of the human complement system and its related diseases.

References

1. Mehan, M. R., Ostroff, R., Wilcox, S. K., Steele, F., Schneider, D., Jarvis, T. C., Baird, G. S., Gold, L., and Janjic, N. (2013) Highly multiplexed proteomic platform for biomarker discovery, diagnostics, and therapeutics. *Complement Therapeutics*, 283-300
2. Jarva, H., Hellwage, J., Jokiranta, T. S., Lehtinen, M. J., Zipfel, P. F., and Meri, S. (2004) The group B streptococcal β and pneumococcal Hic proteins are structurally related immune evasion molecules that bind the complement inhibitor factor H in an analogous fashion. *The Journal of Immunology* **172**, 3111-3118
3. Gustafsson, M. C., Lannergård, J., Nilsson, O. R., Kristensen, B. M., Olsen, J. E., Harris, C. L., Ufret-Vincenty, R. L., Stålhammar-Carlemalm, M., and Lindahl, G. (2013) Factor H binds to the hypervariable region of many Streptococcus pyogenes M proteins but does not promote phagocytosis resistance or acute virulence. *PLoS pathogens* **9**, e1003323
4. Moulin, P., Rong, V., Ribeiro E Silva, A., Pederick, V., Camiade, E., Mereghetti, L., McDevitt, C., and Hiron, A. (2019) Defining the role of the Streptococcus agalactiae Sht-

family proteins in zinc acquisition and complement evasion. *Journal of bacteriology* **201**, e00757-00718
5. Hammerschmidt, S., Agarwal, V., Kunert, A., Haelbich, S., Skerka, C., and Zipfel, P. F. (2007) The host immune regulator factor H interacts via two contact sites with the PspC protein of Streptococcus pneumoniae and mediates adhesion to host epithelial cells. *The Journal of Immunology* **178**, 5848-5858
6. Quin, L. R., Onwubiko, C., Moore, Q. C., Mills, M. F., McDaniel, L. S., and Carmicle, S. (2007) Factor H binding to PspC of Streptococcus pneumoniae increases adherence to human cell lines in vitro and enhances invasion of mouse lungs in vivo. *Infection and immunity* **75**, 4082-4087
7. Yu, Y., Wang, J., Han, R., Wang, L., Zhang, L., Zhang, A. Y., Xin, J., Li, S., Zeng, Y., and Shao, G. (2020) Mycoplasma hyopneumoniae evades complement activation by binding to factor H via elongation factor thermo unstable (EF-Tu). *Virulence* **11**, 1059-1074
8. Madoff, L. C., Paoletti, L. C., Tai, J. Y., and Kasper, D. L. (1994) Maternal immunization of mice with group B streptococcal type III polysaccharide-beta C protein conjugate elicits protective antibody to multiple serotypes. *The Journal of clinical investigation* **94**, 286-292

Appendix A - Copyright Permissions

This appendix includes the copyright permissions for the work compiled in this dissertation.

Published work: Chapter 2

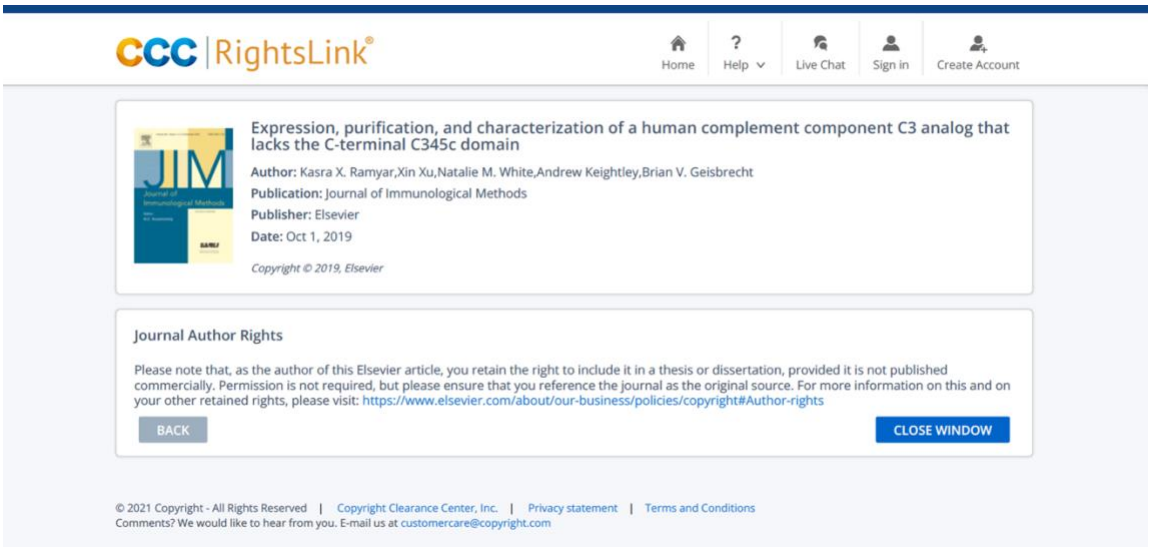

CCC | RightsLink®

Home | Help | Live Chat | Sign in | Create Account

Expression, purification, and characterization of a human complement component C3 analog that lacks the C-terminal C345c domain

Author: Kasra X. Ramyar,Xin Xu,Natalie M. White,Andrew Keightley,Brian V. Geisbrecht

Publication: Journal of Immunological Methods

Publisher: Elsevier

Date: Oct 1, 2019

Copyright © 2019, Elsevier

Journal Author Rights

Please note that, as the author of this Elsevier article, you retain the right to include it in a thesis or dissertation, provided it is not published commercially. Permission is not required, but please ensure that you reference the journal as the original source. For more information on this and on your other retained rights, please visit: https://www.elsevier.com/about/our-business/policies/copyright#Author-rights

BACK | CLOSE WINDOW

© 2021 Copyright - All Rights Reserved | Copyright Clearance Center, Inc. | Privacy statement | Terms and Conditions

Comments? We would like to hear from you. E-mail us at customercare@copyright.com

Published work: Chapter 3

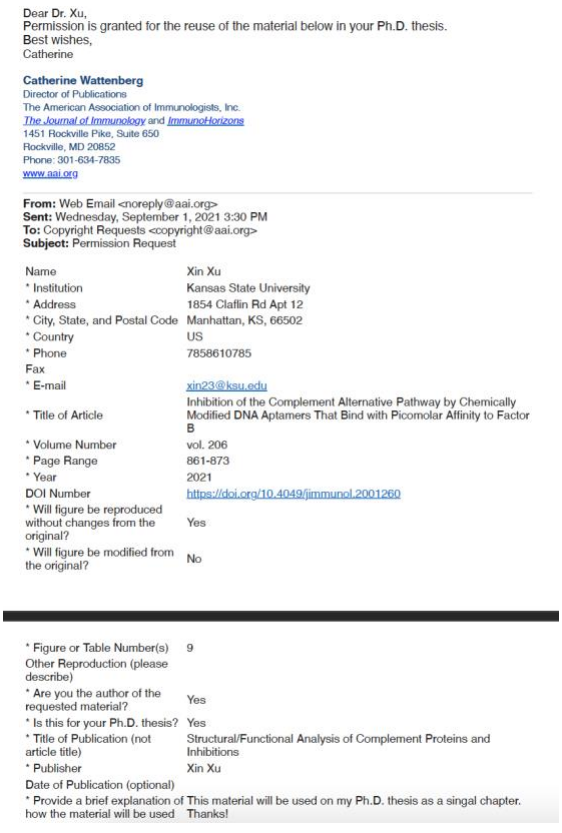

Dear Dr. Xu,
Permission is granted for the reuse of the material below in your Ph.D. thesis.
Best wishes,
Catherine

Catherine Wattenberg
Director of Publications
The American Association of Immunologists, Inc.
The Journal of Immunology and *ImmunoHorizons*
1451 Rockville Pike, Suite 650
Rockville, MD 20852
Phone: 301-634-7835
www.aai.org

From: Web Email <noreply@aai.org>
Sent: Wednesday, September 1, 2021 3:30 PM
To: Copyright Requests <copyright@aai.org>
Subject: Permission Request

Name	Xin Xu
* Institution	Kansas State University
* Address	1854 Claflin Rd Apt 12
* City, State, and Postal Code	Manhattan, KS, 66502
* Country	US
* Phone	7858610785
Fax	
* E-mail	xin23@ksu.edu
* Title of Article	Inhibition of the Complement Alternative Pathway by Chemically Modified DNA Aptamers That Bind with Picomolar Affinity to Factor B
* Volume Number	vol. 206
* Page Range	861-873
* Year	2021
DOI Number	https://doi.org/10.4049/jimmunol.2001260
* Will figure be reproduced without changes from the original?	Yes
* Will figure be modified from the original?	No
* Figure or Table Number(s)	9
Other Reproduction (please describe)	
* Are you the author of the requested material?	Yes
* Is this for your Ph.D. thesis?	Yes
* Title of Publication (not article title)	Structural/Functional Analysis of Complement Proteins and Inhibitions
* Publisher	Xin Xu
Date of Publication (optional)	
* Provide a brief explanation of how the material will be used	This material will be used on my Ph.D. thesis as a singal chapter. Thanks!

Other Images

Figure 1.1 Permission is not required for this non-commercial use.

MDPI Open Access Information and Policy

All articles published by MDPI are made immediately available worldwide under an open access license. This means:

- everyone has free and unlimited access to the full-text of *all* articles published in MDPI journals;
- everyone is free to re-use the published material if proper accreditation/citation of the original publication is given;
- open access publication is supported by the authors' institutes or research funding agencies by payment of a comparatively low **Article Processing Charge (APC)** for accepted articles.

Permissions

No special permission is required to reuse all or part of article published by MDPI, including figures and tables. For articles published under an open access Creative Common CC BY license, any part of the article may be reused without permission provided that the original article is clearly cited. Reuse of an article does not imply endorsement by the authors or MDPI.

Figure 1.2 Permission is not required for this non-commercial use.

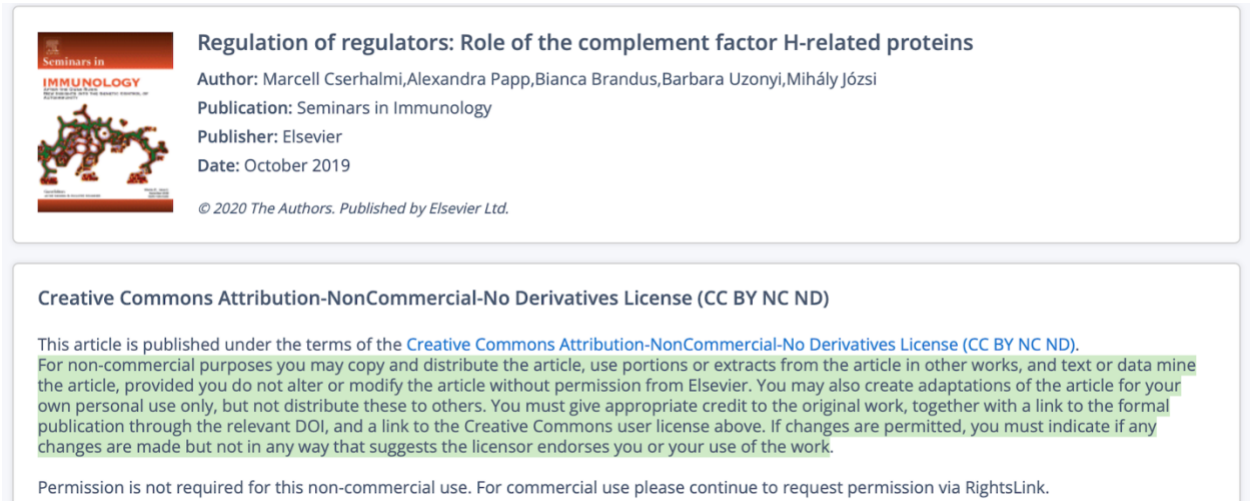

Regulation of regulators: Role of the complement factor H-related proteins

Author: Marcell Cserhalmi,Alexandra Papp,Bianca Brandus,Barbara Uzonyi,Mihály Józsi

Publication: Seminars in Immunology

Publisher: Elsevier

Date: October 2019

© 2020 The Authors. Published by Elsevier Ltd.

Creative Commons Attribution-NonCommercial-No Derivatives License (CC BY NC ND)

This article is published under the terms of the Creative Commons Attribution-NonCommercial-No Derivatives License (CC BY NC ND).
For non-commercial purposes you may copy and distribute the article, use portions or extracts from the article in other works, and text or data mine the article, provided you do not alter or modify the article without permission from Elsevier. You may also create adaptations of the article for your own personal use only, but not distribute these to others. You must give appropriate credit to the original work, together with a link to the formal publication through the relevant DOI, and a link to the Creative Commons user license above. If changes are permitted, you must indicate if any changes are made but not in any way that suggests the licensor endorses you or your use of the work.

Permission is not required for this non-commercial use. For commercial use please continue to request permission via RightsLink.